

**Combinatorial treatment of lung cancer monolayer
cells and their spheroids with tyrosine kinase
inhibitors and salinomycin**

Zhiguang Xiao

Vollständiger Abdruck der von der Fakultät Wissenschaftszentrum Weihenstephan für Ernährung, Landnutzung und Umwelt der Technischen Universität München zur Erlangung des akademischen Grades eines

Doktors der Naturwissenschaften

genehmigten Dissertation.

Vorsitzender: Univ.-Prof. Dr. K. Schneitz
Prüfer der Dissertation: 1. Univ.-Prof. Dr. B. Küster
2. Hon.-Prof. Dr. Dr. h.c. A. Ullrich
(Eberhard-Karls-Universität Tübingen)

Die Dissertation wurde am 24. 11. 2014 bei der Technischen Universität München eingereicht und durch die Fakultät Wissenschaftszentrum Weihenstephan für Ernährung, Landnutzung und Umwelt am 21. 01. 2015 angenommen.

Erklärung

Diese Dissertation wurde im Sinne von § 6 Abs. 6 und 7 der Promotionsordnung von Professor Prof. Dr. Banhard Küster von der Fakultät der Fakultät Wissenschaftszentrum Weihenstephan für Ernährung, Landnutzung und Umwelt.

.

Eidesstattliche Versicherung

Diese Dissertation wurde eigenständig und ohne unerlaubte Hilfe erarbeitet.

München, am 10.09.2014

.....
(Unterschrift des Autors / der Autorin)

Supervisor: Prof. Dr. Axel Ullrich, Dr. Pjotr Knyazev

Dissertation eingereicht am

1. Gutacher: Prof. Dr. Axel Ullrich

2. Gutacher: Prof. Dr. Banhard Küster

Mündliche Prüfung am

Dedicated to cancer patients

ACKNOWLEDGEMENTS

Before beginning a new chapter of my life, I would like to extend a heartfelt thanks to the following people who supported, guided and inspired me throughout the journey of my PhD life.

First and foremost I would like to express my profound gratitude to Prof. Dr. Axel Ullrich (Director, Molecular biology, Max Planck institute of Biochemistry, Martinsried) for providing me the opportunity to complete my doctoral studies in his department. Thanks to his faith in me the last four years and his generous support, I really enjoy to work under an inspiring and friendly atmosphere.

In particular, I am very grateful to Prof. Dr. Bernhard Küster for supervising and promoting this thesis at the Technical University of Munich.

I would also like to extend a heartfelt thanks to my supervisor Dr. Pjotr Knyazev (Senior Scientist, Max Planck institute of Biochemistry, Martinsried) for guiding me through the thesis and paper issues, encouraging and pushing me whenever required. I enjoyed working with him immensely and greatly admire and respect his seemingly endless patience in painstakingly teaching me everything regarding the project.

I further want to acknowledge technical assistance Bianca for helping me with the gene expression profiling and human phospho kinase assay. Thanks for her collaborative work. I also thank Robert and Andreas for their suggestions and discussions during the lab seminars.

I extend my gratitude to Silvia and Renate G. our technical assistants for guiding me during my initial lab work and providing all the cell culture support during my PhD, respectively. A heartfelt gratitude to Tatjana for teaching me RNA extraction and cDNA synthesis.

Special thanks to the lunch members Vijay and Zoltan for the interesting and meaningful discussion during our lunch time. I am also grateful to Vijay for his guidance in the cell sorting. Thanks Zoltan for patiently sorting out technical problems of instruments, specially related to the

ACKNOWLEDGEMENTS

computer. And Simone, thanks for the scientific discussion of my data and the support during my hard time.

I extend my thanks to Verena (Secretary) for supporting me in the entire official paper work. I would like to acknowledge Susanne for preparation of the lab media, and thanks to Attilio for taking care of all the laboratory consumables.

I also extend my thanks to all the lab members for all the scientific as well as non-scientific discussions and all the off-work enjoyment in lab and trips.

I want to extend my gratitude to all my Chinese friends, the salseros and salseras, and Pavel for making my stay in Munich smooth and joyful.

I owe my sincere gratitude to my parents and my sister for their unconditional love, emotional support and belief. I dedicate my doctoral thesis to them.

TABLE OF CONTENTS

ACKNOWLEDGEMENTS.....	1
TABLE OF CONTENTS.....	3
LIST OF FIGURES	9
LIST OF TABLES	11
1. INTRODUCTION	13
1.1. Lung cancer-an overview	13
1.1.1. Lung cancer facts and figures	13
1.1.2. Lung cancer types	14
1.1.2.1. Cellular classification of non-small cell lung cancer	14
1.1.2.2. Small cell lung cancer	15
1.2. Overview of the epidermal growth factor receptor (EGFR) protein kinase family	17
1.2.1. EGFR protein kinases	17
1.2.3. EGFR signaling	20
1.2.4. EGFR mutation in NSCLC	23
1.3. Regular treatment options	24
1.3.1. Local treatment options	25
1.3.1.1. Surgery	25
1.3.1.2. Radiotherapy	25
1.3.2. Systemic treatment options	25
1.3.2.1. Chemotherapy for lung cancer	25
1.3.2.2. Targeted therapy for lung cancer	27
1.4. Mechanisms of acquired drug resistance	29
1.4.1. Clonal evolution model	30
1.4.1.1. Primary resistance1	30

TABLE OF CONTENTS

1.4.1.2	Acquired resistance	30
1.4.2.	Cancer stem cell model	32
1.4.2.1.	Quiescence	33
1.4.2.2.	Active DNA-repair capacity	34
1.4.2.3.	Resistance to apoptosis	35
1.4.2.4.	Increased drug efflux	36
1.4.2.5.	Aldehyde dehydrogenase	37
1.4.2.6.	Tumor Microenvironment.....	38
1.4.2.7.	Pro-survival signaling	39
1.5.	Rational combinations: is there a rationale?	40
1.6.	Metformin (METF)	41
1.7.	Salinomycin (SAL)	42
2.	AIMS.....	45
3.	MATERIALS AND METHODS.....	46
3.1.	Materials.....	46
3.1.1.	Laboratory hardware.....	46
3.1.2.	Laboratory Chemicals.....	47
3.1.3.	Enzymes	48
3.1.4.	Kits and other materials.....	49
3.1.5.	Chemotherapeutic drugs.....	50
3.1.6.	Small molecule tyrosine kinase inhibitors (TKIs)	50
3.1.7.	Putative stem cell killer	51
3.1.8.	Growth factors and ligands	51
3.1.9.	Cell culture media	51
3.1.9.1.	Monolayer cell culture	51

3.1.9.2. Spheroid culture	51
3.1.9.3. Freeze media	51
3.1.10. Stock solutions and commonly used buffers	52
3.1.11. Human cell lines.....	54
3.1.12. Antibodies	55
3.1.12.1. Primary antibodies	55
3.1.12.2. Secondary antibodies	57
3.1.12.3. Therapeutic monoclonal antibody.....	58
3.1.13 Oligonucleotides.....	58
3.1.13.1. siRNAs.....	58
3.1.13.2. Primers for cDNA synthesis	59
3.1.13.3. Primers for conventional and real-time PCR.....	59
3.1.14. Software	61
3.2. Methods.....	62
3.2.1. Methods in mammalian cell culture.....	62
3.2.1.1. General cell culture techniques	62
3.2.1.2. Preparation of polyhema coated plates	62
3.2.1.3. Spheroid generation and cultivation	62
3.2.1.4. Cell seeding and drug treatment	62
3.2.1.5. Single-cell cloning by limiting dilution	63
3.2.1.6. Isolation of different subpopulations	63
3.2.1.7. Sphere formation assay	63
3.2.1.8. Transfection of small interfering RNA (siRNA)	64
3.2.2. Protein analytical methods.....	64
3.2.2.1. Lysis of cells with Triton X-100 lysis buffer.....	64

TABLE OF CONTENTS

3.2.2.2.	Determination of total protein concentration in cell lysates	64
3.2.2.3.	SDS-polyacrylamide-gel electrophoresis (SDS-PAGE).....	65
3.2.2.4.	Western blot	65
3.2.2.5.	Stripping.....	65
3.2.2.6.	Phospho-kinase array	66
3.2.3.	Methods in molecular biology and Cell Biology	66
3.2.3.1.	Total RNA isolation and cDNA synthesis	66
3.2.3.2.	RT-PCR (reverse transcription-PCR) analysis	66
3.2.3.3.	Real-time PCR analysis	67
3.2.3.4.	Flow cytometry	67
3.2.3.5.	Immunofluorescence.....	67
3.2.3.6.	Boyden chamber invasion assay	68
3.2.3.7.	Cell proliferation assays.....	68
3.2.3.8.	Isobologram analysis	68
3.2.3.9.	Statistical analysis.....	69
4.	RESULTS	71
Chapter I.....		71
4.1.	METF and SAL as the best combination for the eradication of NSCLC monolayer cells and their alveospheres (cancer stem cells) irrespective of EGFR, KRAS, EML4/ALK and LKB1 status	71
4.1.1	Characteristics of the NSCLC cell lines used in this study	71
4.1.2.	EGFR family signaling upon EGF and AG1478 treatment.....	74
4.1.3.	Evaluation of the cell viability of chemotherapeutics, TKIs, or mAb in combination with SAL on NSCLC cell lines	79
4.1.3.1.	Single drug sensitivity.....	79

4.1.3.2.	Treatment of NSCLC cell lines with chemotherapeutic agents, TKIs or mAb in combination with SAL.....	80
4.1.4.	SAL enhances METF-induced NSCLC cell growth inhibition	82
4.1.5.	Inhibition of EGFR signaling in NSCLC cells is achieved with the combination of METF and SAL	86
4.1.6.	Cell growth inhibitory effect of combinatorial treatment with METF and SAL is AMPK independent	88
4.1.7.	Human phospho-kinase assay after combinatorial treatment with METF and SAL.	89
4.1.8.	Combination of METF and SAL effectively inhibits sphere formation of NSCLC cell lines with different EGFR, KRAS, EML4/ALK and LKB1 status	91
4.1.9.	Suboptimal Erlotinib stimulates SCM expression of EGFR wt NSCLC cell lines ...	94
4.1.10.	METF abrogates Erlotinib induced apoptosis in NSCLC cell lines independent of the EGFR status.....	96
Chapter II.....		98
4.2.	NSCLC cell line NCI-H1568 heterogeneity as a new approach to investigate chemoresistance.....	98
4.2.1.	SAL interacts synergistically with Erlotinib on cell growth inhibition of NCI-H1568 wt/pool cells.....	98
4.2.2.	Effect of SAL in combination with Erlotinib on EGFR signaling	100
4.2.3.	AKT activation by SAL treatment correlates with increased cellular apoptosis	101
4.2.4.	Lung cancer cell lines in clonal cultures exhibit distinct clonal morphologies	102
4.2.5.	Different NCI-H1568 cell clones possess distinct self-renewal	105
4.2.6.	Quiescence leads to low proliferative capacities of the CSCs	106
4.2.7.	CSCs isolated from NCI-H1568 cells spend longer in the G2 phase of the cell cycle	107
4.2.8.	Evaluation of the expression of CSC related markers in distinct clones	108
4.2.9.	CSCs markedly enhanced the invasive potential of differentiated progeny.....	111

TABLE OF CONTENTS

4.2.10.	EGFR plays a considerable role in mediating the invasive behavior.....	113
4.2.11.	CSCs derived from NCI-H1568 cells survive chemotherapeutic agents and TKIs, but sensitive to the putative stem cell killers SAL and METF.....	116
5.	DISCUSSION	119
5.1.	The addition of SAL doesn't commonly augment the antitumor activity over that achievable with 11 therapeutic drugs in tested NSCLC cell lines.....	119
5.2.	METF modestly inhibits the growth of NSCLC monolayer cells and spheroids in a dose- dependent manner, interacting synergistically with SAL.....	119
5.3.	The inhibitory effect of METF/SAL is mediated by EGFR signaling.....	120
5.4.	Combinatorial treatment with SAL and METF eradicates CSCs	121
5.5.	Antagonistic effect of METF and Erlotinib is valuable for treatment on lung cancer patients with type 2 diabetes.....	122
5.6.	Quiescence emerges as a critical factor of CSC resistance to therapy.....	123
5.7.	CSCs survive traditional chemotherapeutic agents and lead to cancer cell line recurrence	124
5.8.	EMT programs are regulated dynamically by contextual signals that carcinoma cells receive from the microenvironment.....	124
5.9.	Potential value of cancer stem-like clones in the study of CSCs	125
6.	SUMMARY.....	126
7.	ZUSAMMENFASSUNG	128
8.	REFERENCES	130
9.	APPENDIX.....	147
	CURRICULUM VITAE.....	151

LIST OF FIGURES

Figure 1. Statistical representation of cancer cases and deaths in the year 2014.....	13
Figure 2. A schematic diagram of the mouse lung highlighting the spatially distinct cellular environments shown to harbor airway stem / progenitor cells.....	16
Figure 3. Structure of the human EGFR	18
Figure 4. Overview of EGFR family signaling.....	22
Figure 5. Gefitinib- and Erlotinib-sensitizing mutations of EGFR in NSCLC.....	24
Figure 6. CSC involved in drug resistance	32
Figure 7. The possible mechanisms of tumor drug resistance of CSCs.....	33
Figure 8. Interactions between tumor cells and their microenvironment are critical at all stages of tumor development and metastasis.....	39
Figure 9. Downstream effects of AMPK activation by METF resulting in inhibition of tumor growth.....	42
Figure 10. Structural formula of SAL.....	43
Figure 11. Quantitative practical applications of drug combination.....	69
Figure 12. Invasivity of HCC4006 and NCI-H1975 cells by Boyden chamber invasion assay ...	72
Figure 13. Characteristics of NSCLC HCC4006, NCI-H1975 and HCC95 cells	74
Figure 14. EGFR family signaling upon EGF and AG1478 treatment.....	76
Figure 15. Effect of siRNAs on the silencing of EGFR, HER2 and HER3 in HCC4006 cells	78
Figure 16. Treatment of NSCLC cell lines with standard therapeutic drugs, TKIs or mAb in combination with SAL.....	81
Figure 17. SAL increases METF-mediated effects on cell viability of treated NSCLC monolayer cells (2D) and spheroids (3D).	83
Figure 18. SAL enhances growth inhibition after co-administration of METF on NCI-H1650, -H3122 and -H2122 2D and 3D cells.....	84
Figure 19. Isobologram analysis of inhibition of cell viability under combination treatment	85
Figure 20. EGFR signaling in HCC4006, NCI-H1975 and HCC95 2D and 3D upon METF and SAL treatment.	87
Figure 21. AMPK signaling in NSCLC HCC4006, NCI-H1975 and HCC95 cell lines upon METF and SAL combinatorial treatment	89

LIST OF FIGURES

Figure 22. Phospho-kinase signaling after treatment of HCC4006 and NCI-H1975 with METF and SAL 90

Figure 23. Combination of METF and SAL effectively targets CSCs..... 92

Figure 24. METF in combination with SAL markedly inhibits SF in NCI-H3122 and NCI-H2122 cells 93

Figure 25. Elevated SCM expression upon insufficient Erlotinib treatment of EGFR wt NSCLC cell lines 94

Figure 26. Stem cell marker expression under suboptimal doses of Erlotinib treated NSCLC cells with EGFR mutation 95

Figure 27. Effects of Erlotinib and METF on the EGFR signaling and downstream modules AKT, ERK1/2 and PARP..... 97

Figure 28. Effects of combinatorial treatment with Erlotinib and SAL on cell viability of NCI-H1568 cells 99

Figure 29. EGFR downstream signaling in NCI-H1568 cell lines upon combined Erlotinib and SAL treatment 101

Figure 30. The time- and dose-dependent effect of SAL on apoptosis of NCI-H1568 cells..... 102

Figure 31. Phenotypic heterogeneity of NSCLC cell lines..... 105

Figure 32. Clonal heterogeneity of NCI-H1568 cells..... 105

Figure 33. Evaluation of proliferative activity of distinct types of colonies 107

Figure 34. Cell cycle analysis on distinct types of clones 108

Figure 35. Different expressions of SCMs and multidrug resistant genes 111

Figure 36. Invasivity of distinct clones by Boyden chamber invasion assay 112

Figure 37. Expression patterns of EMT related markers in distinct subpopulations of NCI-H1568 cell line..... 114

Figure 38. siRNA-EGFR downregulation of EGFR expression accompanied the reduction of cell invasion 116

Figure 39. Drug sensitivity of NCI-H1568-derived unique clones..... 118

LIST OF TABLES

Table 1. Specificity of EGFR receptors and ligands.....	19
Table 2. Mechanism of action of selected cytotoxic compounds used in cancer therapy	26
Table 3. FDA-approved TKIs and antibodies for treatment of NSCLC patients or for combinatorial application in clinical trials	28
Table 4. Major mechanisms of acquired resistance identified in clinical specimens	31
Table 5. ABC transporters involved in drug resistance	37
Table 6. Characteristics of the NSCLC cell lines used in this study	72
Table 7. Single-drug effects on HCC4006, NCI-H1975 and HCC95 cells	79

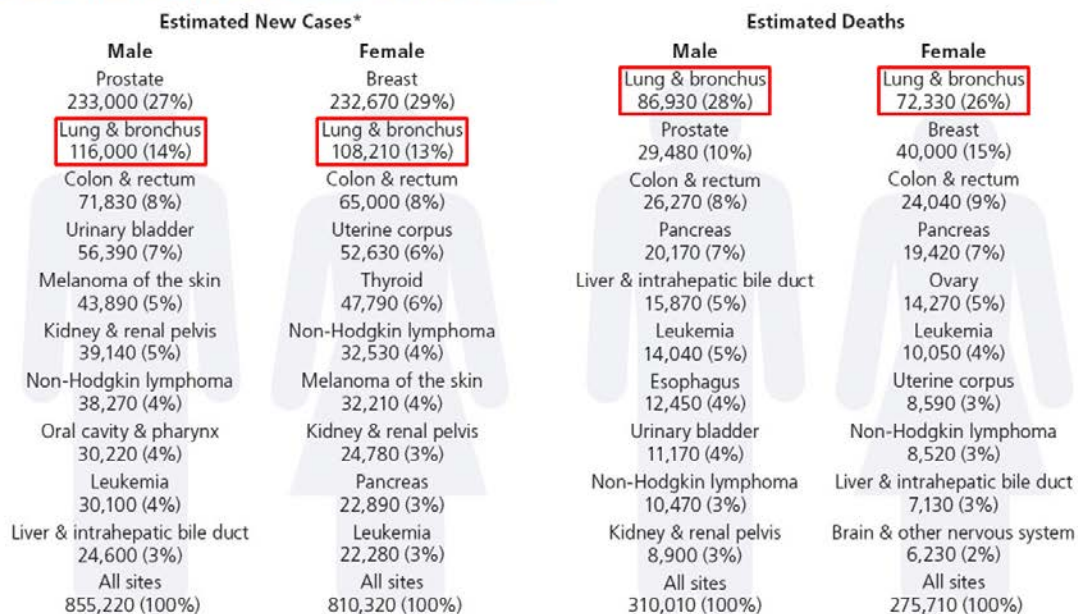
1. INTRODUCTION

1.1. Lung cancer-an overview

1.1.1. Lung cancer facts and figures

Lung cancer accounts for much more deaths than any other cancer all over the world in both men and women (Figure 1). An estimated 159,260 deaths, representing about 27% of all cancer deaths, are expected to occur in 2014. The 1- and 5-year relative survival rates for lung cancer cases diagnosed during 2003-2009 were 43% and 17%, respectively. Only 15% of lung cancers are diagnosed at a localized stage, for which the 5-year survival rate is 54% [1]. These data indicate that lung cancer is the most prevalent malignant disease in modern society and more effective diagnosis and treatments are urgently needed.

Leading New Cancer Cases and Deaths – 2014 Estimates



*Excludes basal and squamous cell skin cancers and in situ carcinoma except urinary bladder.

©2014, American Cancer Society, Inc., Surveillance Research

Figure 1. Statistical representation of cancer cases and deaths in the year 2014. Highlighted areas (Red bordered box) show number of lung cancer new cases and deaths estimated in 2014. (Adapted from Atlanta: American Cancer Society, 2014) [2]

Cigarette smoking is by far the principal risk factor for development of lung cancer, which causes 80-90% of preventable deaths. Gender differences in lung cancer mortality reflect historical diversity in patterns of smoking uptake and cessation over the past 50 years. Nonsmokers account for 10-15% of lung cancer cases, which are often attributed to a combination of genetic factors, exposure to radon gas, asbestos, toxic chemical entities and air pollution from industry, but also including second-hand smoke [1]. As for many cancers, poor diet appears to be associated with increased disease risk [3].

1.1.2. Lung cancer types

According to the World Health Organization diagnosis and classification based primarily on the light microscopic appearance of the malignant cells, occasionally supplemented by immunohistochemical assays, lung cancer have been broadly divided into non-small cell lung cancer (NSCLC) (comprising 80%) and small cell lung cancer (SCLC) (comprising 20%) [4]. NSCLC originates in lung epithelial cells and comprises diverse histological subtypes mainly including adenocarcinoma, squamous, and large-cell carcinomas [5]. The lung cancer subclasses generally follow a proximal-to-distal linear distribution pattern moving distally from the trachea: squamous cell carcinoma (SCC), SCLC and adenocarcinoma [6]. Thus, it is speculated that these different tumour subtypes generated from distinct cells of origin which are located within a specialized regional compartment/microenvironment. Most patients with advanced NSCLC present with metastatic disease and, if left untreated, have a median survival after diagnosis of 4-5 months and a 1-year survival of less than 10% [7]. SCLC mostly arises centrally in a large bronchus and initially responds well to chemo- and radiotherapy, but frequently recurs with refractory to further treatment.

1.1.2.1. Cellular classification of non-small cell lung cancer

Adenocarcinoma (40% of lung cancer)

Adenocarcinoma driven by oncogenic KRAS mutant form seems to be originated from targeted cells located in the bronchioalveolar duct junction (BADJ), a region where the airways terminate and form alveoli (Figure 2). BADJ which contains a rare cell population, termed as

bronchioalveolar stem cells, exhibits progenitor cell-like features and is found to co-express the Clara cell-specific marker (CC10) and the alveolar-specific marker (surfactant protein C) [8, 9]. Adenocarcinoma is currently the most common histological form of lung cancer in many countries, and also the most common major type of lung cancer seen in female non-smokers [10].

Squamous cell carcinoma (25% of lung cancer)

The histopathology and gene expression profiling patterns of mouse lung SCC-like lesions indicated their high expression of keratin 5/14, and transcription factor p63 that controls adult stem/progenitor cell regulation. Thus these cells were speculated to resemble tracheal basal cell progenitors [11] (Figure 2). SCC are located at the submucosal gland duct junctions or intracartilaginous boundaries [12, 13] and are associated most strongly with a history of tobacco smoking than other histological subtypes [14].

Large cell carcinoma (10% of lung cancer)

Large cell carcinoma represents an exceptionally heterogeneous group of poorly differentiated malignant neoplasms generated from transformed epithelial cells in the lung. This type of lung cancer can occur in any part of the lung and tends to grow and spread quickly. Large cell carcinoma can be histologically discriminated primarily by the large and round shape.

Other subtypes (5% of lung cancer): There are also a few other subtypes of NSCLC, such as carcinoids, carcinosarcomas, pulmonary blastomas, giant and spindle cell carcinomas. They are very rare and will not be explained further.

1.1.2.2. Small cell lung cancer

SCLC mostly localizes to the midlevel bronchioles and can be stained diffusely and strongly with a range of neuroendocrine markers (CK7, CK20, CD56), and transcription factors (thyroid transcription factor-1) which play important roles in neuroendocrine (NE) differentiation (Figure 2). The modern SCLC hypothesis suggests that a rare population of NE cells is the progenitors of

SCLC. In the epithelial lining of the bronchi there are neuroendocrine bodies, which harbor pulmonary neuroendocrine cells (PNECs) that are associated with variant Clara expressing cells (vCEs). Two hypotheses explain the origin of lung NE tumors, neither from PNECs nor from less-differentiated progenitor-like cells (e.g., vCE).

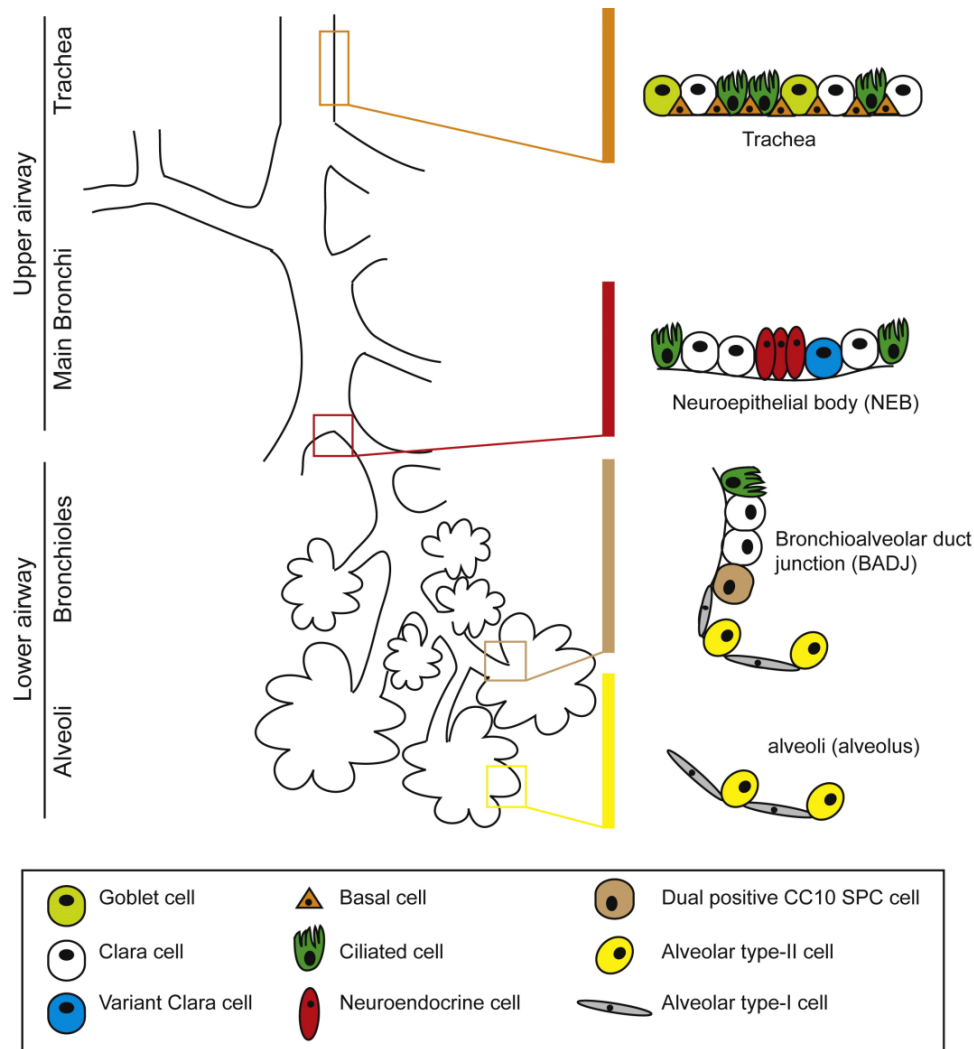


Figure 2. A schematic diagram of the mouse lung highlighting the spatially distinct cellular environments shown to harbor airway stem / progenitor cells. The mouse lung consists of three main levels of conducting airways: the trachea, bronchi and bronchioles. Candidate epithelial niches (depicted on the right hand side) have been identified and found to exist in spatially defined regions: the tracheal submucosal gland ducts, neuroendocrine bodies (NEB) of the bronchi/bronchioles, and the broncholalveolar duct junction (BADJ). (Adapted from Sutherland KD and Berns A, 2010) [15]

1.2. Overview of the epidermal growth factor receptor (EGFR) protein kinase family

1.2.1. EGFR protein kinases

EGFR protein family consists of four structurally related receptor tyrosine kinases (RTKs), ErbB1/HER1/EGFR [16], ErbB2/HER2 [17], ErbB3/HER3 [18, 19], and ErbB4/HER4 [20]. The gene symbol, ErbB, is derived from the name of erythroblastosis leukemia viral oncogene B to which these receptors are homologous [21]. In order to exclude misunderstanding, further EGFR, HER2, HER3 and HER4 will be used. Human receptors of this family exhibit approximately 40-45% sequence identity and are ubiquitously expressed in epithelial, mesenchymal, and neuronal cells and their cellular progenitors [21, 22]. This family members are composed of an extracellular domain (see below), a single hydrophobic transmembrane segment of 19-25 amino acid residues, and an intracellular domain of about 540 amino acid residues that contains (1) a 40-residue juxtamembrane (JM) segment, (2) a 270-residue protein kinase domain, and (3) a 230-residue carboxy terminal tail (Figure 3) [21]. The glycosylated extracellular domain contains four subdomains: subdomains I and III contain numerous leucine segments involved in ligand binding, and subdomains II and IV are cysteine-rich and participate in the formation of disulfide bonds. Subdomain II also contains the dimerization loop required for homo- and heterodimer formation with EGFR family members [21].

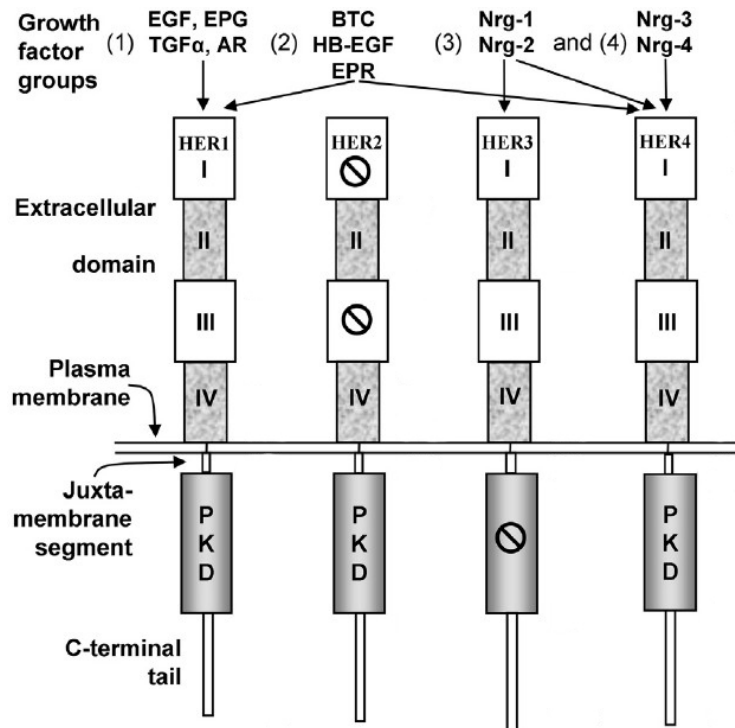


Figure 3. Structure of the human EGFR. Extracellular subdomains I and III participate in ligand binding. Those of ligand-impaired HER2 are marked with the stop symbol \emptyset . The carboxy terminal tail contains several tyrosine residues that can be phosphorylated. The kinase activity of HER3 is defective, where is marked with the stop symbol. The growth factor groups (1-4) that bind to the receptors are indicated. EGF, epidermal growth factor; TGF α , transforming growth factor- α ; AR, amphiregulin; BTC, betacellulin; HB-EGF, heparin-binding EGF-like growth factor; EPR, epiregulin; NRG1/2/3/4, neuregulin1/2/3/4. (Adapted from Roskoski Jr R, 2004) [21]

Like all protein RTKs, the four EGFR family members are able to form 10 homo- and heterodimers. HER2 has no known high-affinity ligand, however, unphysiological overexpression of this receptor can transform cells in a ligand-independent manner [21]. In this respect, amplification of HER2 is found in > 30% of human breast cancers and correlates with aggressive metastatic diseases [23]. HER2 is the favored dimerization partner for all the other EGFR family members [24], and its heterodimer combinations with EGFR or HER3 exhibit robust signaling activity [25]. The theoretical HER3 homodimers would be non-functional as the

kinase-impaired receptor requires transphosphorylation through heterodimerization with other EGFR family members, most notably the ligand binding-impaired HER2 [21]. RTK heterodimer conformation allows HER3 to serve as an efficient phosphotyrosine scaffold, leading to the activation of downstream signaling and triggering cancer progression and resistance.

There are 11 different, but structurally related ligands, each a 6-10 kilodalton (kDa) small soluble protein, that serve as specific agonists for EGFR family receptors (Table 1). Specifically, seven ligands bind to EGFR, none bind to ligand binding-impaired HER2, two bind to kinase-impaired HER3, and seven growth factors bind to HER4. Activation of EGFR family receptors requires proteolysis of the transmembrane precursors to release the diffusible ligands. Members of the ADAM (a disintegrin and metalloprotease) family of metalloproteases are playing the role in executing precursor cleavage. Protein ectodomain shedding involved in cleavage processing and liberation of extracellular fragment function as a post-translational modification that regulates the activity of the growth factor [26].

Table 1. Specificity of EGFR receptors and ligands

Ligand	Receptor			
	EGFR	HER2	HER3	HER4
EGF	+	-	-	-
TGF- α	+	-	-	-
HB-EGF	+	-	-	+
Amphiregulin	+	-	-	-
Betacellulin	+	-	-	+
Epigen	+	-	-	-
Epiregulin	+	-	-	+
Neuregulin-1	-	-	+	+
Neuregulin-2	-	-	+	+
Neuregulin-3	-	-	-	+
Neuregulin-4	-	-	-	+

+ and - signify ability and inability to activate each of the EGFR receptors respectively.

(Adapted from Linggi B and Carpenter G, 2006) [27]

1.2.3. EGFR signaling

Binding of ligand to the extracellular domain induces receptor dimerization and activation of the cytoplasmic kinase, which in turn leads to auto- or transphosphorylation and initiation of downstream signalling events. The EGFR signal is propagated through different intracellular modules and adaptor proteins, involving cross talks to parallel pathways and strong feedback loops on different levels [28]. Tyrosine phosphatases, as the main negative feedback loop, dephosphorylate activated EGFR and *casitas b*-lineage lymphoma (CBL) working as a proto-oncogene E3 ubiquitin protein ligase causes internalization/degradation of RTK/ligand forms. Each receptor pairing of EGFR family allows the signaling complex to activate different combinations of signaling pathways, including the phosphatidylinositide 3-kinase (PI3K)/AKT/phosphatase and *tensin* homologue (PTEN), the Ras/Raf/MEK/ERK, the phospholipase C (PLC γ), Src kinases and signal transducer and activator of transcription (STAT) pathways within untransformed and cancer cells [28]. These and other EGFR signaling modules mediate cell adhesion, proliferation, motility, angiogenesis and organogenesis [29].

HER3, an important heterodimer partner, launches critical surviving signaling cascade in cancers, with a special emphasis on EGFR-mutant lung cancer and HER2-amplified breast cancer. HER3 receptor possesses six potential PI3K binding sites in its cytoplasmic tail and is therefore the preferred dimerization partner when specific apoptosis signaling occurs via the PI3K/AKT pathway. The regulatory subunit (p85) of PI3K binds to docking sites of phosphotyrosines in HER3 that leads to a strong activation of PI3K [30]. The activated enzyme catalyzes the phosphorylation of cell membrane-bound phosphatidylinositol 4, 5-bisphosphate (PIP₂) to form phosphatidylinositol 3, 4, 5-trisphosphate (PIP₃), which attracts the protein-serine/threonine kinase AKT, known as protein kinase B (PKB), to bind to with high affinity (Figure 4) [31]. PTEN, a tumor suppressor protein, catalyzes the hydrolysis of PIP₃ to form PIP₂ and inorganic phosphate; its activation negatively regulates the AKT/PKB pathway. In lung cancer, this pathway is overactive, thus reducing apoptosis and consequently allowing cell division and increasing cell survival. However, unlike HER2 partnering with HER3, EGFR is able to directly signal PI3K via GAB1, suggesting that EGFR mutant cancer can adapt and activate PI3K/AKT

pathway in the absence of HER3 function [32]. Mutant form of EGFR often activates PI3K via HER3 and propagates HER3 signaling in order to promote resistance to EGFR inhibitors [33].

The mitogen-activated protein kinases (MAPKs) regulate diverse cellular functions, including cell proliferation, differentiation, cell survival and apoptosis [34]. The best-known MAPKs include the extracellular signal-regulated kinases 1 and 2 (ERK1/2), the c-Jun N-terminal kinases (JNK) and p38 subfamilies, which relay various stress signals, like membrane damage, oxidative stress, and heat shock. The binding of adaptor protein growth factor receptor-binding protein (Grb2) or Src homology 2 domain containing (Shc) to phosphotyrosines in the EGFR family leads to the formation and activation of the Ras/Raf/MEK/ERK1/2 signaling modules (Figure 4) [35]. In this pathway, Grb2 associates with several phosphotyrosine residues in EGFR, HER2/3/4 via SH2 domain and binds to son of sevenless (SOS) through its SH3 domain [36]. Kinase activity of RKT forms binding site to recruit Grb2-SOS complex to the plasma membrane. In this case, SOS functions as a GTP exchange protein, once binds to cell membrane can activate the proto-oncogene product P21 H-Ras and K-Ras, which stimulate a series of serine/threonine protein kinases. Upon activation, mitogen activated protein kinase-MAPK (ERK) can translocate into the nucleus and activate gene transcription machinery.

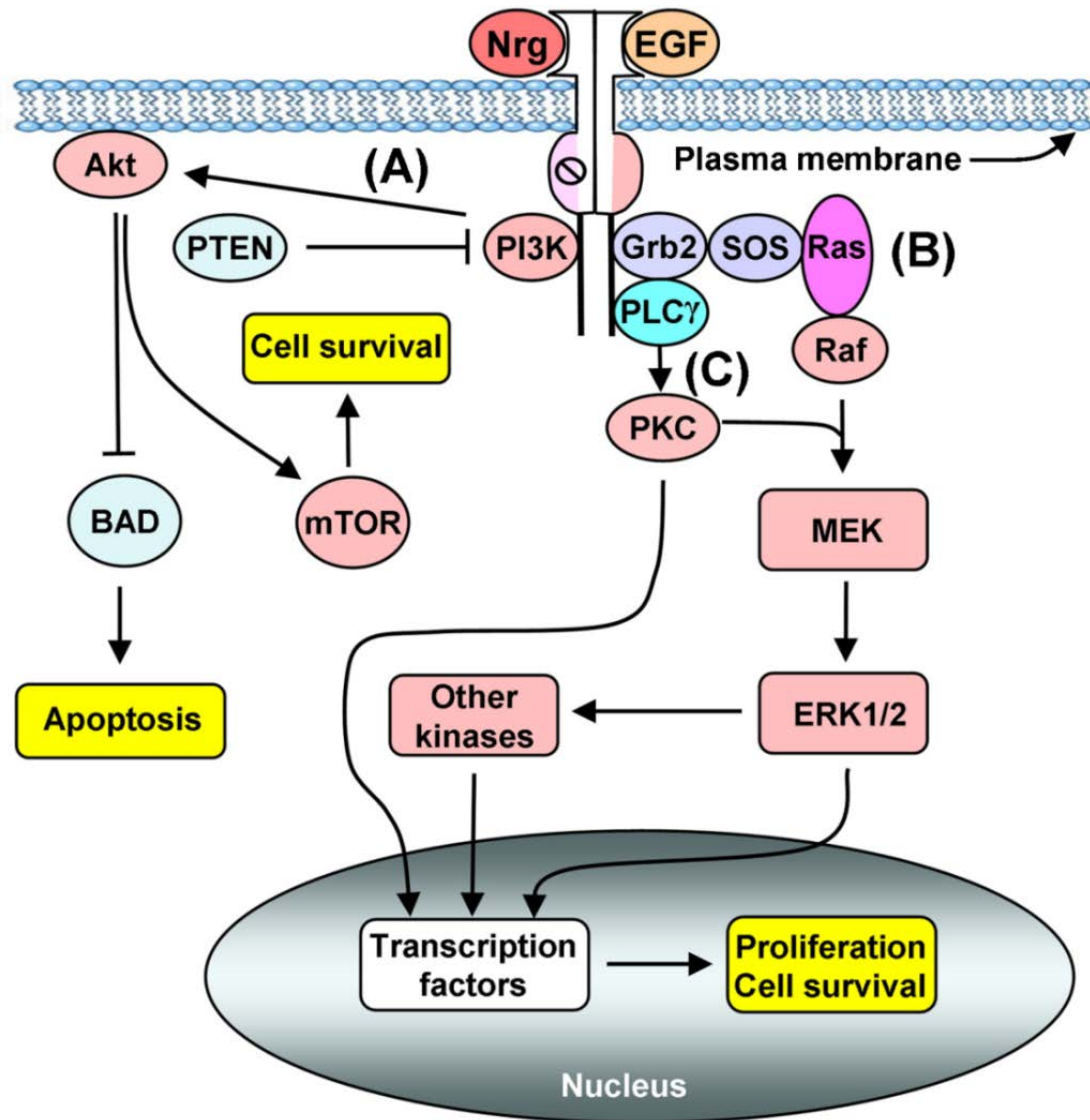


Figure 4. Overview of EGFR family signaling. The main downstream signaling modules include (A) PI3K, (B) Ras/Raf/MEK/ERK1/2, and (C) PLC γ . PI3K, PLC γ , and Grb2 bind to phosphotyrosines in the carboxy terminal tail of the receptors to initiate the signaling process. The PI3K regulatory subunit binds to kinase-impaired HER3, which is denoted by a stop symbol. (Adapted from Roskoski Jr R, 2004) [21]

1.2.4. EGFR mutation in NSCLC

The EGF receptor is highly expressed on the cell surface of > 60% of NSCLC, and notably, the majority of the cases are correlated with a poor prognosis [37]. In a large unselected series of NSCLC samples, EGFR mutations exist in around 10% of cases in Western Europe and North America, but in a higher proportion 30-50% of cases in East Asian-descent individuals, and over half are related with adenocarcinomas with bronchioloalveolar features that occur frequently among non-smokers [37].

As indicated in Figure 5, the most prevalent EGFR kinase domain mutations, representing approximately 45% of EGFR mutations in lung tumors, are in-frame deletions of exon 19, nested around the LREA string of amino-acids located between residues 747-750 of the EGFR polypeptide. Another sensitive and recurrent mutation is the L858R substitution in exon 21, within the activation loop of EGFR, which accounts for a bit less with 40-45% of EGFR mutations. Nucleotide substitutions in exon 18 (e.g., G719C or G719S) have been detected and comprise another 5% of EGFR mutations. All these “classic” EGFR mutations result in enhanced EGFR signaling and are associated with *in vitro* and *in vivo* dramatic and lasting response to EGFR-TKIs Gefitinib and Erlotinib, which were designed to competitively bind to the adenosine triphosphate (ATP)-binding site of the enzyme. Variants that exhibit certain mutations in the EGFR gene constantly drive uncontrolled cell division, in addition to predicting a positive responsiveness for EGFR-TKIs; it also highlighted the crucial importance of targeted therapy for a subset of NSCLC. The most noteworthy, occur relatively rare with < 10% of cases, of which T790M substitution can either be linked to primary resistant to abrogate the inhibitory activity of TKIs, or might be presented as the secondary mutation bypassing the continued requirement for the original target. In general, most instances are associated with acquired resistance [38]. Recently, D761Y, a T790M-like secondary mutation in exon 19 of EGFR, which co-exist with the L858R-EGFR point mutation was also reported to be associated with refractory to Gefitinib and Erlotinib in NSCLC cells [39].

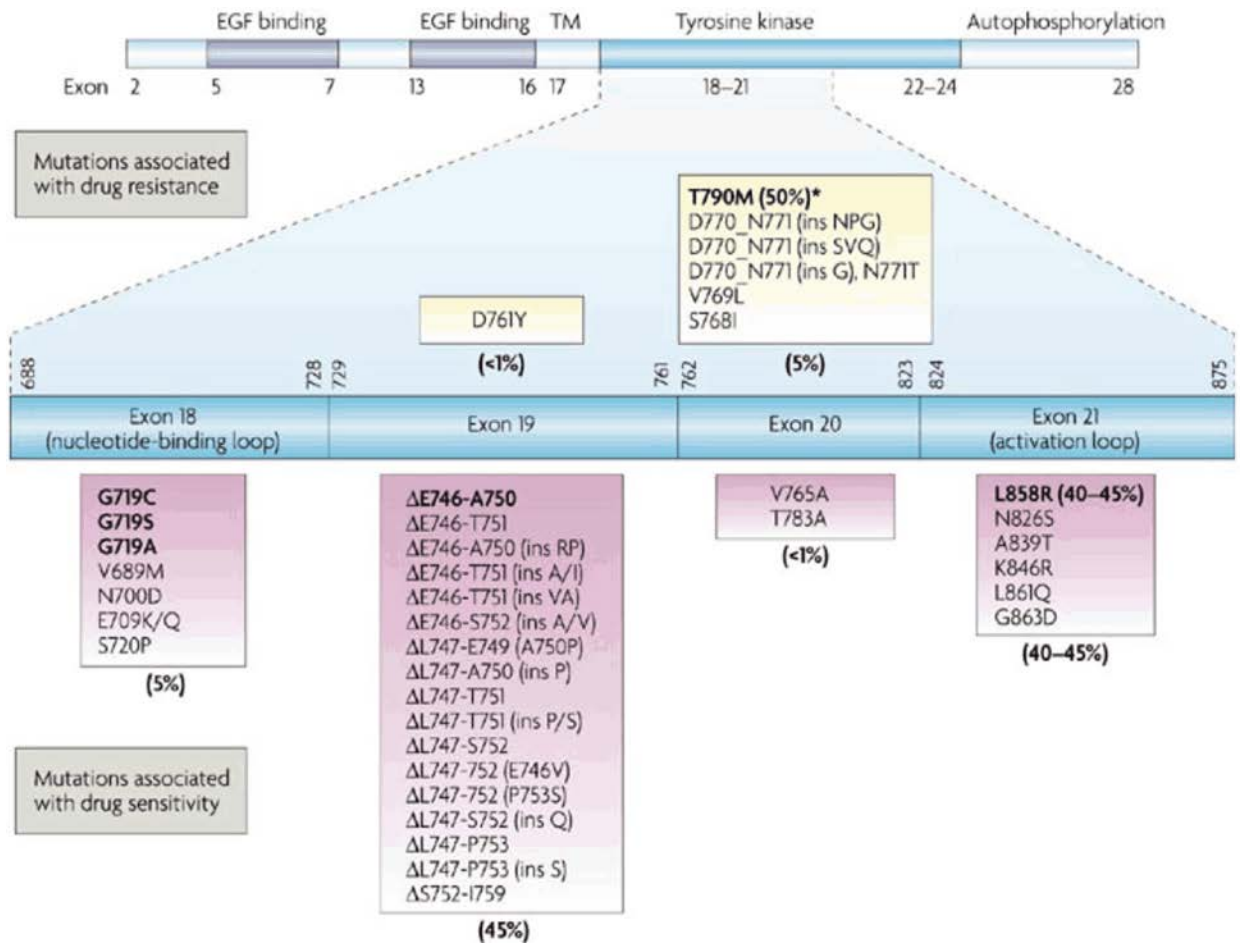


Figure 5. Gefitinib- and Erlotinib-sensitizing mutations of EGFR in NSCLC. A cartoon representation of EGFR showing the distribution of exons in the extracellular domain (EGF binding), transmembrane domain (TM) and intracellular domain (comprising the tyrosine kinase and autophosphorylation regions). Magenta boxes contain a detailed list of EGFR mutations in 18-21 exons that are associated with sensitivity to Gefitinib or Erlotinib. (Adapted from Sharma SV et al., 2007) [40]

1.3. Regular treatment options

Life-saving therapies for lung cancer have advanced dramatically in the past two decades, driving long-term outcomes for many patients. Various treatment options are available in the clinic for patients with lung cancer. They may be applied alone, but most often they are applied in a combination of different types. A choice of strategy is strongly based on the type and the stage of

cancer. In addition, the factors like age, physiological condition of patients will also be taken into consideration. Treatment options for lung cancer can be characterized as follows.

1.3.1. Local treatment options

1.3.1.1. Surgery

Surgery is the most common and effective treatment for early-stage NSCLC when cancer cells have not spread out of the local region and metastasized to lymph nodes. Since SCLC tends to spread to distant parts of the body when it is diagnosed, surgery was not recommended except if it is found at an early stage and with a small tumor size. The type of surgery depends on many factors, such as the size of the cancer, its location within the lung, general state of health and lung functions.

1.3.1.2. Radiotherapy

Radiation therapy works by damaging the DNA of cancerous cells to induce cell death. Radiotherapy operating at early-stage lung cancer is aimed to eliminate cancer cells. For NSCLC, radiotherapy is often used for cancers that grow right at the top of the lung, where tumors can be very close to the nerves that supply the arm and are difficult to operate on. Meanwhile, radiotherapy was suggested after or alongside chemotherapy as part of adjuvant therapy for early stage SCLC, as it can help prevent lung cancer recurrence.

1.3.2. Systemic treatment options

1.3.2.1 Chemotherapy for lung cancer

Chemotherapy is the main treatment for SCLC, as its operation can help control overt disseminated disease. The growth of lung cancer, for example, may spread to adjacent lymph nodes and metastasize to the brain. Chemotherapeutic drugs circulate in the bloodstream around the body to effectively treat cells that have broken away from the lung tumour and spread to

other parts of the body even if they are too small to be seen on a scan. Their side effects are typically related to the inhibition of normal cell proliferation, with a narrow window of selectivity for cancer cells.

Combination of different chemotherapeutic drugs, including either Cisplatin or Carboplatin, was used to either improve the results, lessen the side effects, or both. For instance, EP-Cisplatin plus Etoposide, Carboplatin plus Etoposide, Gemcitabine plus Carboplatin (GemCarbo), Caclphosphamide, Doxorubicin plus Vincristine (CAV), CAV plus Etoposide (CAVE), Doxorubicin, Cyclophosphamide plus Etoposide (ACE) (Table 2).

Table 2. Mechanism of action of selected cytotoxic compounds used in cancer therapy

Cytotoxic agents	Mechanism of action	Acute toxicity	Delayed toxicity
5-Fluorouracil	An anti-metabolite that inhibits thymidylate synthase, DNA synthesis and function, and RNA function	Nausea, diarrhea	Myelosuppression, hand-foot syndrome, neurotoxicity
Cisplatin	A first-generation platinum-based drug that binds to and cross-links DNA, which inhibits DNA synthesis and function	Severe nausea and vomiting	Myelosuppression, nephrotoxicity, peripheral
Carboplatin	A second-generation platinum-based drug whose mechanism of action is the same as Cisplatin	Nausea and vomiting	Myelosuppression, nephrotoxicity, peripheral neuropathy
Doxorubicin	An anthracycline antibiotic that intercalates with DNA, inhibits the progression of topoisomerase II, and produces oxygen-dependent single and double stranded DNA breaks with subsequent inhibition of DNA function	Nausea and vomiting, cardiotoxicity, vesicant	Myelosuppression, cardiotoxicity, alopecia
Etoposide	DNA topoisomerase II inhibitor that causes DNA strand breakage	Nausea and vomiting	Myelosuppression, alopecia

Gemcitabine	A nucleoside analog that inhibits DNA synthesis, repair, and function, ribonucleotide reductase, and RNA function	Nausea, rash, flu-like symptoms	Myelosuppression, edema
Paclitaxel	An anti-mitotic taxane that binds to and enhances polymerization of microtubules and inhibits their function	Nausea and vomiting, hypersensitivity reaction	Myelosuppression, peripheral neuropathy, alopecia

(Adapted from Roskoski Jr R, 2004) [21]

1.3.2.2. Targeted therapy for lung cancer

Targeted agents were designed selectively to modulate the activity of proteins essential for uncontrolled cell growth or to target specific molecular pathways responsible for maintenance and development of cancer (Table 3). Because of this relative selectivity, targeted therapy usually causes fewer toxic effects on normal cells and less side effect for cancer patients as well. The main classes and agents that are now being used in lung cancer treatment include:

Inhibitors of EGFR: Afatinib (Gilotrif®), Erlotinib (Tarceva®), Gefitinib (Iressa®); monoclonal antibody Centuximab (Erbitux®)

Treatment with an EGFR kinase inhibitor in EGFR mutant NSCLC patients leads to a superior overall response rate, a prolonged progression-free survival and an improved quality of life compared to cytotoxic chemotherapy.

Inhibitors of vascular endothelial growth factor (VEGF): monoclonal antibody Bevacizumab (Avastin®)

Tumor-angiogenesis plays a crucial role in tumor growth, propagation and metastasis formation. Among several angiogenic activators, the VEGF and its receptors represent one of the major inducers of tumor angiogenesis.

Inhibitor of EML4-ALK: Crizotinib

The anaplastic lymphoma kinase (ALK) rearrangements define a unique molecular subset of NSCLC, and 4-6% of all NSCLC cases contain an EML4 (echinoderm microtubule-associated protein-like 4)-ALK translocation [41]. This abnormal gene fusion, in many cases, promotes and maintains the malignant behavior of the cancer cells [42]. ALK inhibitors lead to apoptosis *in vitro* and tumor shrinkage *in vivo*, thus demonstrating the phenomenon of “oncogene addiction”.

Table 3. FDA-approved TKIs and antibodies for treatment of NSCLC patients or for combinatorial application in clinical trials

Drugs	Company	Target (year approved)	Indications
Small molecule inhibitors			
Afatinib/ Gilotrif®	Boehringer Ingelheim	EGFR (2013)	First-line treatment of NSCLC with exon 19 deletions or the exon 21 L858R mutation.
Erlotinib/ Tarceva®	Genentech/OSI	EGFR (2004)	First-line treatment of NSCLC with exon-19 deletions or the exon 21 L858R mutation or second-line treatment following cytotoxic therapy and first-line treatment of pancreatic cancer in combination with gemcitabine.
Gefitinib/ Iressa®	AstraZeneca	EGFR (2003)	Second-line treatment of NSCLC after cytotoxic therapies. Approved in dozens of countries worldwide, but approval was withdrawn in the United States.
Lapatinib/ Tykerb®	GlaxoSmithKline	EGFR/HER2 (2007)	Second-line treatment of patients with Capecitabine for HER2-positive breast cancer who have previously received cytotoxic chemotherapy or trastuzumab and with letrozole in post-menopausal hormone receptor-positive breast cancer.

Sunitinib	Pfizer	PDGFRs, vEGFR, KIT (2006)	Treatment of renal cell carcinoma and Imatinib-resistant gastrointestinal stromal tumor
Dasatinib	Bristol-Myers Squibb	BCR/Abl, Src, c-Kit, ephrin receptors (2006)	First line use in patients with chronic myelogenous leukemia and Philadelphia chromosome-positive acute lymphoblastic leukemia.
Bosutinib/ SKI-606	Wyeth- Pfizer	BCR/Abl, Src (2012)	Adult patients with Philadelphia chromosome-positive chronic myelogenous leukemia with resistance, or intolerance to prior therapy
Monoclonal antibodies			
Cetuximab/ Erbix®	ImClone/ Eli Lilly/ Bristol-Myers Squibb	EGFR (2004)	Wild-type KRAS colorectal cancer in combination with cytotoxic therapies and head and neck cancers in combination with radiation therapy or cytotoxic chemotherapy.
Panitumumab/ Vectibix®	Genentech	EGFR (2006)	Second-line treatment for metastatic colorectal cancer following cytotoxic therapies. It is not indicated for KRAS-positive mutations or mutation status unknown.

(Adapted from: Roskoski Jr R, 2004.) [21]

1.4. Mechanisms of acquired drug resistance

In many, if not all instances, cancer patients who initially respond to medication eventually develop resistance, resulting in tumour recurrence. The inevitable development of chemoresistance is a persistent problem during the treatment of local and disseminated disease, and greatly limits the ability of therapeutic drugs to significantly prolong patient survival. Thereafter, a better understanding of the molecular and cellular mechanisms is crucial as it provides important clues for better addressing cancer therapy.

Two current ideas that attempt to describe the establishment and maintenance of tumor initiation and heterogeneity are the clonal evolution model and the cancer stem cell (CSC) hypothesis.

1.4.1. Clonal evolution model

According to clonal evolution model, genetic drift and stepwise natural selection allow the best suitable genotypes to survive and re-establish the tumor.

1.4.1.1 Primary resistance

Various EGFR mutation status partially explain differential TKI sensitivities. ``Classic`` EGFR mutations, involving exon 19 deletions and exon 21 L858R substitution, are associated with marked sensitivity to TKIs [43]. Conversely, Exon 20 insertions or duplications, which represent ~5% of EGFR mutations, are resistant to EGFR inhibitors. Additionally, in lung cancer EML4-ALK fusion variants and ALK fusion partners to some extent account for heterogeneous Crizotinib responses [44]. Besides, intrinsic resistance to EGFR TKIs may also be due to secondary genetic alterations that co-occur with sensitizing EGFR mutations. For instance, T790M gatekeeper mutation and MET amplification have been reported in EGFR-mutant tumors before TKI exposure [45].

1.4.1.2 Acquired resistance

Development of additional genetic alterations in the primary oncogene, which commonly arise through additional secondary mutations or through gene amplification of the kinase target (Table 4), facilitates continued downstream signaling. Alternatively, resistance can occur independent of genetic changes. This emerges through activation of signal transduction pathways, alterations in tumor histology, or drug targets associated specific metabolic changes [43, 46, 47]

Table 4. Major mechanisms of acquired resistance identified in clinical specimens

Mechanism	Estimated Frequency (%)	References
EGFR TKI resistance		
Genetic alterations in EGFR		
T790M mutations	50	[38]
D761Y, T854A, and L747S mutations	< 5	[39, 48]
EGFR amplification	8	[49]
Bypass signaling tracts		
MET amplification	5-22	[50]
AXL activation	×	[51, 52]
HER2 amplification	12	[53]
PIK3CA mutations	5	[49]
PTEN mutations	4-8	[54]
BRAF mutations	1	[55]
CRKL amplification	9	[56]
HGF overexpression	1 of 2 cases	[57]
Phenotypic alterations		
Transformation to SCLC	3-14	[49]
ALK TKI resistance		
Genetic alterations in ALK		
ALK secondary mutations (e.g., L1196M)	22-36	[41, 42]
ALK gene amplification	7-18	[58]
Bypass signaling tracts		
EGFR activation	44	[44]
KIT gene amplification	15	[44]

HGF, hepatocyte growth factor; CRKL, v-CRKL avian sarcoma virus CT10-homolog-like; ×, not evaluated.

(Modified from Gainor JF and Shaw AT, 2013) [59]

1.4.2. Cancer stem cell model

The remarkable ability of NSCLC to recur despite favorable responses to initial local and/or systemic therapy suggests that a small fraction with enormous capacity for self-renewal and regeneration exist in minimal residual disease, termed ‘‘cancer stem cells (CSCs)’’, these cells are believed to be a phenotypically distinct population that exhibits a generalized resistance and possesses tumor initiation. As illustrated in Figure 6, CSC gave rise to highly proliferative progenitors or transiently amplifying cells comprising the bulk of tumor mass, and ultimately defined the histological type of the cancer. First-line chemotherapeutic drugs, TKIs and biologic agents that target cell proliferation are more effective against proliferating over dormant CSCs. Consequently, quiescent, slow-cycling cells at diffusion distances from tumor blood vessels are likely to exhibit relatively resistant to therapy. As such, a number of mechanisms of chemoresistance in CSCs are summarized in Figure 7.

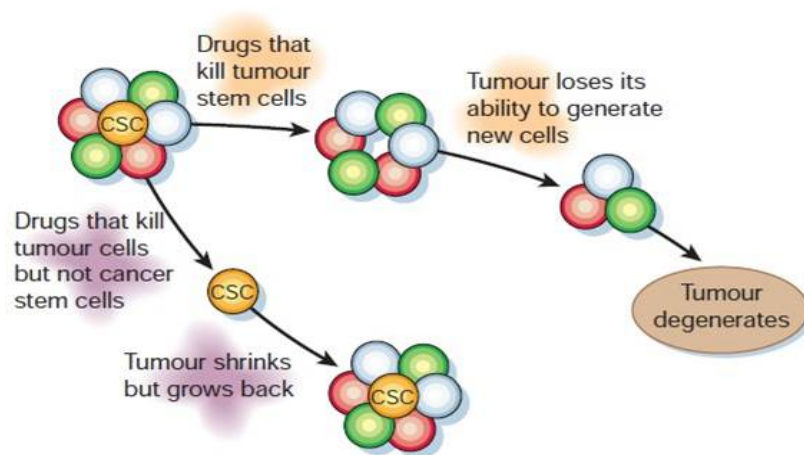


Figure 6. CSC involved in drug resistance. The CSC model states that a distinct subpopulation of tumor cells with stem cell-like properties is responsible for resistance, metastasis and relapse. Tumor heterogeneity and hierarchy are generated by aberrant downstream differentiation of one single CSC. (Adapted from Tannishtha Reya et al., 2001) [60]

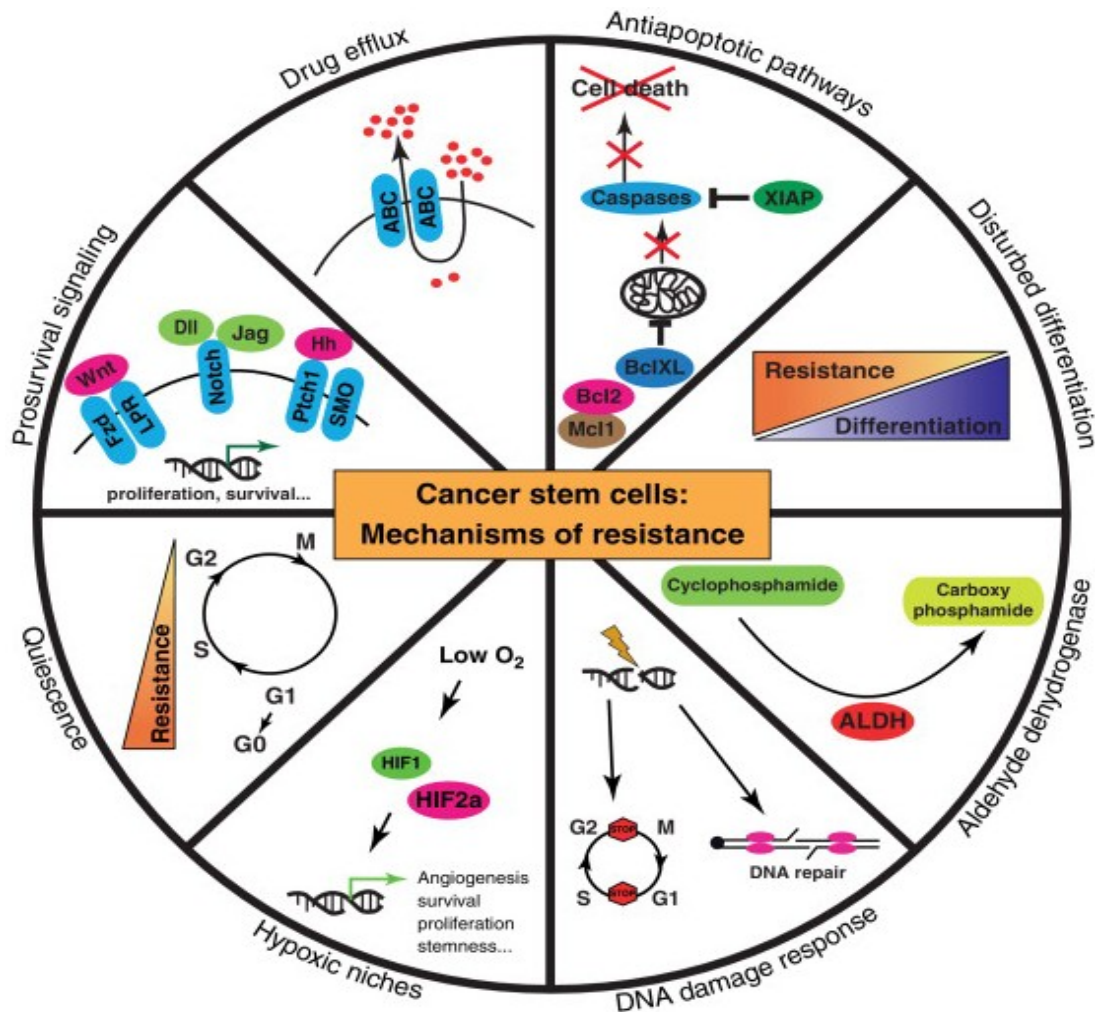


Figure 7. The possible mechanisms of tumor drug resistance of CSCs. (Adapted from Sotiropoulou PA et al., 2014.) [61]

1.4.2.1. Quiescence

Conventional chemo- and radiotherapy selectively target rapidly proliferating cells, potentially leaving a subpopulation with slow-cycling. Infrequent division or a quiescent nature of CSCs appears to be necessary for preserving self-renewal and accumulating mutations, which may provide added resistance to offspring to protect tumors from later rounds of treatment. CSCs often hijack stem cell resistance mechanisms by acquiring mutations that overactivate other signaling pathways or bypass track signaling emanating from specific kinases. Over a period of time and due to stimuli release of cytokines, growth factors, heat-shock proteins and hypoxia

induced factors that are associated with tumour cell death, these dormant stem cells are induced to re-enter the cell cycle and to produce progenitor cells that can re-establish the tumor. In vitro and in vivo experimental evidence has shown that several types of tumor, including brain, pancreas and glioblastoma, contain a slower cycling transient population, which has often been correlated with drug resistance [62-64]. Chen and colleagues using a transgenic mouse model of glioma identified a labeled relatively quiescent subpopulation survived temozolomide treatment. More importantly, after elimination of those cells, tumor growth was arrested in parallel with mouse survival prolongation [64]. Reduced cycling may help maintain the stem cell pool, limit cell damage, decrease prodeath signals and increase the potential for CSC survival. Additional time in S or G2 phase of the cell cycle couples with increased DNA repair protein activity may afford a survival advantage over bulk cells that continuously accrue DNA damage and ultimately are forced to undergo apoptosis. Given that quiescence emerges as a critical factor of CSC resistance to therapy, novel drugs targeting slow-cycling cells or stimuli factors inducing CSC proliferation and differentiation in aggressive cells creating metastasis could have proven efficient therapeutic regimens.

1.4.2.2. Active DNA-repair capacity

Different external and internal agents associated with genotoxic stress lead to DNA-damage generation, which can trigger a complex network of mechanisms to repair the cell injuries or to avoid its cell cycle progression. Activation of highly conserved DNA-damage-response (DDR) signaling pathways is critical to prevent the development of diseases associated with genomic instability [65]. CSCs have been shown to have enhanced DDR activation as a mechanism to effectively repair DNA damage and enhance chemoresistance [66]. In a pioneer study, Bao and colleagues demonstrated that a fraction of tumor cells expressing CD133 contributed to glioma radio-resistance through activation of the DNA damage checkpoint response and an increase in DNA repair capacity. In addition, the radio-resistance can be reversed using checkpoint kinase 1 (CHK1) and checkpoint kinase 2 (CHK2) inhibitors [67]. Under hypoxic conditions, following the initial response to DNA damage, two major signaling pathways - Ataxia telangiectasia mutated (ATM) and ATM and Rad-3-related (ATR) are activated, which can subsequently regulate cell cycle by phosphorylating downstream kinases CHK2 and CHK1, respectively. The

enhanced DDR and checkpoint activation offer a delay in the cell cycle progression, providing more time and effective repair to damaged DNA [68]. The maintenance of genomic stability and integrity is indispensable for cancer cell survival and for the inheritance of traits to offspring to benefit cancer progression [69].

1.4.2.3. Resistance to apoptosis

Compared to differentiated cells, stem cells naturally express elevated levels of death preventive proteins, such as members of the BCL-2 family and inhibitors of apoptosis. The BCL-2 protein family members which regulate the permeabilization of the outer mitochondrial membrane are very important in regulation of coordination and balance between cell survival and apoptosis. The apoptotic response to chemotherapy is regulated by the crosstalk of proteins that function in controlling cell survival (such as BCL-2, MCL1 and BCL-XL) and apoptosis (such as BAD, BAX and BAK). Considering the integral effect of BCL-2 family members on cancer cell survival and tumor development, there have been extensive efforts to study their connection with CSCs. High expression levels of anti-apoptotic molecules, conferring resistance to therapy, have been demonstrated for limited number of primary tumors and cell lines [70, 71]. Currently the function of CD133⁺ (prominin 1) is unknown, however, it's detected to highly express in hematopoietic stem cells, endothelial progenitor cells, glioblastoma, neuronal, glial stem cells [72-74]. In glioblastoma a subpopulation of CD133⁺ cells from primary cell lines overexpress anti-apoptotic genes BCL-2, BCL-XL, XIAP and FLIP in comparison with the CD133⁻ cancer cells [75], and BCL-2 suppression sensitized CSC-like cells lines to TNF-related apoptosis-inducing ligand (TRAIL) treatment *in vitro* and in xenograft models. TRAIL is working to induced cell death via methylation of the caspase-8 promoter to inhibit caspase-8 expression. In colon cancer, Interleukin-4 (IL-4) protects CD133⁺ cells from chemotherapy through the upregulation of c-FLIP, BCL-XL, and PED anti-apoptotic proteins. Consistently, treatment with IL-4 neutralizing antibody strongly enhanced the antitumor efficacy of oxaliplatin and 5-fluorouracil through selective sensitization of this 2% of tumor cells [76]. Studies also indicated that prostate CSCs from primary cell lines can be sensitized to apoptosis through pharmacological inhibition of BCL-2, survivin and XIAP [77, 78]. Chemotherapeutic-induced cell death is generally programmed by apoptosis; therefore, targeting the apoptotic pathway

could be an important therapeutical option in clinic. The increased ratio of pro-apoptotic to anti-apoptotic proteins in signal pathways via targeting at anti-apoptotic members of the BCL-2 family could lead to elimination of CSCs and prevent tumor recurrence.

1.4.2.4. Increased drug efflux

A wide variety of chemotherapeutic drugs are extruded from cells by ATP-binding cassette (ABC) transporters, resulting in multidrug resistance which is a major obstacle in the success of cancer treatment and better outcome in cancer patients [79]. In clinical practice, traditional chemotherapy can kill most cells within a solid tumor, however, a small fraction of cells (CSCs) are drug resistant and finally drive tumour recurrence. One important characteristic of CSCs that can be distinguished from other normal cells in the tumour is their high expression levels of ABC transporters known to protect cells from drug damage via efflux pumping mechanisms (Table 5). 48 ABC transporters are classified into seven families by the Human Genome Organization. P-glycoprotein also named multidrug resistance protein 1 (MDR1) or ATP-binding cassette sub-family B member 1 (ABCB1), is the most extensively-studied ABCB family member and confers efficient removal of drug compounds. ATP-binding cassette sub-family G member 2 (ABCG2), alternatively referred to as breast cancer resistance protein (BCRP), is controlling resistance to most of Topoisomerase I or II inhibitors such as Doxorubicin. Today it is unclear exactly how these proteins can transport such a wide variety of drugs out of cells, several observations support the hydrophobic vacuum cleaner model which states that, P-glycoprotein works as an ATP-activated efflux pump to activate a lateral drug-vacuum system that exists in the multi-drug resistance cell [80].

Cancer cells detected by enhanced efflux of Hoechst 33342 through ABC transporters are known as the "side population (SP)" and can be isolated by flow cytometry. Hoechst efflux assay was originally documented to isolate murine hematopoietic stem cells [81]. Subsequently, SP analysis has been successfully applied to identify a subpopulation of CSC-like cells in a variety of solid tumors, including lung, ovarian, gastrointestinal and breast [82-84].

Table 5. ABC transporters involved in drug resistance

Gene	Protein/alias	Chemotherapeutic drugs effluxed by transporter
ABCA2	ABCA2	Estramustine
ABCB1	PGP/MDR1	Colchicine, Doxorubicin, Etoposide, Vinblastine, Paclitaxel
ABCC1	MRP1	Doxorubicin, Daunorubicin, Vincristine, Etoposide, Colchicine, Camptothecins, Methotrexate
ABCC2	MRP2	Vinblastine, Cisplatin, Doxorubicin, Methotrexate
ABCC3	MRP3	Methotrexate, Etoposide
ABCC4	MRP4	6-mercaptopurine, 6-thioguanine and Metabolites; Methotrexate
ABCC5	MRP5	6-mercaptopurine, 6-thioguanine and Metabolites
ABCC6	MRP6	Etoposide
ABCC11	MRP8	5-flurouracil
ABCG2	MXR/BCRP	Mitoxantrone, Topotecan, Doxorubicin, Daunorubicin, Irinotecan, Imatinib, Methotrexate

(Adapted from Dean M et al., 2005) [85]

1.4.2.5. Aldehyde dehydrogenase

Currently, 19 aldehyde dehydrogenase (ALDH) enzymes have been identified within the human genome. The most widely studied ALDH1 functions as a cytosolic enzyme responsible for catalyzing the oxidation to a variety of intracellular aldehydes [86]. ALDH enzymatic activity safeguards the cell against cytotoxic drugs, and ALDH-mediated oxidation of aldophosphamide to carboxyphosphamide represents the critical mechanism of the therapeutic drug cyclophosphamide detoxification [86]. Increased ALDH1 expression has been reported in normal stem cell clones and CSC isolated from leukemia and various solid tumors, such as head and neck, breast, prostate, pancreas cancer [87-89]. ALDH activity may thus been successfully employed as a common marker for stem and progenitor cells in normal and malignant tissues. Using tissue microarrays and immunostaining, it has been shown that high expression of this stem/ progenitor cell marker in human breast and prostate tumors is a powerful predictor of poor clinical outcome [86]. Indeed, Dylla et al. took xenograft models of colorectal tumors and identified that ALDH1 activity is a major mediator of resistance to classical chemotherapeutic

agent cyclophosphamide treatment. Noteworthy, knocking down with ALDH1-targeted shRNA restored the sensitivity of tumors to cyclophosphamide in vivo [90]. Given that ALDH1 is crucial for both normal stem cell and CSC function, the development of specific ALDH inhibitors would mediate CSC sensitization to therapy and facilitate the clinical application of stem cell concepts.

1.4.2.6. Tumor Microenvironment

Paralleled to normal stem cells, CSCs preferentially reside and maintain their stemness in a physiologically limited and specialized microenvironment called the "niche". CSCs interact with microenvironmental niches, which are likely to be well endowed with a blood supply, support their growth and regulate their fate. Maintaining a balance between self-renewal and differentiation is the key for the homeostatic regulation of stem cells, which can be controlled by direct interaction with surrounding cells or in an indirect paracrine manner. CSCs in different tissues differ in their niches. Several types of cancer have been investigated to define the constitution and function of the niches, including the intestinal epithelium, hematopoietic bone marrow, epidermis, and brain [91-93]. The niches for other solid tumors are still not well identified, however, it has also been hypothesized that niches for hematopoietic, liver and lung can be "hijacked" by the CSCs for invasion and metastasis [94].

Once receiving the extrinsic factors (such as cytokines, epigenetic factors and stress) released from the niche, CSCs exit from quiescence, undergo an epithelial-mesenchymal transition (EMT) and generate metastatic progenitor cells into the blood vessels to start secondary lesions in the same or other organs (Figure 8). Survival of disseminated non-CSCs, also known as transit-amplifying progenitors and differentiated cells, at distant sites is a limiting step, as the vast majority of infiltrating cancer cells die from the host defense. More frequently, some survivors endowed with invasive capability quickly convert into epithelial like cells (CSCs) through the processes of phenotypic plasticity, and coopt a supportive niche for thriving in the new environment. This explained why post-treatment mainly targeting metastasis mesenchymal cells failed to eradicate the cancer, because CSCs frequently active from the dormant state and regenerate the cell pool after each drug treatment cycle.

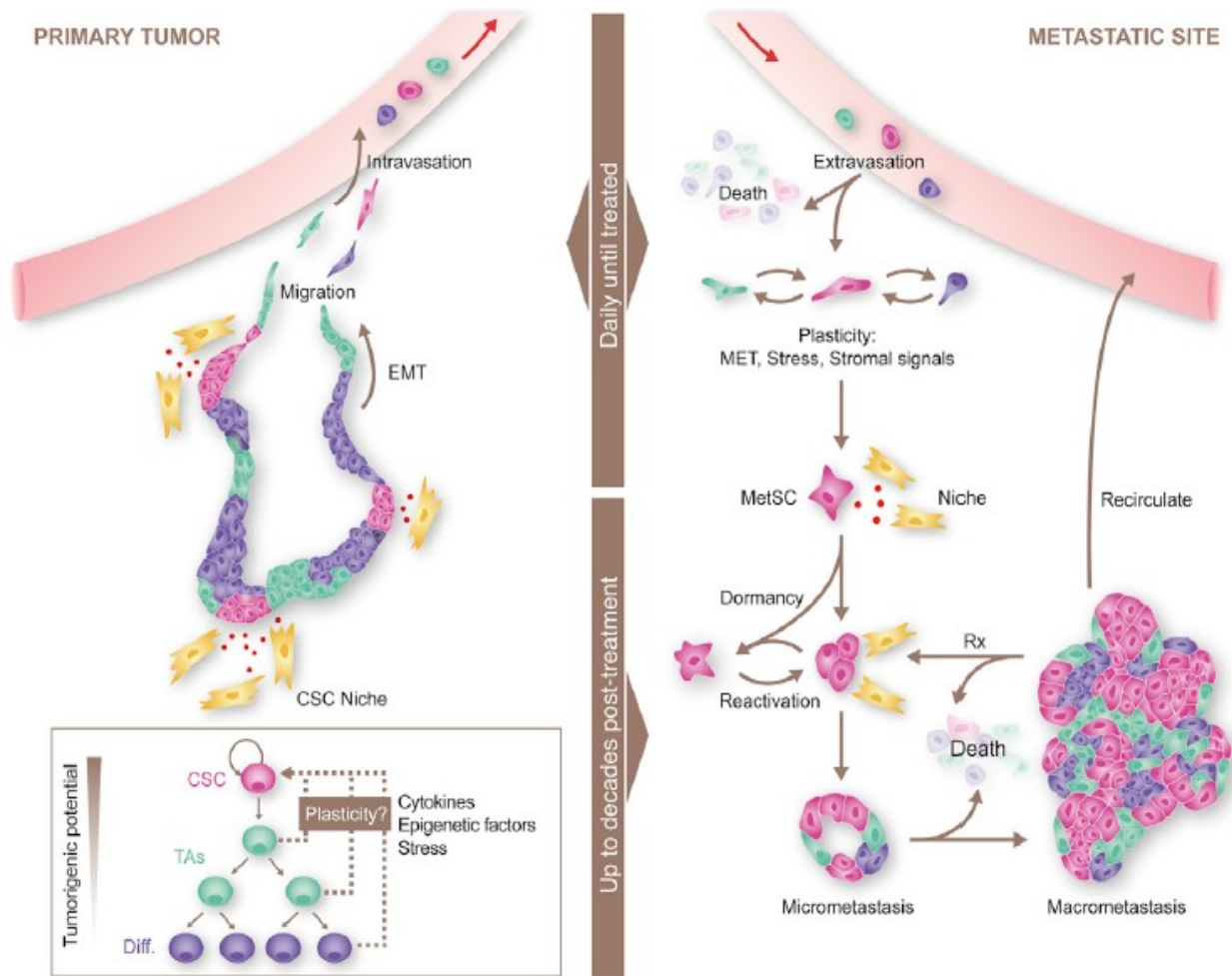


Figure 8. Interactions between tumor cells and their microenvironment are critical at all stages of tumor development and metastasis. (Adapted from Oskarsson T et al., 2014) [95]

1.4.2.7. Pro-survival signaling

Similar to their normal counterparts, CSCs rely upon developmental signaling pathways, which induced by intrinsic and extrinsic developmental cues contribute to the regulation of stem cell/progenitor cell self-renewal and differentiation. Drug treatment triggered a multifactorial signaling, with an activation of pro-survival signaling acting as an adaptive response to therapy for CSCs. Several signaling pathways associated with cell survival, are preferentially activated in CSCs. The elucidation of pathways that regulate these cells led to the identification of potential therapeutic targets (see above).

Emerging data from many human tumors have suggested the role of Wnt/ β -catenin signaling pathway in regulating both self-renewal of CSCs and oncogenesis [96], and its high expression in bone marrow suggests the role in regulating haematopoietic stem cells [96].

The strongest evidence to data for the role of Hedgehog (Hh) signaling in CSC is in glioblastoma [97], chronic myeloid leukemia [98] and breast cancer [99]. Recent work from myeloma demonstrated Hh signaling can act through multiple signaling modes to mediated interactions between CSCs and microenviromental niche [100].

Inappropriate Notch activation through cell-to-cell interaction accelerates cell proliferation and restricts differentiation and apoptosis, moreover, this signaling pathway retains stem cell viability via asymmetric cell division [101]. Notch signaling has been suggested to regulate CSCs in various types of cancers, including breast cancer [102], gliomas [103] and embryonal brain tumors [104].

These pathways rarely operate alone, at least during cancer development; instead, cross-talk occurs often on multiple levels of the signaling cascade. These broader complex signaling networks might indicate the need for combination of inhibition regiments to target CSCs effectively.

1.5. Rational combinations: is there a rationale?

As the mechanisms responsible for drug resistance become clearer, several strategies for countering this phenomenon are beginning to emerge. Attempts to overcome resistance mainly involve the use of combination drug therapy using different classes of drugs with minimally overlapping toxicities to allow maximal effective dosages and with narrowest cycle intervals for bone marrow recovery [105]. Specified, combing drugs that have different modes and sites of action we want to create complementary/synergistic rather than just additive effect. Most currently used chemotherapeutic drugs selectively inhibit rapidly dividing cells within the tumour, however spare the slowly dividing or dormant but inherently resistant CSCs and, thus,

may not lead to long-term benefits. Alternatively, it may be preferable to develop combinatorial treatment that specifically targets both CSC and non-CSC population.

1.6. Metformin (METF)

The biguanide Metformin (METF) is regarded as the most widely prescribed anti-hyperglycaemic drug for type 2 diabetes in the world [106]. The glucose lowering effects conducted by METF is largely believed through repression of hepatic gluconeogenesis and an increase of insulin sensitivity. Over a decade ago, METF has gained broad attention for its ability to decrease cancer incidence and mortality in diabetic patients [107-109]. Preclinical study demonstrated that in vitro treatment with METF inhibited growth of various human cancer cell types, including those of thyroid carcinoma [110], prostate [111], gastric [112], breast [113] and glioblastoma [114]. Numerous in vivo studies also indicated METF functions as an antitumor agent. One of the early observations done by Anisimov et al. showed that METF slowed aging rate, increased the life span and inhibited spontaneous carcinogenesis in female transgenic HER2/ neu mice [115]. The anticancer effects of METF are associated with activation of AMPK leading to various downstream effects (Figure 9).

Several reports also showed the potential use of METF in preventing metastasis via mitigating both EMT and CSC. The first report published by Hirsch et al. demonstrated that METF at the low doses inhibited cellular transformation and selectively killed CSCs in four genetically different types of breast cancer. Taking a step further, when given along with Doxorubicin, this combination effectively reduced tumor mass and prevented relapse [116]. Later study also suggested combination of METF with Trastuzumab setting overcame in vivo primary resistance generated by CD44^{high} CD24^{low} phenotype [117].

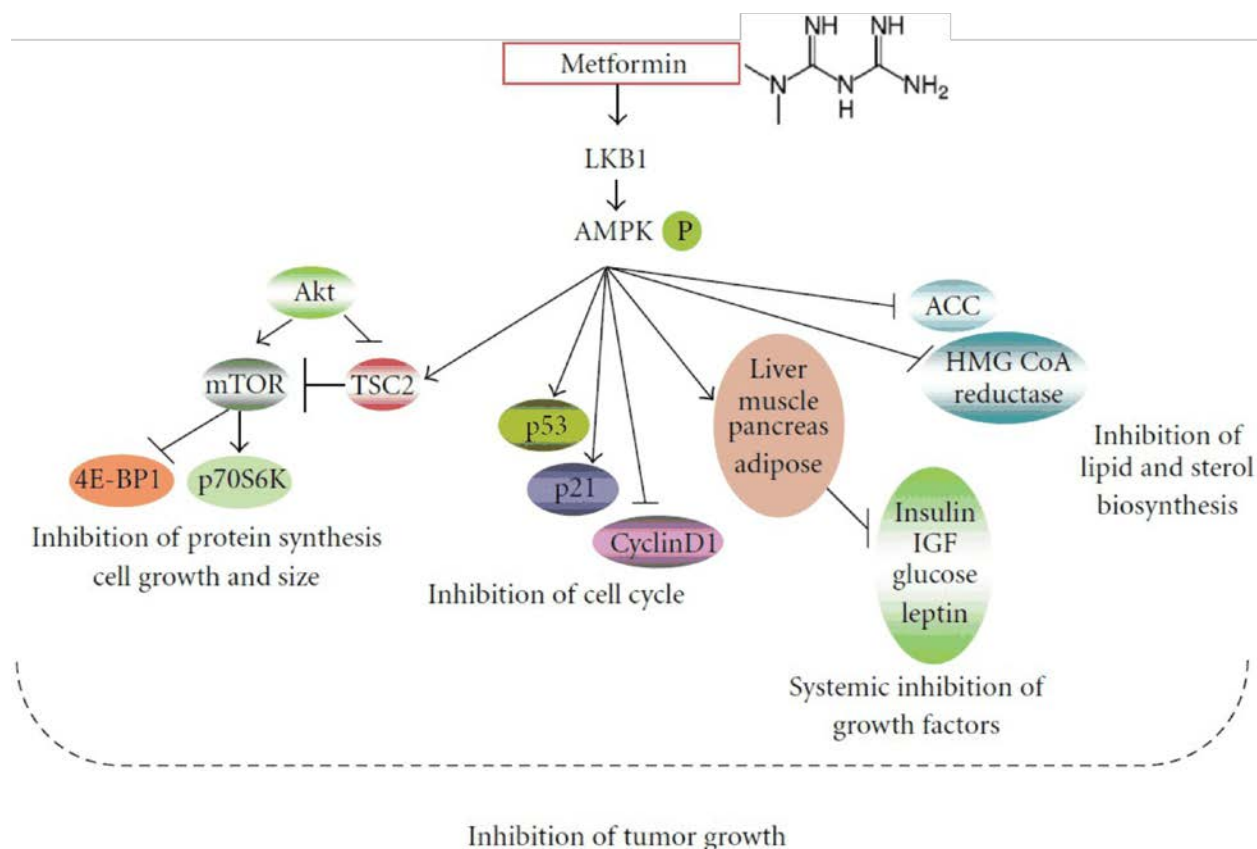


Figure 9. Downstream effects of AMPK activation by METF resulting in inhibition of tumor growth. Activation of AMPK by METF results in myriad effects that include (1) inhibition of mTOR, resulting in inhibition of protein synthesis and cell growth; (2) activation of p53 and p21 along with inhibition of cyclins, resulting in cell cycle arrest; (3) inhibition of lipid and sterol biosynthetic pathways; (4) having a systemic effect on vital organs involved in glucose balance that results in reduced levels of growth factors like insulin, IGF, and leptin. (Modified from Rattan R et al.,2012) [118]

1.7. Salinomycin (SAL)

Salinomycin (SAL) is a carboxylic polyether ionophore (Figure 10) that has been widely used in chicken fodder as an agricultural antibiotic to prevent bacterial and coccidiosis [119]. In 2009, Gupta et al. used EMT this property of CSCs to develop a high-throughput screen, which successfully identified SAL specifically targets CSCs through the induction of differentiation

[120]. After that, SAL has been identified to selectively kill CSC-like cells in some tumor types, including breast cancer and leukemia [120, 121]. Although the mechanism of action underlying the elimination of CSCs by SAL specifically remains unknown, numerous work has uncovered an increasing number of relevant mechanisms and modes of action of SAL in human CSCs and cancer cells.

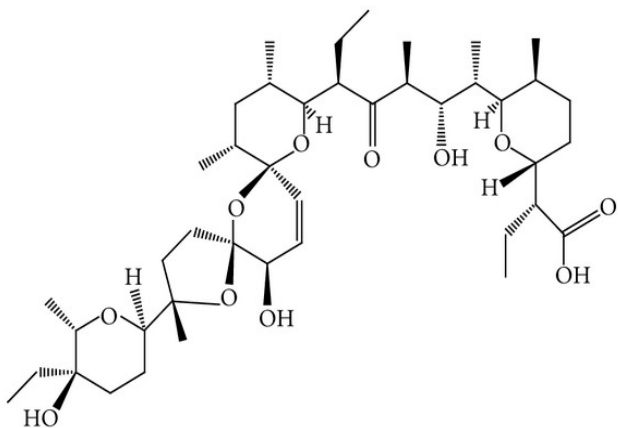


Figure 10. Structural formula of SAL. The pentacyclic molecule with a unique tricyclic spiroketal ring system has a mass of 751 Da, a molecular formula of $C_{42}H_{70}O_{11}$, a melting point of 113 °C, and a UV absorption at 285 nm. (Adapted from H. Kinashi et al., 1973) [122]

Induction of apoptosis and cell death: SAL has been shown to induce apoptosis in CSCs of different origin, such as acute myeloid leukemia, hepatocellular carcinoma, prostate and breast cancer [123-126]. In particular, SAL triggered apoptosis of PC-3 cells by intrinsic mitochondrial pathway that induced activation of the caspase-3-mediated cleavage of poly ADP ribose polymerase (PARP) [126]. Overall, induction of apoptosis or non-apoptosis cell death by SAL in cancer cells seems to be cell type dependent.

Interference with ABC transporters: One of the mechanisms of SAL' action against CSCs was identified as interference with ABC transporters. Specifically, SAL acts as a potent inhibitor of P-glycoprotein to prevent chemotherapeutic drugs from pumping out of tumor cells, thus effectively enhance the action of the agents [127, 128]. Human leukemia stem cell-like cells exhibit resistance to a broad spectrum of chemotherapeutic drugs by virtue of expression of functional ABC transporters [121].

Inhibition of the Wnt/ β -catenin signaling pathway: Increasing evidence suggests that Wnt signaling pathway is required for the maintenance or self-renewal of stem-like cells within a tumor [129, 130]. In particular, Lu and colleagues identified that treatment of primary chronic lymphocytic leukemia cells with SAL caused degradation of Wnt coreceptor lipoprotein receptor related protein 6, suppressed the expression of Wnt target genes LEF1, cyclin D1, and fibronectin, and impaired cell survival [131].

Inhibition of oxidative phosphorylation: Transformed human mesenchymal stem cells have been shown to increase their dependency on oxidative phosphorylation [132]. It is well known that tumor cells possess an increased glucose uptake via enhanced cell proliferation [133]. This observation can be extended to the putative CSCs along with bioenergetics changes during transformation. In this context, SAL is known to inhibit oxidative phosphorylation in mitochondria [134] that may contribute to the elimination of CSCs by SAL.

Cytoplasmic and mitochondrial K^+ efflux: Abnormal expression of potassium channels has been frequently observed in different types of cancer, such as colon cancer [135] and acute myeloid leukaemia [136], which can alter tumor behavior and provide advantages for tumor growth. SAL acts as a K^+ ionophore that interferes with transmembrane K^+ potential and promotes the rapid release of K^+ from mitochondria and cytoplasm [137]. Pharmacological manipulation of K^+ channels can increase tumor cell apoptosis and bring benefit to clinic treatment.

Differentiation of CSCs: SAL is capable of inducing differentiation of CSCs and to induce epithelial reprogramming of cells that had undergone EMT [120]. This is in concert with the finding that SAL downregulated the expression of genes associated with either CSCs or normal mammary epithelial progenitor cells [120].

2. AIMS

Lung cancer is the leading cause of cancer deaths worldwide. Due to late presentation, disease relapse and lack of curative systemic therapy, the overall prognosis is poor with less than 5 year survival. EGF receptor is frequently overexpressed in NSCLC, activation of which results in the phosphorylation of downstream proteins that can induce cell proliferation, invasion and metastasis. Recently, the CSC theory proposes that cancers are maintained by small subpopulations of tumor cells that possess stem or progenitor cell characteristics. Salinomycin, a polyether antibiotic, acting as a highly selective potassium ionophore and widely used as an anticoccidial drug, was recently shown to act as a specific inhibitor of CSCs.

Most of the current therapies that against cancer and also other diseases consist of empirically designed combination strategies. The primary aim is a mutual enhancement of the therapeutic effects, while other benefits may include decreased side effects and the delay or prevention of drug resistance. Based on this, we performed the following studies.

In the first chapter of this study, we aimed to evaluate the effects of chemotherapeutic agents (Paclitaxel, Carboplatin, Gemcitabine), TKIs (Gefitinib, Erlotinib, Afatinib, Lapatinib, Sutent, SKI-606, Dasatinib), Ab (Erbix) or Metformin in combination with Salinomycin, a drug targeting CSCs, in NSCLC cell lines. Due to their architectural resemblance to tumors and the enrichment for CSC subpopulation, spheres were generated to identify the best combination for complete tumor control. Additionally, elucidate the mechanism behind the proliferation inhibition and apoptotic induction activities via combinatorial treatment.

In the second chapter of this PhD Project, we intent to determine whether the morphological heterogeneity typically found in NSCLC cell lines is underlying a characteristic pattern of cancer stem cells and their differentiated progeny, and how different cellular properties related to drug resistance are predicted by such cell polymorphism.

3. MATERIALS AND METHODS

3.1. Materials

3.1.1. Laboratory hardware

Arrayscan VTI HCS Reader	Thermo Fisher Scientific, Schwerte
Balances	Kern 572, Kern & Sohn GmbH, Balingen
	Mettler AE200, Mettler Toledo, Giessen
Centrifuges	Biofuge pico, Heraeus, Hanau
	Universal 320, Hettich, Thermo Fisher Scientific, Schwerte
	Sorvall super T21
Coulter Counter®, Beckman Coulter 21™	Beckman Coulter GmbH, Krefeld
FACScan flow cytometer	BD Biosciences (Heidelberg, Germany)
ELISA reader	Bio Tek, USA
Film processor, Optimax® 2010	Protec, Oberstenfeld
Incubator HERAccl® 150	Thermo Scientific, Munich
LightCycler, StepOnePlus	Applied Biosystems, Darmstadt
Microscopes	Zeiss Axio Observer.A1, Jena
	Zeiss ID 02, Jena
Multichannel pipette, eline®1200	Biohit, Rosbach
Orbital shaker, Red Rotor	Hoefer Scientific, Kehl/Rhein
Pipetboy	INTEGRA Biosciences GmbH, Fernwald
Polyacrylamide gel electrophoresis system	ATTO, Japan

Sterile laminar air hood	Biogard hood, Sanford
Spectrophotometer, Nanodrop ND 000	Thermo Fisher Scientific (Schwerte, Germany)
Vortex Genie 2TM	Bender and Hobein, Swizerland
Western blotting chamber, “semidry” system	Workshop MPI of Biochemistry, Martinsried

3.1.2. Laboratory Chemicals

Acrylamide	Serva, Heidelberg
Ampicillin	Roche, Mannheim
Aprotinin	Sigma, Taufkirchen
APS (ammonium peroxodisulfate)	Bio-Rad, München
BSA (Bovine serum albumin)	Sigma, Taufkirchen
Crystal violet	Sigma, Taufkirchen
Deoxynucleotides (dG/ A/ T/ CTP)	Roche, Mannheim
DTT (Dithiothreitol)	Sigma, Taufkirchen
Ethidium bromide	Sigma, Taufkirchen
Fish Gelatin, G7765	Sigma, Taufkirchen
Formaldehyde	Polysciences, Inc.
Hoechst 33342	Sigma, Taufkirchen
HEPES (N-(2-Hydroxyethyl) piperazine-N-(2-ethanesulfonic acid))	Serva, Heidelberg
L-Glutamine (GibCo)	Invitrogen, Eggenstein
Lipofectamine RNAiMAX	Invitrogen, Eggenstein
Mowiol 4-88 (ROTH)	Carlroth, Karlsruhe
Penicillin/Streptomycin	Gibco, Eggenstein

PMSF (Phenylmethanesulfonyl fluoride)	Sigma, Taufkirchen
Ponceau S	Sigma, Taufkirchen
Propidium Iodide	Sigma, Taufkirchen
Protein marker, PageRuler™ Prestained Protein Ladder	Fermentas, St. Leon-Rot
Polyhema	Sigma, Taufkirchen
RNase inhibitor	Fermentas, St. Leon-Rot
SDS (Sodium dodecyl sulfate)	Roth, Karlsruhe
Sodium azide	Serva, Heidelberg
Sodium fluoride	Sigma, Taufkirchen
Sodium orthovanadate	Sigma, Taufkirchen
Sugar	Merck, Millipore
TEMED (N,N,N',N'-Tetramethylethylenediamine)	Serva, Heidelberg
Triton X-100	Serva, Heidelberg
Tween 20	Sigma, Taufkirchen

3.1.3. Enzymes

AMV reverse transcriptase	Roche, Mannheim
Fast SYBR® Green Master Mix	AB Applied Biosystems, Darmstadt
REDTaq ReadyMix	Sigma, Taufkirchen
Trypsin (GibCo)	Invitrogen, Eggenstein

3.1.4. Kits and other materials

48-well chemotaxis chamber	Neuro Probe; Cabin John, MD
Cell culture materials	BD Falcon, Heidelberg
	Corning, USA
	Falcon, UK
	Greiner, Solingen
	Nunc, Denmark
	LONZA; Germany
CellTiter-Glo luminescent cell viability assay	Promega, USA
Coverslip	MENZEL, Germany
CryoTube™ vials	Nunc, Denmark
Enhanced Chemi Luminescent (ECL) Kit	PerkinElmer/NEN, Köln
Hyperfilm™ MP	Amersham Pharmacia, Freiburg
Nitrocellulose transfer membrane, PROTAN® BA85 0.45 µm	Whatman, Dassel
MicroAmp® Fast Optical 96-Well Reaction Plate	AB Applied Biosystems (Darmstadt, Germany)
Micro BCA Protein Assay Kit	Pierce, Sankt Augustin
Parafilm	Dynatech, Denkendorf
QIAGEN RNase Mini Kit	Qiagen, Hilden
QIAquick PCR Purification Kit (50)	Qiagen, Hilden
StemElite ID System	Promega, Madison, WI
Standard 48-well chemotaxis chamber	Neuro Probe; Cabin John, MD
Sterile filter 0.22 µm, MCE membrane	Millipor, Schwalbach
Sterile filter 0.22 µm, cellulose acetate	Nalge Company, USA

Syringe Norm-Ject 12 ml	BD Falcon, Heidelberg, Henke-Sass Wolf, Tuttlingen
Whatman 3MM	Whatman, Rotenburg/Fulda
96, 6 Well Clear Flat Bottom ULA Microplates	Corning, Hong Kong
Costar™ 96-Well Black Clear-Bottom Plates	Corning, Thermo Fisher Scientific

3.1.5. Chemotherapeutic drugs

Carboplatin	Santa Cruze, CA
Gemcitabine	Sigma, Taufkirchen
Paclitaxel	Sigma, Taufkirchen

3.1.6. Small molecule tyrosine kinase inhibitors (TKIs)

Afatinib	SelleckChem
Dasatinib	Vichem Chemie, Hungary
Erlotinib	Vichem Chemie, Hungary
Gefitinib	Vichem Chemie, Hungary
Lapatinib	Vichem Chemie, Hungary
Metformin	Sigma, Taufkirchen
SKI 606	Vichem Chemie, Hungary
Sutant	Vichem Chemie, Hungary
Tyrphostin AG1478	Cell Signaling, MA

3.1.7. Putative stem cell killer

Salinomycin	Sigma, Taufkirchen
-------------	--------------------

3.1.8. Growth factors and ligands

EGF	Peprtech, USA
FGF	Sigma, Taufkirchen

3.1.9. Cell culture media

The media and the additives were obtained from Gibco™ (Invitrogen, Eggenstein), unless otherwise indicated. Media were supplemented to the requirements of each cell line.

3.1.9.1. Monolayer cell culture

RPMI 1640 with 10% FBS, 2 mM L-Glutamine, 50 U/ml Penicillin and 50 µg/ml Streptomycin SALE and SALC were cultured in Small Airway Growth Media (SAGM™ Medium) (LONZA, CC-3119) supplemented with the contents of the SAGM™ SingleQuots™ Kit (LONZA, CC-4124).

3.1.9.2. Spheroid culture

Dulbecco's Modified Eagle Media/F12 (1:1) supplemented with 30% Glucose, Hepes (Serva), Progesterone (Sigma), Putrescine (Sigma), B27, EGF (Peprtech), FGF (Sigma), ITSS (Roche), Heparin (Sigma) and NaHCO₃ (Invitrogen).

3.1.9.3. Freeze media

90% FBS, 10% DMSO

For SALE and SALC: 80% SAGM, 10% DMSO, and 10% serum

3.1.10. Stock solutions and commonly used buffers

All solutions and buffers were prepared with Millipore water, unless indicated otherwise.

Acrylamide solution	30% (w/v)	Acrylamid
	0.8% (w/v)	Bisacrylamid
Ammoniumbicarbonate buffer (ABC)	500 mM	Ammoniumbicarbonat
DTT	1 M	DL-Dithiothreitol in ABC buffer
DNAase I (RNase free)	1 M	PEQLAB Biotechnologie GMBH, Erlangen
DNA loading buffer (6 ×)	0.05%	Bromphenol blue
	0.05%	Xylencyanol
	30%	Glycerol
	100 mM	EDTA pH 8.0
2% Formaldehyde	400 ml	10% Formaldehyde
	100 ml	1 × PBS
	19 g	Sugar
HNTG	20 mM	HEPES, pH 7.5
	150 mM	NaCl
	0.1%	TritonX-100
	10%	Glycerol
	10 mM	Na ₄ P ₂ O ₇
Laemmli buffer (3 ×)	100 mM	Tris/HCl, pH 6.8
	3%	SDS
	45%	Glycerol
	0.01%	Bromphenol blue
	7.5%	β-Mercaptoethanol

Blocking solution	5%	Goat serum
	1 ×	PBG (see below)
NET-gelatin	50 mM	Tris/HCl, pH 7.5
	5 mM	EDTA, pH 8.0
	0.05%	Triton X-100
	150 mM	NaCl
	0.25%	Gelatin
PBS	137 mM	NaCl
	27 mM	KCl
	80.9 mM	Na ₂ HPO ₄
	1.5 mM	KH ₂ PO ₄ , pH 7.4
PBG	0.5%	Bovine Albumen
	0.045%	Fish Gelatine
PBT	0.1%	Triton X-100
	1 ×	PBS
Propidium-Iodide buffer	0.1%	Na-Citrate
	0.1%	Triton
	20 μM	Propidium Iodide
Running buffer (4×)	0.5 M	Tris/HCl, pH 8.8
	0.4%	SDS
Staining buffer	20%	Methanol
	0.5%	Crystal violet
Stripping buffer	62.5 mM	Tris/HCl, pH 6.8
	2%	SDS

TE (10/0.1)	10 mM	Tris/HCl, pH 8.0
	0.1 mM	EDTA, pH 8.0
Transblot-SD buffer	50 mM	Tris/HCl, pH 7.5
	40 mM	Glycine
	20%	Methanol
	0.004%	SDS
Tris-glycine-SDS buffer	25 mM	Tris/HCl, pH 7.5
	200 mM	Glycine
	0.1%	SDS
Triton X-100 lysis buffer	50 mM	HEPES, pH 7.5
	150 mM	NaCl
	1 mM	EDTA
	10%	Glycerol
	1%	Triton X-100
	10 mM	Na ₄ P ₂ O ₇
	100 µg/l	Aprotinin
	10 mM	NaF
	1 mM	PMSF
	2 mM	VaO ₅

3.1.11. Human cell lines

Cell line	Histology	Reference
HCC4006	Adenocarcinoma	ATCC, USA
NCI-H1975	Adenocarcinoma	ATCC, USA

PC9	Adenocarcinoma	ATCC, USA
HCC827	Adenocarcinoma	ATCC, USA
NCI-H1650	Adenocarcinoma	ATCC, USA
NCI-H1568	Adenocarcinoma	ATCC, USA
NCI-H2122	Adenocarcinoma	ATCC, USA
HCC2935	Adenocarcinoma	ATCC, USA
NCI-H3255	Adenocarcinoma	Dr. Roman Thomas, Blackfield, AG, Köln, Germany
NCI-H3122	Adenocarcinoma	Dr. Roman Thomas, Blackfield, AG, Köln, Germany
HCC2279	Adenocarcinoma	Dr. Roman Thomas, Blackfield, AG, Köln, Germany
HCC95	Squamous cell carcinoma	Dr. Roman Thomas, Blackfield, AG, Köln, Germany
SALC	Small airway epithelial cells+hTERT+SV40	Dr. Roman Thomas, Blackfield, AG, Köln, Germany
SALC-KRAS	Small airway epithelial cells+hTERT+SV40+KRAS	Dr. Roman Thomas, Blackfield, AG, Köln, Germany

3.1.12. Antibodies

3.1.12.1. Primary antibodies

Recognized protein	Description	Reference
pEGFR	Rabbit, monoclonal; detects endogenous EGFR phosphorylated at Tyr1173	#4407; Cell Signaling, (MA, USA)
EGFR	Mouse, monoclonal; recognizes amino acids 1020-1046 of human EGFR	610017; BD Transduction Laboratories (CA, USA)

pHER2	Rabbit, polyclonal; detects endogenous HER2 phosphorylated at Tyr1248	#2247; Cell Signaling, (MA, USA)
HER2	Rabbit, polyclonal; recognizes amino acids 1243-1255 of human HER2	06-562; Millipore (Schwalbach, Germany)
pHER3	Rabbit, monoclonal; detects endogenous HER3 phosphorylated at Tyr1289	#4791; Cell Signaling, (MA, USA)
HER3	Mouse, monoclonal, clone 2F12; against 1295-1323 of human HER3	05-390; Millipore (Schwalbach, Germany)
pAKT	Rabbit, polyclonal; recognizes endogenous Akt1 phosphorylated at Ser473	#9271; Cell Signaling, (MA, USA)
AKT1/2/3 (H-136)	Rabbit, polyclonal; against amino acids 345-480 of human Akt1	Sc-8312; Santa Cruz, (CA, USA)
pERK1/2	Rabbit, polyclonal; recognizes phospho-p44/P42	#9101; Cell Signaling, (MA, USA)
ERK1 (K-23)	Rabbit, polyclonal; against a peptide mapping within subdomain Xi of ERK1 of rat origin	Sc-94; Santa Cruz, (CA, USA)
pAMPK α	Rabbit, polyclonal; detects endogenous AMPK phosphorylated at threonine 172, and both α -1 and α -2 isoforms of the catalytic subunit	#2531; Cell Signaling, (MA, USA)
AMPK α	Rabbit, polyclonal; detects endogenous AMPK α protein, and both α -1 and α -2 isoforms of the catalytic subunit	#2532; Cell Signaling, (MA, USA)
pmTOR	Rabbit, polyclonal; detects endogenous mTOR phosphorylated at Ser2448	#2971; Cell Signaling, (MA, USA)
mTOR (7C10)	Rabbit, monoclonal; detects endogenous levels of total mTOR protein	#2983; Cell Signaling, (MA, USA)
pP70 S6K	Rabbit, polyclonal; detects human, mouse p70 S6 phosphorylated at Thr412	07-018; Millipore (Schwalbach, Germany)
P70 S6K	Rabbit, polyclonal; detects amino acids 26-43 of rat p70 S6 Kinase	07-402; Millipore (Schwalbach, Germany)

PARP	Rabbit, polyclonal; detects endogenous levels of full length PARP (116 kDa), as well as the large fragment (89 kDa) of PARP resulting from caspase cleavage	#9542, Cell Signaling, (MA, USA)
Ki-67	Rabbit, polyclonal; Synthetic peptide conjugated to KLH derived from within residues 1200 - 1300 of Human Ki67	ab15580; Abcam, (Cambridge, UK)
Nanog (H-155)	Rabbit, polyclonal; against amino acids 151-305 mapping at the C-terminus of Nanog of human origin	Sc-33759; Santa Cruz, (CA, USA)
β -catenin	Mouse, monoclonal; detects amino acids 571-781 of mouse β -Catenin	610154; BD Transduction Laboratories (CA, USA)
AXL (C-20)	Goat polyclonal; against a peptide mapping at the C-terminus of AXL of human origin	Sc-1096; Santa Cruz, (CA, USA)
CD44	Mouse, monoclonal, detects endogenous levels of total CD44 protein	#3570; Cell Signaling, (MA, USA)
Tubulin	Mouse, monoclonal, ascites	T 9026; Sigma (Taufkirchen, Germany)

3.1.12.2. Secondary antibodies

For western blot analysis corresponding secondary antibodies conjugated with horseradish peroxidase (HRP) were utilized.

Recognized protein	Description	Reference
Mouse IgG	Goat polyclonal, HRP-conjugated	Sigma, Taufkirchen, Germany
Rabbit IgG	Goat polyclonal, HRP-conjugated	Bio-Rad, Munich, Germany

For immunofluorescence analysis corresponding secondary antibodies conjugated with fluorochrome were utilized.

Antigen	Fluorescent	Host	Reference
Mouse IgG	Alexa Fluor 546	Goat	Molecular Probe, A11003
Rabbit IgG	Alexa Fluor 546	Goat	Molecular Probe, A11010
Goat IgG	Alexa Fluor 488	Donkey	Molecular Probe, A11055
Rabbit IgG	Cy2	Goat	Jackson Immuno Research, 111-225-045
Mouse IgG	Cy3	Goat	Jackson Immuno Research, 115-165-003
Mouse IgG	Cy2	Goat	Jackson Immuno Research, 115-225-003
Mouse IgG	FITC	Goat	Sigma, F5387

3.1.12.3. Therapeutic monoclonal antibody

Antibody	Reference
Cetuximab (Erbix) (Erbix)	Max-Planck Apotheke, Martinsried, Germany

3.1.13 Oligonucleotides

3.1.13.1. siRNAs

20 μ M Stock dissolved with Millipore water. Aliquots were stored at -20 °C.

Target	Sequence	Reference
EGFR	Sense: CUGACUCCGUCCAGUAUUGAUdTdT	Ambion (TX, USA)
	Antisense: dTdTGACUGAGGCAGGUCAUAACUA	
HER2	Sense: GUUGGAUGAUUGACUCUGAtt	Ambion (TX, USA)
	Antisense: UCAGAGUCAAUCAUCCAACat	
HER3	Sense: GAAUGAAUUCUCUACUCUAtt	Ambion (TX, USA)
	Antisense: UAGAGUAGAGAAUUCAUUCat	

Scramble	Sense: GAACUUCAGGGUCAGCUUGCCUU	Ambion (TX, USA)
	Antisense: GGCAAGCUGACCCUGAAGUUCUU	

3.1.13.2. Primers for cDNA synthesis

Name	Sequence (5'-3')	Reference
K1	AAGCAGTGGTATCAACGCAGAGTACT(30) N-1N	MWG Biotech, Germany
K2	AAGCAGTGGTATCAACGCAGAGTACGCGGG	MWG Biotech, Germany

N-1=A, G or C; N=A, C, G, T

3.1.13.3. Primers for conventional and real-time PCR

Primers for real-time PCR were diluted in Millipore water to final concentration of 100 pmol/ μ l. Aliquots were stored at -20 °C.

Primers for conventional PCR

The working concentrations of CD44, MMP1 and Tubulin were 5, 5 and 10 pmol/ μ l, respectively.

Target	Sequence (5'-3')
CD44-F	GATCCACCCCAATTCCATCTGTGC
CD44-R	AACCGCGAGAATCAAAGCCAAGGC
MMP1-F	CGACTCTAGAAACACAAGAGCAAGA
MMP1-R	AAGCTTAGCTTACTGTCACACGCTT
Tubulin-F	AAGTGACAAGACCATTGGGGGAGG
Tubulin-R	GGGCATAGTTATTGGCAGCATC

Primers for real-time PCR

Target	Sequence (5'-3')
ALDH-F	AGCAGGAGTGTTTACCAAAGA
ALDH-R	CCCAGTTCTCTTCCATTTCCAG
AXL-F	TTTCTCCTGCGAAGCCCATA
AXL-R	ATGCCACGCGGATGTGATAA
ABCG2-F	AGATGGGTTTCCAAGCGTTCAT
ABCG2-R	CCAGTCCCAGTACGACTGTGACA
BMI1-F	GATGAATTCGTCACTGTGAATAACGATTT
BMI1-R	TCTAGATCTACAATCATTCTGAATGCAT
CD44-F	TCCAACACCTCCCAGTATGACA
CD44-R	GGCAGGTCTGTGACTGATGTACA
CD133-F	GCTCAGACTGGTAAATCCCC
CD133-R	GACTCGTTGCTGGTGAATTG
E-cadherin-F	CGGGAATGCAGTTGAGGATC
E-cadherin-R	AGGATGGTGTAAGCGATGGC
EGFR-F	GTGACCGTTTGGGAGTTGATGA
EGFR-R	GGCTGAGGGAGGCGTTCTC
ABCC1-F	ATGTCACGTGGAATACCAGC
ABCC1-R	GAAGACTGAACTCCCTTCCT
Nanog-F	CAAAGGCAAACAACCCACTT
Nanog-R	TCTGCTGGAGGCTGAGGTAT
Oct4-F	ACATCAAAGCTCTGCAGAAAGAACT
Oct4-R	CTGAATACCTTCCCAAATAGAACCC
Periostin-F	CAGTTTTGCCCATGACCATG

Periostin-R	ATAGCGCTGCGTTGTGGTG
Slug-F	CATGCCTGTCATACCACAAC
Slug-R	GGTGTCAGATGGAGGAGGG
Snail-F	GAGGCGGTGGCAGACTAG
Snail-R	GACACATCGGTCAGACCAG
Sox2-F	TCCCATCACCCACAGCAAATGA
Sox2-R	TTTCTTGTCGGCATCGCGGTTT
hHPRT-F	TGACACTGGCAAAACAATGCA
hHPRT-R	GGTCCTTTTCACCAGCAAGCT

3.1.14. Software

software	Reference
AIDA	Raytest, Germany
Photoshop CS3	Adobe Systems Inc, San Jose
ImageJ	National Institutes of Health, USA
CorelDRAW	COREL, USA

3.2. Methods

3.2.1. Methods in mammalian cell culture

3.2.1.1. General cell culture techniques

All cell lines were cultivated in a humidified 93% air, 7% CO₂ HERAcell® 150 incubator at 37 °C and routinely assayed for mycoplasma contamination using a bisbenzimidazole staining kit (Sigma). Cell lines (American Type Culture Collection, USA) were routinely grown according to the supplier's instructions. Before seeding, cell numbers were counted with a Coulter Counter (Coulter Electronics).

3.2.1.2. Preparation of polyhema coated plates

2.4 g polyhema was dissolved completely in 20 ml 95% ethanol by rotating at 65 °C. Solution was filtered through a sterile 0.22 µm pore size filter and served as stock. Opaque-walled 96-well plates were coated with 50 µg/ml polyhema with the volume of 30 µl and dried under the laminar flow overnight. Plates can be stored indefinitely at room temperature prior to use.

3.2.1.3. Spheroid generation and cultivation

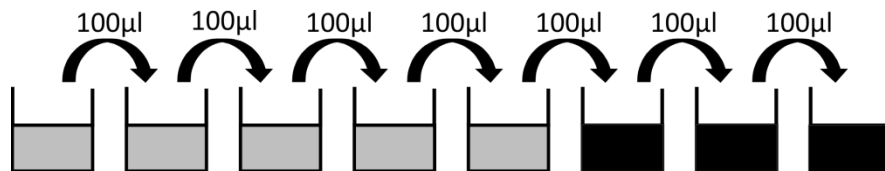
Monolayer cells after trypsinized were seeded in ultra-low adherent 96- or 6-well plates. Except NCI-H1650, cells were seeded in polyhema coated opaque-walled 96-well plates for sphere generation and drug treatment.

3.2.1.4. Cell seeding and drug treatment

Opaque-walled 96-well plates with clear bottoms were used for monolayer cells culture. The number of cells used per cell line was determined empirically, cells from HCC4006, NCI-H1975, HCC95, NCI-H1650, NCI-H2122, NCI-H3122 were seeded at 5×10^4 , 7.5×10^4 , 1.3×10^5 , 1×10^5 , 2.2×10^5 , 1.2×10^5 cells/well, respectively. Drug treatments were performed next day after seeding. Cells were exposed to drugs 3 days for cell viability assay and 48 hours for western blot analysis.

3.2.1.5. Single-cell cloning by limiting dilution

NSCLC cells after trypsin were harvested and resuspended in fresh medium to generate a single-cell suspension with a density of 1000 cell/ml. Then, 100 μ l single-cell suspension was dispensed into each well of the first column in 96-well plates. A way of two-fold dilution (see below) was conducted until the last column. Next day after plating, each well was checked under the microscope, like wells containing only a single cell were marked, and wells with no cells or with more than one cell were excluded. 50 μ l fresh medium was supplied each 5 days during the 2 weeks cell culture.



Black square ■: indicated these wells have the possibility to contain only one single cell.

3.2.1.6. Isolation of different subpopulations

Limited-dilution assay and spheroid differentiation were carried out to determine the clonal composition of each tumor cell line. Individual clones that yielded colonies within 7–21 days were designated CSCs, first line differentiation (1st DF) cells or second line differentiation (2nd DF) cells based on their colony morphology. Colonies were grown to confluence and transferred to 6-well plates where they were maintained until near confluent, at which time they were replated in 10 cm dishes and propagated under conditions where they retain their morphology. Specifically, cells were split 1:6 and passaged every 3 days.

3.2.1.7. Sphere formation assay

To examine the effect of drugs in the sphere formation ability, monolayer cells were treated with Metformin, Salinomycin alone or combination for 48 hours, then cells were trypsinized and replated with 5.000 and 10.000 cells in ultra-low adherent 96-well plates for sphere generation in the continued presence of drugs as before. Cells were transferred into opaque-walled 96-well

plates with clear bottoms over a 4 day period, and the number of spheres per well was reflected by detection of viable cells.

3.2.1.8. Transfection of small interfering RNA (siRNA)

Cells were plated at 60% to 80% confluence in 6-well plates and incubated with medium containing no antibiotics 24 hours before transient transfection with siRNA mixed with Lipofectamine RNAiMax reagent (Invitrogen) according to the manufacturer's protocol. 21-nucleotide siRNA specific for EGFR, HER2 and HER3 as well as a corresponding scrambled (control) siRNA were list in the materials. Briefly, 9 μ l Lipofectamine RNAiMax reagent and siRNA (90 pmol) were diluted in 150 μ l Opti-MEM separately and formed siRNA-reagent complex was incubated for 5 minutes before adding to cells. After 48 or 96 hours, cells were harvested for western blotting to analyze knockdown efficiency or applied for cell viability detection, respectively.

3.2.2. Protein analytical methods

3.2.2.1. Lysis of cells with Triton X-100 lysis buffer

Monolayer cells or spheroids harvested from ultra-low adherent 6-well plates were washed by cold PBS one time, and lysed in lysis buffer containing 50 mM HEPES [pH 7.5], 150 mM NaCl, 1 mM EGTA, 10% Glycerol, 1% Triton X-100, 10 mM $\text{Na}_4\text{P}_2\text{O}_7$, 1 μ g/ml Aprotinin, 1mM PMSF and 1 mM Orthovanadat. Insoluble cell fragments were removed under centrifugation at $13.000 \times g$ for 20 minutes at 4 $^\circ\text{C}$, then stored at -80 $^\circ\text{C}$ or directly subjected to western blot analysis.

3.2.2.2. Determination of total protein concentration in cell lysates

Protein concentration was measured using the Micro-BCA Protein Assay Kit (Pierce, Sankt Augustin) following manufacturer's instructions. The absorbance was obtained at 570 nm on a BioTek ELISA reader.

3.2.2.3. SDS-polyacrylamide-gel electrophoresis (SDS-PAGE)

SDS-PAGE was conducted as described previously (Sambrook, 1990). 35 μ g total proteins with 3 \times or 6 \times Laemmli buffer were heated at 95 $^{\circ}$ C for 5 minutes to remove the inappropriate ingredients, and separated on the acrylamide percentage 7.5 or 10% SDS PAGE gel (depends on the size of the target protein in the sample). The electrophoresis was stopped when the downmost sign of the protein marker almost reaches the foot line of the glass plate. SDS-PAGE running was done in an ATTO polyacrylamide gel electrophoresis system with the setting voltage at 20 mA per stacking gel and 35 mA per separating gel.

3.2.2.4. Western blot

Western blot was conducted as described previously (Gershoni and Palade, 1982). After electrophoresis, the protein-containing polyacrylamide gel was placed in direct contact with a nitrocellulose membrane and ``sandwiched`` between 8 sheets of Whatmann 3 MM in the presence of transblot-SD buffer. Transfer was last for 3 hours at 0.8 mA/cm² using a ``semidry``-blot system. Following transfer, proteins were stained with Ponceau S (2 g/l in 2% TCA) 5 min with shaking in order to visualize marker protein bands. The membrane was then de-stained in Millipore water and incubated in NET-gelatin at room temperature for at least 1 hour with shaking to block unspecific sites. Afterwards, membranes were placed in the interesting primary antibody with the dilution 1:1000 or 1:2000 in NET-gelatin overnight at 4 $^{\circ}$ C. The next day, membranes were rinsed 3 \times 12 minutes in NET-gelatin and incubated for 1 hour at room temperature with horseradish peroxidase-conjugated antibody (see Table 8) with the appropriate dilution in NET-gelatin. After additional rinse (3 \times 12 minutes), detection was performed using an ECL reagent with X-ray films.

3.2.2.5. Stripping

Membranes were stripped and re-probed to investigate more than one interest protein on the same blots. Therefore, the membrane was incubated with stripping buffer at 52 $^{\circ}$ C for 1 hour with some agitation. Afterwards the membrane was rinsed at least 5 \times for up to 1 hour in NET-gelatin before it was incubated with another detection antibody overnight.

3.2.2.6. Phospho-kinase array

The Proteome Profiler Phospho-Antibody Array Kit (ARY003) from R&D Systems was performed following manufacturer's instructions. Spot densities were analyzed using AIDA program (Germany). The average density of duplicated spots was determined and normalized for the relative changes of phosphorylation of 43 kinases and 2 related total proteins.

3.2.3. Methods in molecular biology and Cell Biology

3.2.3.1. Total RNA isolation and cDNA synthesis

Total RNA was extracted using the RNAeasy kit (QIAGEN) and purified through a column of oligo (dT)-cellulose (Stratagene, United States). Synthesis of cDNA was carried out with 5 µg 7.5 µl Poly(A) + RNA, 5 × reverse transcriptase buffer (Roche Diagnostics, Mannheim, Germany), 0.1 mM DTT, 10 µM dNTP, 20 U AMV reverse transcriptase (Roche Diagnostics, Mannheim, Germany). The reaction mixture also contained primers K1 and K2 (MWG Biotech, Germany). Mixture was incubated at 42 °C for 1-2 hours in the incubator to avoid evaporation, followed with 10 µl TE 10/1 at 72 °C for 7 minutes to stop reaction. cDNA after synthesis was purified using PCR purification KIT (QIAGEN) and used as the template for PCR amplification after 1:40 dilution.

3.2.3.2. RT-PCR (reverse transcription-PCR) analysis

REDTaq ReadyMix (Sigma-Aldrich) was used for PCR amplification reactions (20 µl) according to the manufacturer's recommendations. Cycling conditions were as follows: (i) 2 minutes at 94 °C; (ii) 30 seconds at 94 °C; (iii) 30 seconds at each annealing temperature; (iv) 1 minute at 72 °C; and (v) 5 minutes at 72 °C. The steps (ii–iv) were repeated in each cycle number. Samples without template were used as the negative control for excluding contamination, and RNA from human placenta was used as positive control. PCR products were size-fractionated by 2% agarose gel electrophoresis and DNA was visualized by ethidium bromide staining. Annealing temperature and cycle number for CD44, MMP1 and Tubulin were 62 °C 30 cycles, 60 °C 40 cycles and 57 °C 25 cycles, respectively.

3.2.3.3. Real-time PCR analysis

All quantitative PCR reactions (20 μ l) were carried out in the StepOne plus Real-Time PCR system (Applied Biosystems) using Fast SYBR Green Master Mix (AB Applied Biosystems, Darmstadt, Germany). The $2^{-\Delta\Delta CT}$ method was used to analyze the relative fold change in gene expression with hypoxanthine phosphoribosyltransferase (HPRT) (Applied Biosystems) as an endogenous control. All specimens were evaluated in triplicates.

3.2.3.4. Flow cytometry

$1-2 \times 10^6$ cells grown in 6-well plates were harvested by trypsinization, washed twice and resuspended in 1 ml of PBS. The cells were fixed by adding 9 ml of 70% ice cold ethanol followed by 30 minutes incubation at 4 °C. Cells were stained with 0.1% (v/v) Triton X-100, 10 g/mL PI (Molecular Probes, Inc.), and 100 μ g/mL DNase-free RNase A in PBS at room temperature in the dark for 30 minutes. Cell cycle distribution was determined by FACScan flow cytometer (BD Biosciences, Heidelberg, Germany) and analyzed by CellQuest software (BD Biosciences).

3.2.3.5. Immunofluorescence

Sterile coverslips (MENZEL) were placed in the 24-well plate before cell seeding, when adherent cells were grown to the desired confluence, remove medium from live cells, followed with 2 times washes of 1 \times PBS. Cells were fixed in 2% paraformaldehyde made in PBS for 30 minutes at room temperature. After 1 time 1 \times PBS wash, cells were further fixed in 1% paraformaldehyde at room temperature for 10 minutes. Monolayer cells were washed additional 2 times to remove residual paraformaldehyde, and submerged in PBS at 4 °C until use. Cells were permeabilized with 0.1% Triton X-100 in PBS solution for 10 minutes, followed with 1 time wash of 1 \times PBS. Then cells were first blocken for 10 minutes in 100 mM Glycine in 1 \times PBS, and further blocken in 5% goat serum in PBG for 1 hour. Afterwards, cells were placed the desired primary antibody with the dilution 1:300 ~ 500 in 300 μ l 5% goat serums in PBG overnight at 4 °C. The next day, cells were rinsed 3 \times 10 minutes in 5% goat serum in PBG and incubated for 1 hour at room temperature with fluorochrome-labeled secondary antibody with the

appropriate dilution (1:400 ~ 800) in 5% goat serum in PBG. After additional rinse (3×10 minutes), Hoechst 33342 stain at concentration of 1 mg/100 ml in ddH₂O was performed for 5 minutes. Coverslips were mount with a drop of mounting medium Mowiol 4-88 (Carlroth), and kept in dark at 4 °C overnight before detection.

3.2.3.6. Boyden chamber invasion assay

50.000 cells resuspended in 350 μ l of serum-free medium were seeded into the Matrigel-coated inserts of the Boyden chamber (BD Biosciences, Heidelberg, Germany). In the bottom chamber 750 μ l medium with 10% FCS was served as chemoattractant. Cells were permitted to migrate for 36 hours, then fixed and stained with crystal violet. Pictures were taken on a Zeiss Observer.A1 microscope (Zeiss). The value of the migrated cells was calculated from at least three wells for each experiment group and analyzed with the Photoshop CS3 extended measurement feature.

3.2.3.7. Cell proliferation assays

Drug treatments were performed next day after cell seeding and proliferation was measured 72 hours later using CellTiter-Glo luminescent cell viability assay (Promega, USA), following manufacturer's instructions. As a slight adaptation to spheroid specificity, the mixture was transferred into an opaque white cell culture plate after pipetting up and down 3 times, and incubation time was extended to 20 minutes accordingly. Each point represents as a percentage of the DMSO treated control. Experiments were set up in 4 replicate wells and repeated thrice.

3.2.3.8. Isobologram analysis

According to the Chou-Talalay method for evaluation of drug combination, the combination index (CI) was calculated using the CalcuSyn software (Biosoft) and quantitatively defined the effect between two drugs, with $CI < 1$ (synergism), $CI = 1$ (additivity) and $CI > 1$ (antagonism).

Figure 11 indicated the depiction of typical quantitative diagnostic graphics generated by the computer simulation. a, the Fa-CI plot (Chou-Talalay plot). b, the classic isobologram (for the

constant ratio combination design). c, the normalized isobologram (Chou-Chou plot) for the non-constant ratio combination design. d, the Fa-DRI plot (Chou-Martin plot) for the constant ratio combination design. When all single drug parameters (m and D_m values) are available, the CI values can be calculated for the non-constant ratio combinations. But no computer simulation for Fa-CI plot or the Fa-DRI plot is possible due to changing ratios.

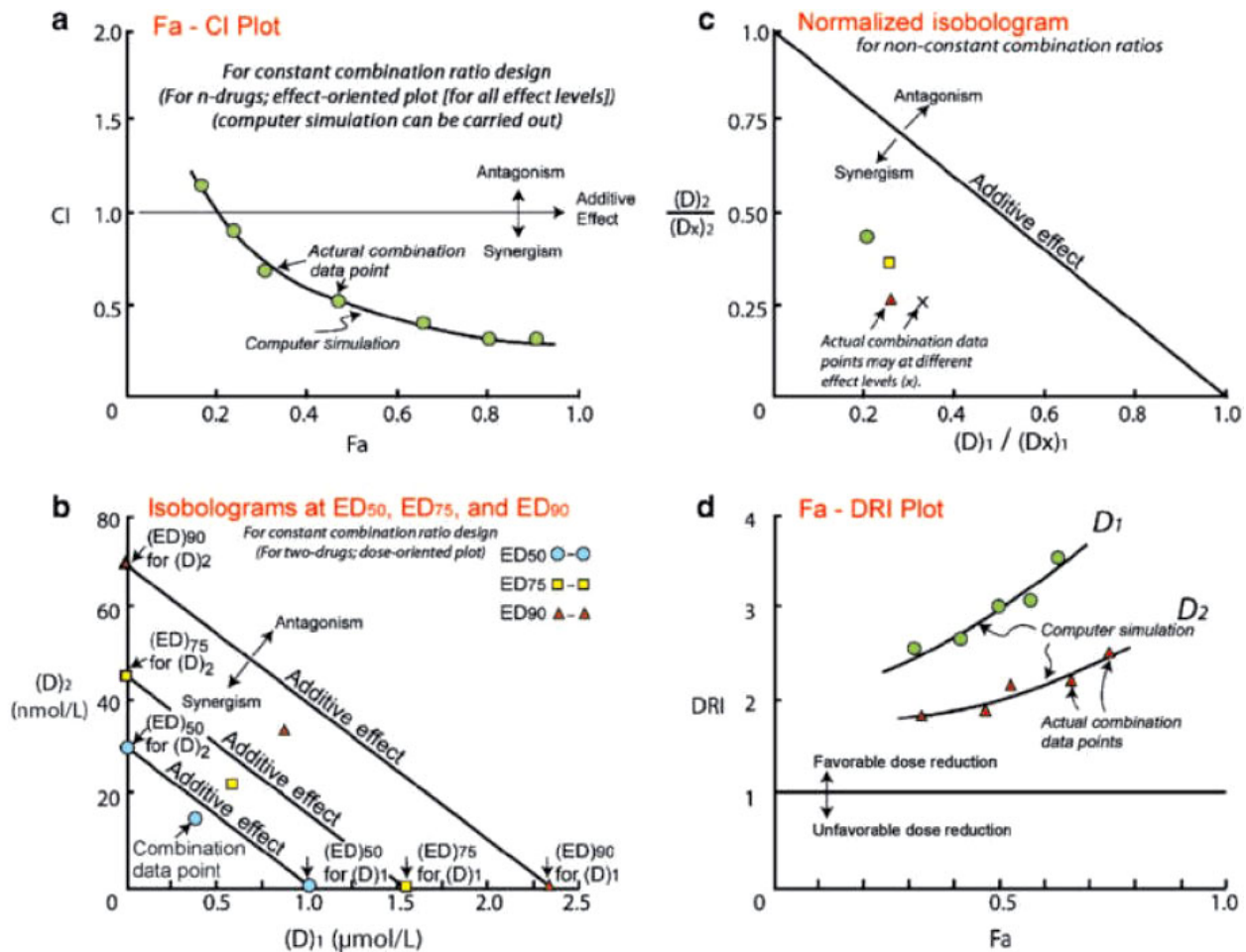


Figure 11. Quantitative practical applications of drug combination. (Adapted from Ting-Chao Chou, 2010) [138]

3.2.3.9. Statistical analysis

Data were represented as mean \pm SD from three independent experiments unless stated otherwise. Statistical analysis was performed by one-way analysis of variance (ANOVA), and statistical

MATERIALS AND METHODS

significance (**P < 0.01, *P < 0.05) was evaluated with the unpaired 2-tailed Student t test to assess difference between treated and control samples.

4. RESULTS

Chapter I

4.1. METF and SAL as the best combination for the eradication of NSCLC monolayer cells and their alveospheres (cancer stem cells) irrespective of EGFR, KRAS, EML4/ALK and LKB1 status

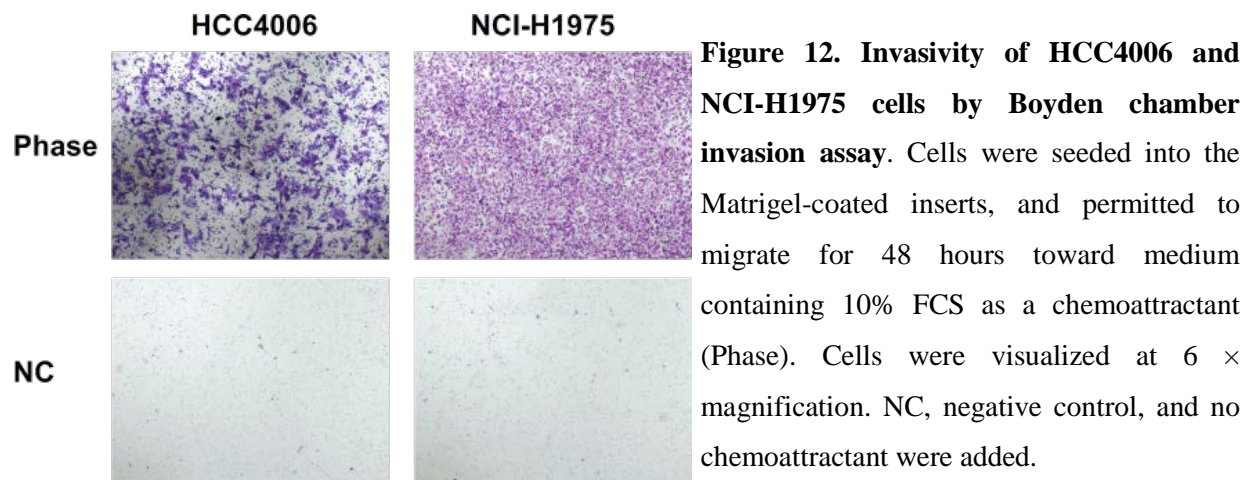
4.1.1 Characteristics of the NSCLC cell lines used in this study

After chemical genomics based cell line selection, 11 NSCLC cell lines were chosen for evaluation (Table 6). Three of them were initially investigated in more details in order to gain the best combination that can target both CSCs and differentiated tumor cells. The HCC4006 adenocarcinoma cell line has an EGFR deletion in exon 19 and EGFR amplification with the copy number 5.2, and acquired half maximal inhibitory concentration (IC_{50}) of Gefitinib at 0.25 μ M. However, NCI-H1975 adenocarcinoma cells, which harbor both the L858R substitution associated with sensitivity to Gefitinib and the “gatekeeper” T790M missense mutation linked with resistance to EGFR-TKIs, are refractory to Gefitinib ($IC_{50} > 20 \mu$ M). The HCC95 cell line is derived from SCC with wt EGFR and an IC_{50} value of $> 10 \mu$ M for Gefitinib. Furthermore, all cell lines carry wt KRAS, BRAF, LKB1 and PTEN genotypes; in addition, HCC4006 and NCI-H1975 cells possess motility and invasivity (Figure 12).

Table 6. Characteristics of the NSCLC cell lines used in this study

NSCLC cell line	Histology	EGFR genotype [139, 140]	PTEN, KRAS or LKB1 mutation	Gefitinib (IC ₅₀ , μM)
HCC4006	AD	del E746–A750 Amplification	None	0.25
NCI-H1975	AD	L858R and T790M	None	> 20
HCC95	SCC	wt	None	> 20
NCI-H1650	AD	del E746–A750	PTEN	11.7
NCI-H2122	AD	wt	KRAS, LKB1	> 10
NCI-H3122	AD	wt	EML4/ALK	> 10
NCI-H1568	AD	wt	None	> 20
HCC2935	AD	del E746–S752	None	0.11
NCI-H3255	AD	L858R	None	0.089
HCC2279	AD	del E746–A750	None	0.048
HCC827	AD	del E746–A750	None	0.04

AD: adenocarcinoma, SCC: squamous cell carcinoma.



There are several possible methodologies available to characterize the CSCs, for instance, fluorescence-activated cell sorting (FACS) analysis (based on common antigens presenting on cell membranes of viable cells, like CD44 and CD133), stem cell marker (SCM) expression, tumor sphere formation (SF) in serum-free media, side population phenotype identification by efflux of dye and an intracellular enzyme ALDH activity [141-143]. In our study we applied all these methods, however, for drug screening we routinely used two of them. One of which is tumor SF that is increased with CSC population and function. From the morphology, as shown in Figure 13A, we found HCC4006 cells assembled into highly compact three-dimensional (3D) alveospheres with a spherical cavity inside, whereas the 3D structure of NCI-H1975 cells was less cohesive. In the HCC95 cell line, the initial loose aggregates seen at day 1 gradually and randomly increased into relatively compact spheroids after one week in culture. These morphological characteristics of 3D outgrowth of these cell lines could indicate the existence of a functional heterogeneity of CSCs, which may vary from tumor to tumor, depending on their mutations and distinct genetic profiles. Another used strategy is the investigation of SCM expression. Until now, to our knowledge, there is no apparent consensus about the “best marker” by which to identify CSCs, hence, here we chose the widely accepted SCMs for characterization. Real-time PCR demonstrated that in HCC4006 cells (Figure 13B, upper), SCMs Nanog, CD133, Sox2, BMI1 and the multi-drug transporters ABCG2, ABCC1 were higher expressed (1.6 ~ 5.2 folds) in alveospheres over in two-dimensional (2D) monolayer cells. Similar gene upregulation patterns (2.3 ~ 6.7 folds) were observed in NCI-H1975 3D cells, including additional elevated CD44 (Figure 13B, middle). However, HCC95 spheroids showed increased CD44, Sox2, BMI1 and ABCG2 marker expression (1.2 ~ 3.2 folds) (Figure 13B, bottom). In common, Sox2, BMI1 and ABC transporters can be identified as SCMs for the evaluation of CSCs in the tested NSCLC.

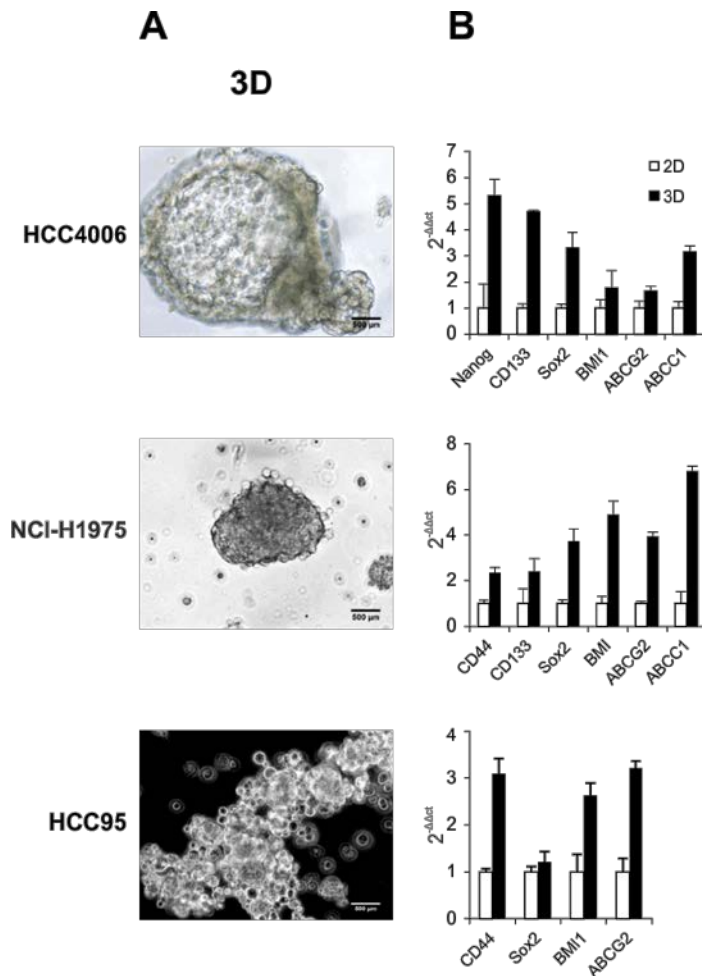


Figure 13. Characteristics of NSCLC HCC4006, NCI-H1975 and HCC95 cells.

(A) Phase-contrast micrographs of spheroids. Cells were placed in non-serum free medium in non-adherent culture flasks to form spheroids. (B) Real-time PCR analyzed expression levels of SCMs and ABC transporters in monolayer cells (2D) and spheroids (3D).

4.1.2. EGFR family signaling upon EGF and AG1478 treatment

To gain insight into the functional role of the EGFR family signaling in these three cell lines, we examined HER2 and HER3 phosphorylation in serum-starved conditions with and without AG1478 (specific TKI for EGFR) and EGF treatment. After 24 hours serum starvation of HCC4006 and NCI-H1975 cells, EGFR and HER2 were still activated and could be further phosphorylated upon 50 ng/ml EGF stimulation (Figure 14A and B, upper panel). In contrast, there was no EGFR and HER2 phosphorylation in HCC95 cells (EGFR wt), except with the addition of EGF (Figure 14C, upper panel). EGF-mediated EGFR and HER2 phosphorylation was completely prevented by 30 minutes of AG1478 pretreatment in HCC4006 and HCC95 cells, but persisted at a high level in the NCI-H1975 cell line, as substitution of a threonine at the

gatekeeper position (T790M), results in a steric hindrance that may interfere with the binding of TKIs (Figure 13A-C, upper panel) [38]. In HCC4006 and HCC95 cells, the preferred heterodimerization partner HER3 was constitutively activated and no further phosphorylation was observed after EGF stimulation. AG1478 treatment entirely inhibited pHER3, as well as pEGFR and pHER2 in HCC4006 cells, whereas the blockade of HER3 transactivation was gradually released along the reduced AG1478 concentrations in HCC95 cells (Figure 14A and C, middle panel). In contrast, under starve condition, HER3 phosphorylation in NCI-H1975 cells was totally suppressed compared with untreated control cells, and remained so despite EGF stimulation (Figure 14B, middle panel).

Concerning the constitutive EGFR phosphorylation in HCC4006 and NCI-H1975 cells, we wish to determine whether the downstream signaling is activated. In HCC4006 cells, EGFR continued to activate PI3K/AKT and MAPK/ERK signaling, and AKT and ERK1/2 can be further phosphorylated with the addition of EGF (Figure 14A, lower panel). AG1478 treatment completely inhibited pERK1/2 and caused a dramatic reduction of pAKT. In contrast, ERK1/2, but not AKT, was constitutively phosphorylated in NCI-H1975 cells (Figure 14B, lower panel). Our findings suggest that the ERK1/2 pathway is preferentially activated by the EGFR T790M mutation. AKT and ERK1/2 can be further phosphorylated with EGF stimulation, but were minimally affected by AG1478 treatment. In HCC95 cells, pAKT is constitutively activated in serum-starved condition as a result of HER3 permanent phosphorylation, while TKI AG1478 completely abrogated pAKT and pERK1/2 signaling (Figure 14C, lower panel).

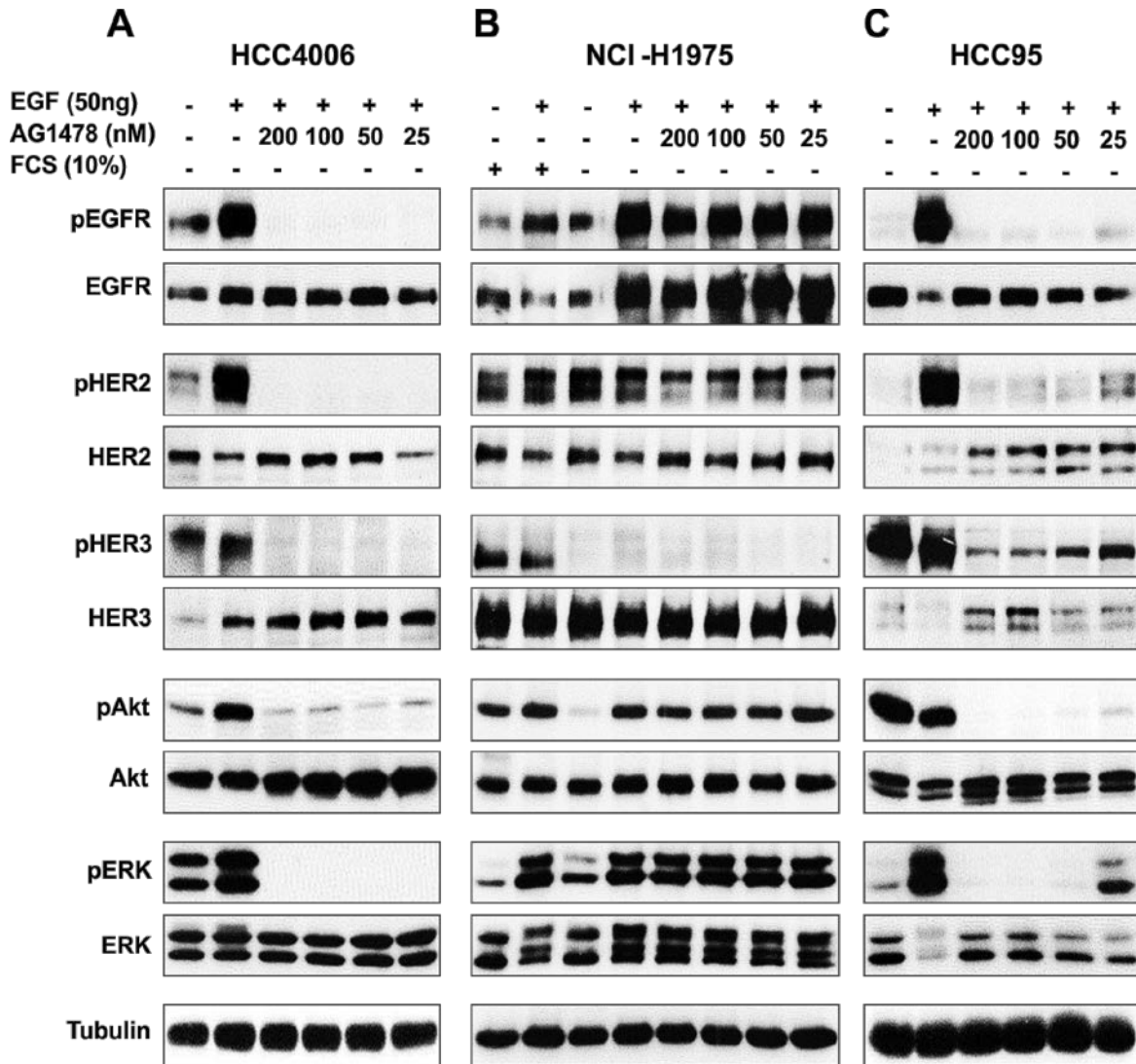


Figure 14. EGFR family signaling upon EGF and AG1478 treatment. Western blot analysis of extracts from serum starved HCC4006, NCI-H1975 and HCC95 cells, untreated or treated with indicated concentrations of AG1478 TKI for 30 minutes, followed by stimulation with 50 ng/ml EGF for 10 minutes. Expression and phosphorylation of EGFR, HER2, HER3, and the downstream signaling molecules AKT and ERK1/2 have been evaluated. Tubulin was used as a loading control.

Then we ask whether EGFR overexpression was necessary to activate AKT and to drive NCI-HCC4006 cell survival? After 48 hours siRNA transfection, western blot assay was applied to test the changes of EGFR, HER2 and HER3 expression. As depicted in Figure 15A and B, the expression levels of these three proteins were effectively suppressed by specific siRNAs when compared with the scrambled control group. We further found that knockdown of EGFR markedly inhibited HER2 and HER3 phosphorylation and slightly suppressed pAKT and pERK (Figure 15A). HER2 and HER3 are the potent activators of the PI3K/AKT and MAPK/ERK pathway, respectively, which were reflected by the downregulation of the activated forms of both elements after specific knockdown of target proteins HER2 and HER3 (Figure 15B and C). Furthermore, siRNA-mediated inhibition of EGFR and HER2 triggered apoptosis shown by cleavage PARP in HCC4006 cells harboring mutant EGFR. As we know, HER2 and HER3 both required EGFR for heterodimerization, which seem to be the important factors contributing to HCC4006 EGFR signaling amplification. Dual-inhibition of EGFR + HER2 or EGFR + HER3 totally abolished the activation of AKT, and also enhanced pERK suppression. Later on, cell viability assay was conducted to determine the effect of siRNA on growth ability. The knockdown of HER2 or HER3 alone or in combination does not significantly affect cancer cell proliferation, while single siRNA of EGFR and the simultaneous inhibition of EGFR + HER2 or EGFR + HER3 decreases cell proliferation to a relative level of $69 \pm 3\%$ compared to the scrambled control group (Figure 15D and E).

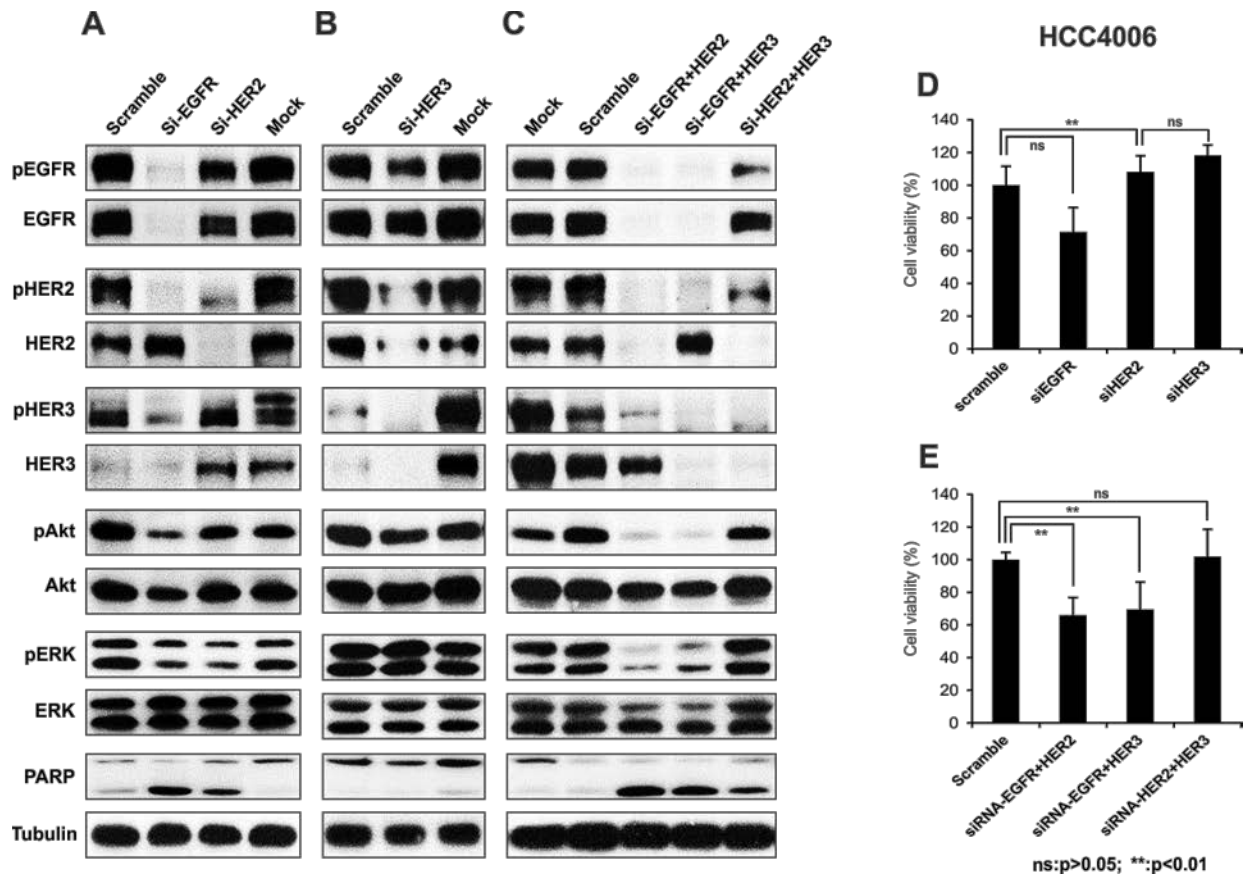


Figure 15. Effect of siRNAs on the silencing of EGFR, HER2 and HER3 in HCC4006 cells. (A-C) Western blot evaluated EGFR signaling after single or double siRNA transfection of EGFR, HER2 and HER3. (D) The decreased number of viable cells after siRNA-mediated specific knockdown of EGFR. (E) Double siRNA knockdown with EGFR + HER2 or EGFR + HER3 enhanced growth inhibition.

These observations suggest that HCC4006 and NCI-H1975 cells, with somatic gain-of-function mutation and “gatekeeper” T790M substitution, respectively, both undergo EGFR-dependent AKT phosphorylation. However, in EGFR wt HCC95 cells, persistent HER3 signaling is associated with acquired resistance to TKIs by permanent activation of AKT.

4.1.3. Evaluation of the cell viability of chemotherapeutics, TKIs, or mAb in combination with SAL on NSCLC cell lines

4.1.3.1. Single drug sensitivity

The initial experiments were set up to screen the responsiveness of NSCLC cell lines HCC4006, NCI-H1975 and HCC95 to combinatorial treatment with SAL and various inhibitors. To that end, we first treated cells with increasing concentrations of chemotherapeutic agents, TKIs and mAb Erbitux for 72 hours. Data showed that HCC4006 cells were very resistant ($IC_{50} > 10 \mu M$) to Gemcitabine, Sutent, Carboplatin (130 $\mu g/ml$) and Erbitux ($IC_{50} > 200 \mu g/ml$), resistant ($1 \mu M < IC_{50} < 10 \mu M$) to SAL, Dasatinib, Lapatinib, SKI-606 and METF (2.5 mM), and sensitive ($IC_{50} < 1 \mu M$) to Afatinib, Paclitaxel, Erlotinib and Gefitinib (Table 7). In contrast, due to EGFR secondary T790M mutation in EGFR, the NCI-H1975 cell line was refractory to all the tested drugs, except Afatinib and Paclitaxel. HCC95 cells were only sensitive to the putative stem cell killer SAL, with IC_{50} value of 50 nM (Table 7).

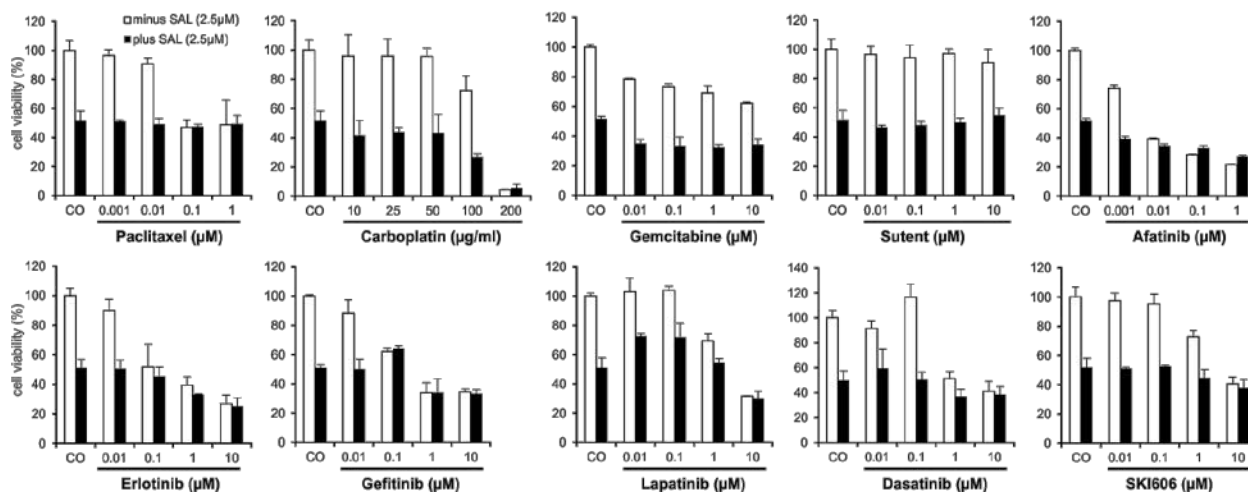
Table 7. Single-drug effects on HCC4006, NCI-H1975 and HCC95 cells

IC_{50} (μM) Drug	Cell line	HCC4006	NCI-H1975	HCC95
Paclitaxel		0.1	0.14	>20
Carboplatin		130 $\mu g/ml$	52.3 $\mu g/ml$	63.5 $\mu g/ml$
Gemcitabine		>10	5.8	>20
Sutant		>10	>20	>20
Afatinib		0.0082	1.3	16.3
Erlotinib		0.15	>10	>20
Gefitinib		0.25	>20	>20
Dasatinib		3	>10	20.3
Lapatinib		3.78	>10	>20
SKI-606		7.3	12.8	16.8
Erbitux		>200 $\mu g/ml$	>200 $\mu g/ml$	>200 $\mu g/ml$
Metformin		2.5 mM	4 mM	6.8 mM
Salinomycin		2.5	5	0.05

4.1.3.2. Treatment of NSCLC cell lines with chemotherapeutic agents, TKIs or mAb in combination with SAL

Next we examined the growth inhibitory effects of the therapeutic drugs in combination with SAL at its IC₅₀. Exposure of HCC4006 cells to SAL didn't significantly increase the cytotoxicity of chemotherapeutic agents, TKIs and Erbitux (Figure 16A). In NCI-H1975 cells, 5 μM SAL enhanced apoptotic effect of Carboplatin at 50 μg/ml and TKIs > 10 μM treatment (Figure 16B), whereas low-dose SAL only potentiated the sensitivity to Carboplatin and Gemcitabine at the indicated concentrations in HCC95 cells (Figure 16C). We didn't observe any inhibitory difference after Erbitux application with 5 different concentrations, so for all three cell lines Erbitux in combination with SAL was not shown in the Figure 16. Collectively, these data suggested that in all three cell lines, the addition of SAL doesn't commonly augment the antiproliferative activity over that achievable with the 11 therapeutic drugs available in the clinic.

A HCC4006



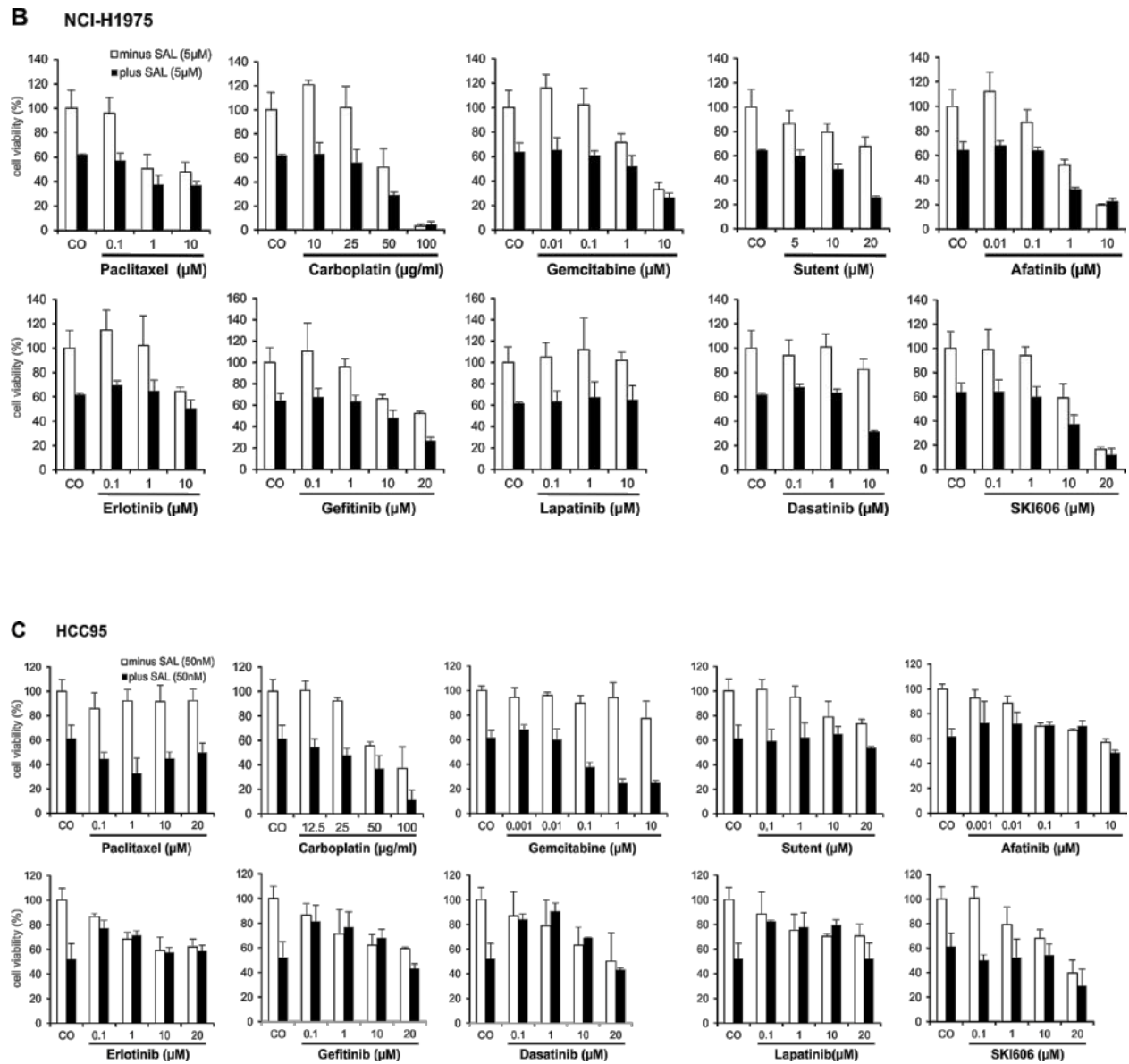


Figure 16. Treatment of NSCLC cell lines with standard therapeutic drugs, TKIs or mAb in combination with SAL. NSCLC HCC4006, NCI-H1975 and NCI-H1650 were exposed to various therapeutic drugs, TKIs, or mAb in combination with SAL for 72 hours. Cell viability was measured via CellTiter-Glo cell viability assay and plotted as a percentage of the viability of DMSO treated cells (control). CO, control.

4.1.4. SAL enhances METF-induced NSCLC cell growth inhibition

As depicted in Figure 17A, METF significantly inhibited the growth of HCC4006, NCI-H1975 and HCC95 monolayer cells in a dose-dependent manner at the 72-hour time point, as revealed by CellTiter-Glo cell viability assay. The mean IC_{50} values of METF were 2.5 mM for HCC4006, approximately 5 mM for both NCI-H1975 and HCC95, indicating that the Gefitinib sensitive cell line HCC4006 with the EGFR in-frame deletion displayed the highest sensitivity to METF. We next examined the efficacy of METF in combination with SAL, to investigate whether SAL could sensitize cancer cells to METF. We observed that SAL, with a fixed dose (IC_{50} value), potentiated the growth inhibitory effects of different concentrations of METF in all three cell lines (Figure 17A). Combined treatment caused a significantly greater inhibition in cellular viability relative to either drug alone on 2D cells.

Consistent with cell growth inhibition, microscopic examination revealed a substantial decrease of cell density and cell death induction upon combinatorial treatment (Figure 17C). More specifically, treatment with 2.5 μ M SAL induced vacuole formation in HCC4006 cells, and the number of vacuoles increased after co-administration of METF, whereas either drug alone or in combination promoted NCI-H1975 cells to a more mesenchymal phenotype. HCC95 cells are mainly composed of two different types of cells, which are epithelial-type-cells directly attaching to the plate surface, and apoptotic-like cells sitting on the top of epithelial-like cells, which changed to the mesenchymal type after SAL or METF single application and almost vanished when these two drugs were combined.

Spheroids were considered as an *in vitro* model to mimic some aspects of tumor heterogeneity and hierarchy controlled by CSCs. Exposure of alveospheres of HCC4006, NCI-H1975 and HCC95 cells to the same concentrations of METF turned out to be less effective than 2D, whereas co-exposure to SAL significantly enhanced METF efficiency (Figure 17B).

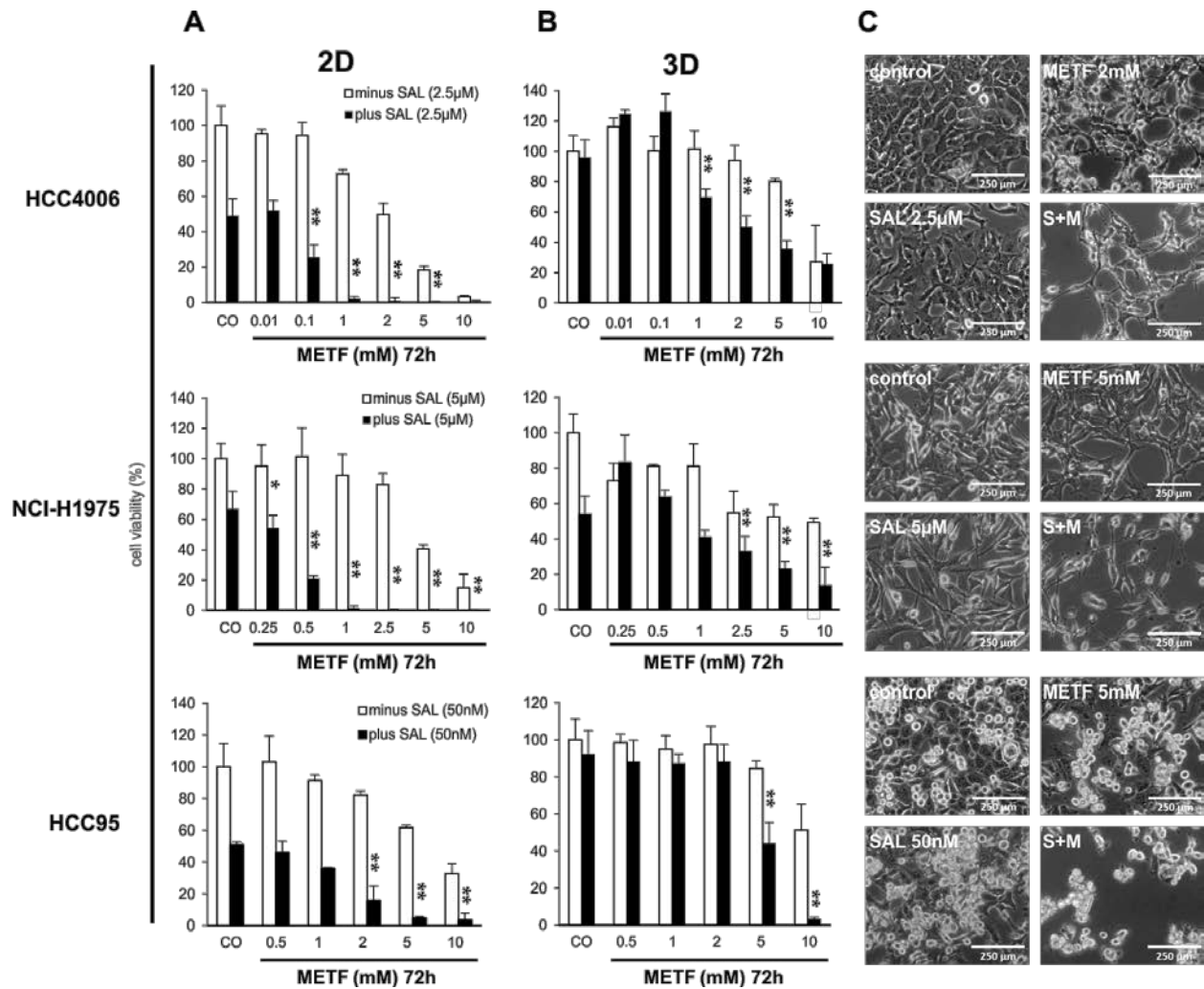


Figure 17. SAL increases METF-mediated effects on cell viability of treated NSCLC monolayer cells (2D) and spheroids (3D). Culture HCC4006, NCI-H1975 and HCC95 monolayer cells (2D) (A) and spheroids (3D) (B) for 72 hours in the presence of increasing amounts of METF with and without SAL. Cell growth was assessed using CellTiter-Glo cell viability assay and plotted as a percentage of the viability of DMSO treated cells (control). The asterisks indicate significant differences versus SAL (** $P < 0.01$, * $P < 0.05$). (C) Microscopic examination after 48 hours drug treatment. CO, control; S+M, combination of SAL and METF.

RESULTS

To determine if the cytotoxic effects of METF/SAL complex are limited to these three cell lines, we treated a panel of additional NSCLC cell lines with different genetic characteristics, namely NCI-H1650 (EGFR del E746–A750, PTEN null), NCI-H2122 (EGFR wt, KRAS mutation, LKB1 inactivation) and NCI-H3122 (EGFR wt, EML4-ALK translocation) [54, 144]. These data confirmed that co-administration of METF and SAL elicited stronger inhibition of cell growth of 2D and 3D cells of these additional cell lines over single treatment (Figure 18). Of note, alveospheres derived from the NCI-H2122 cell line were more sensitive than monolayer cells to either drug alone or their combination (Figure 18, middle panel).

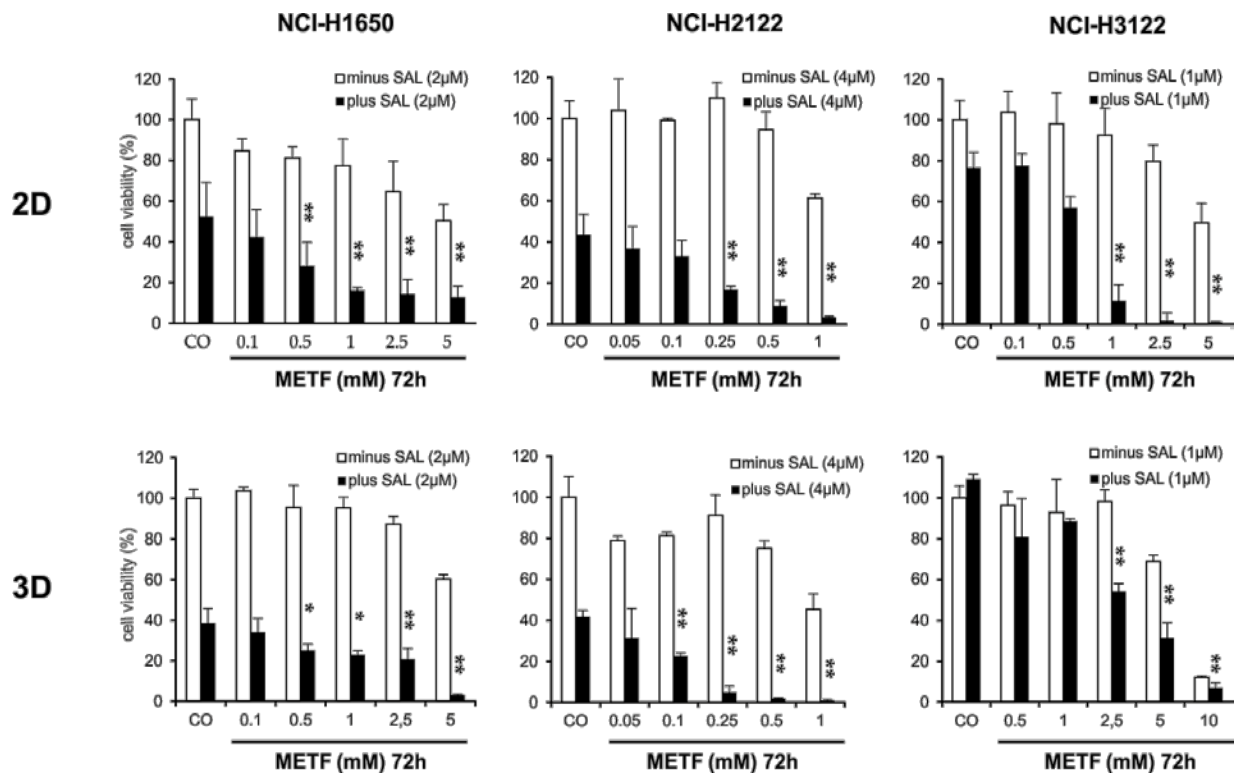


Figure 18. SAL enhances growth inhibition after co-administration of METF on NCI-H1650, -H3122 and -H2122 2D and 3D cells. Culture NCI-H1650, NCI-H3122 and NCI-H2122 monolayer cells (2D) and spheroids (3D) for 72 hours in the presence of increasing amounts of METF with and without SAL. Cell growth was assessed using CellTiter-Glo cell viability assay and plotted as a percentage of the viability of DMSO treated cells (control). The asterisks indicate significant differences versus SAL (**P<0.01, *P<0.05). CO, control.

To determine whether the combination of METF and SAL has synergistic or merely additive activity, we performed isobologram analysis to assess their inhibitory effects [138, 145]. In our data, specific effect with IC_{50} , IC_{65} and IC_{75} levels have been selected for NCI-H1975, HCC95 and HCC4006 cells, respectively (Figure 19). These 3 data points showed similar cell growth inhibition having been achieved via co-administration of METF and SAL. As indicated in the isobologram, all dose pairs fell below the straight line, which reflected a synergistic effect. Moreover, treatment of these three lung cancer cell lines with SAL synergized with all indicated concentrations of METF on cell growth inhibition.

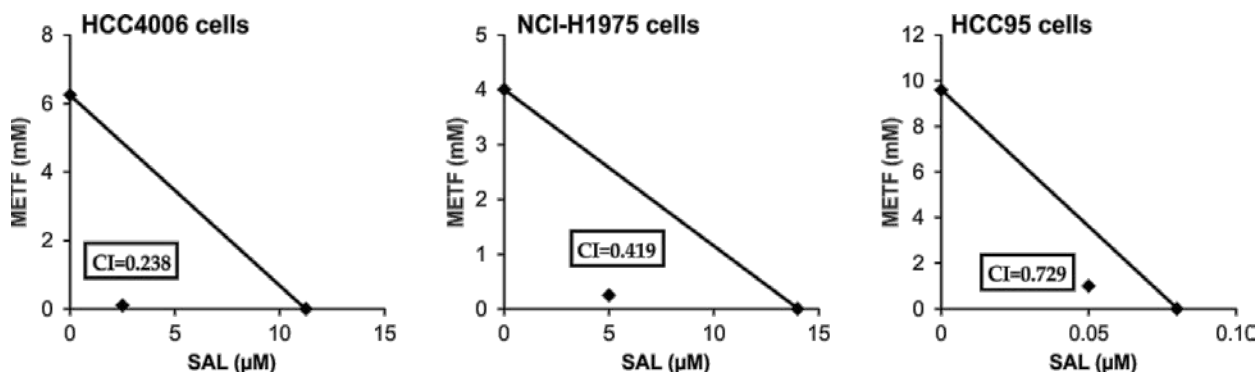


Figure 19. Isobologram analysis of inhibition of cell viability under combination treatment. Data points (♦) reflecting the concentrations of METF and SAL were plotted as the ordinate and abscissa respectively, and were represented as average of three independent experiments.

Taken together, these findings suggest that METF, which modestly inhibits the growth of NSCLC monolayer cells and alveospheres in a dose-dependent manner, interacts synergistically with SAL.

4.1.5. Inhibition of EGFR signaling in NSCLC cells is achieved with the combination of METF and SAL

To further characterize the downstream EGFR signaling pathway that might correlate with the observed growth inhibition, we examined the effect of the two drugs on the expression of several key regulators as biomarkers of response. Using western blot analysis, a weak inhibition of EGFR, HER2 and the downstream regulators of signaling AKT and ERK1/2 expression and phosphorylation could be detected after 48 hours treatment of HCC4006 cells with METF or SAL alone, in addition to the pHER2 inhibition after exposure to single agent SAL (Figure 20A). In contrast, these endogenous proteins showed a pronounced downregulation after combinatorial treatment. As depicted in Figure 20B, pEGFR was highly sensitive to SAL in NCI-H1975 cells, and the inhibition of pEGFR and pHER2 was METF dose dependent. This combination-induced reduction of phospho-status of EGFR, HER2, and the mediators AKT and ERK1/2 was further augmented after co-administration of 5 mM METF and 5 μ M SAL. Cell death development of tested cell lines was assessed by PARP cleavage. Here we observed that co-administration increased the levels of cleaved PARP in both cell lines (Figure 20A and B, lower panel). In HCC95 cells, single-agent treatment with METF and SAL didn't show obvious inhibition on total and phosphorylated EGFR, HER2, AKT and ERK1/2, however, the activated forms of these investigated proteins were highly suppressed under their combination (Figure 20C).

To corroborate this strong inhibition on an in vitro tumor model, multicellular alveospheres were also exposed to METF and SAL. Here we mainly focused on the expression and activated forms of EGFR and downstream mediators AKT and ERK1/2. Clearly, as shown in Figure 20D, alveospheres generated from HCC4006 cells were more resistant than monolayer cells, and a distinct effect was observed after treatment with 5 mM METF and 2.5 μ M SAL, which displayed in 2D the inhibition of tubulin protein expression. In contrast, NCI-H1975 3D cells can defend higher dose administration, since 5 or 10 mM METF in combination with 5 μ M SAL inhibited phosphorylation of EGFR and ERK1/2 compared with single drug treatment, but still not sufficient to completely block this pathway (Figure 20E). For alveospheres generated from these two cell lines, more rounds of treatment could be necessary for further suppression of proteins mentioned above and induction of cell death. In HCC95 spheres, co-administration of 10 mM METF entirely abrogated pAKT and pERK1/2 (Figure 20F).

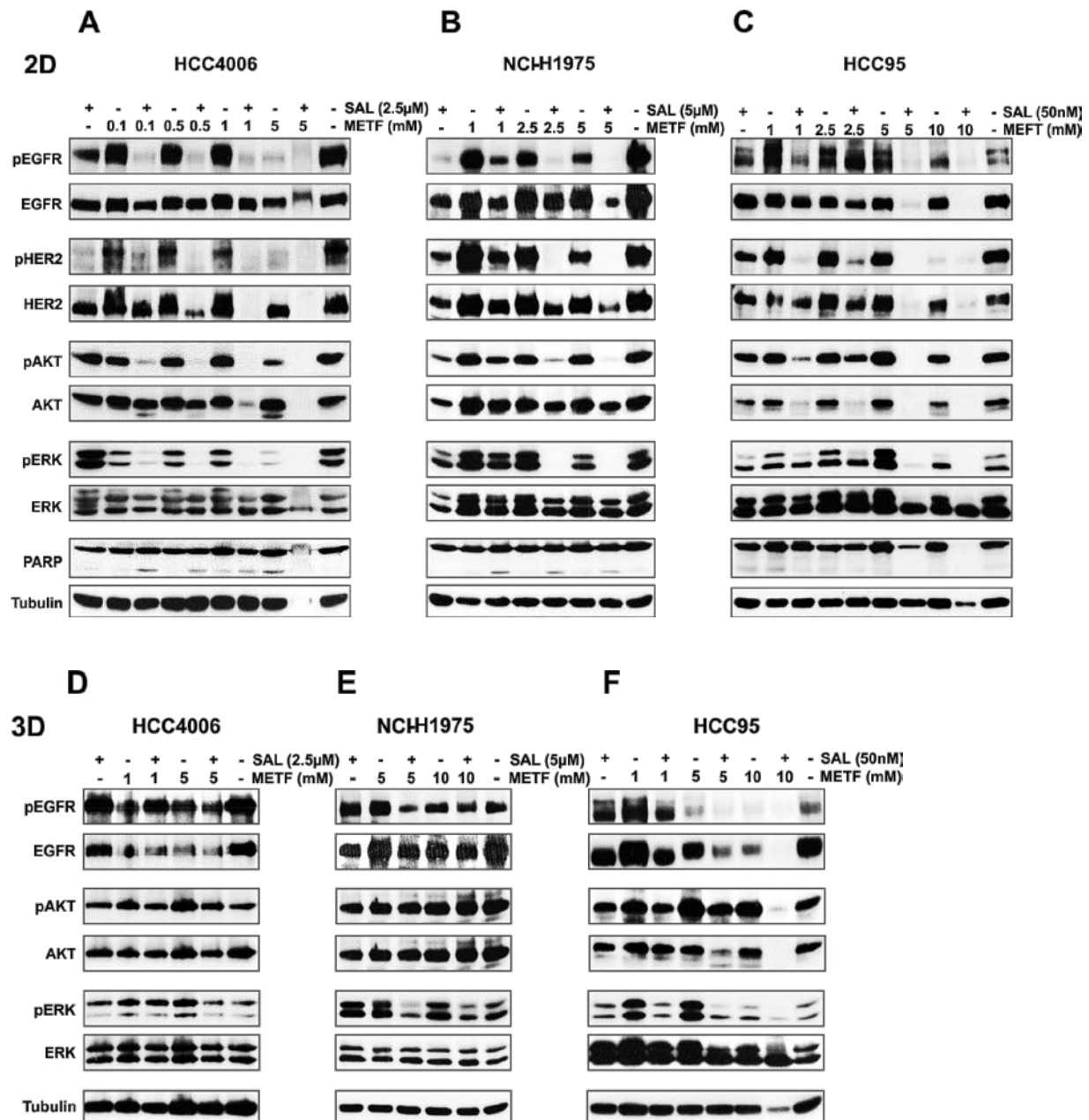


Figure 20. EGFR signaling in HCC4006, NCI-H1975 and HCC95 2D and 3D upon METF and SAL treatment. (A-C) Monolayer cells-2D and (D-F) spheroids-3D were exposed to the indicated concentrations of METF, SAL and their combinations for 48 hours, as specified. After harvesting, cells were lysed and prepared for western blot analysis of downstream molecules of EGFR signaling. Tubulin served as a loading control.

4.1.6. Cell growth inhibitory effect of combinatorial treatment with METF and SAL is AMPK independent

METF, as an AMPK-activating compound, is widely used to suppress cancer cell proliferation. To analyze whether the cell growth inhibitory effect of treatment with METF and SAL is also mediated by activation of the AMPK signaling pathway, several key proteins and associated phosphorylation status have been evaluated. At the indicated two concentrations, METF activated AMPK in a dose-dependent manner in the HCC4006 and HCC95 cell lines (Figure 21A and C), while negatively regulated phosphorylations of AMPK and downstream molecules mTOR and p70 s6k in NCI-H1975 cells (Figure 21B). The results suggested that METF functions as a potent AMPK-independent antiproliferative agent, and AMPK activation may be due to physiological adaptation to metabolic stress. The combination of SAL and lower dose METF (1 mM for HCC4006, 2.5 mM for both NCI-H1975 and HCC95) strongly induced AMPK activation and associated mTOR and p70 s6k downregulation. In contrast, co-administration of 5 mM METF caused a near-complete abolition of activated forms of these proteins, and a clear suppression of total protein expression was seen in all three cell lines (Figure 21). Overall, SAL potentiated the inhibitory effect of high dose METF, in our case 5 mM, on NSCLC cell proliferation through unique AMPK-independent mechanisms.

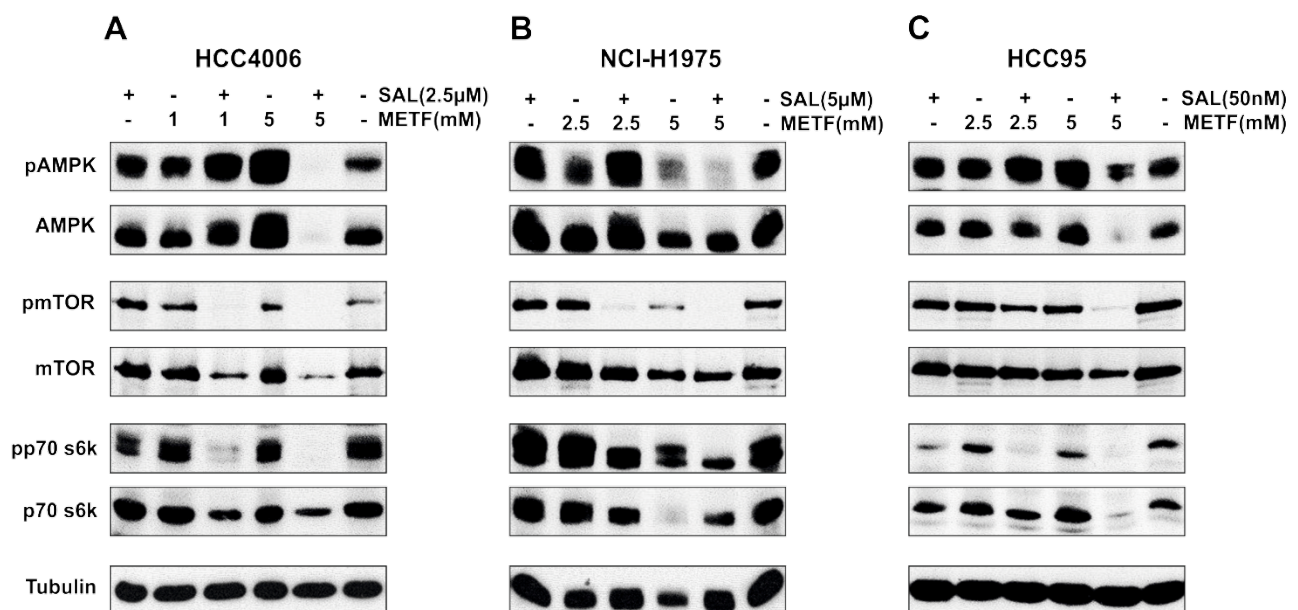


Figure 21. AMPK signaling in NSCLC HCC4006, NCI-H1975 and HCC95 cell lines upon METF and SAL combinatorial treatment. (A-C) Monolayer cells were exposed to the indicated concentrations of METF, SAL and their combinations for 48 hours, as specified. After harvesting, cells were lysed and prepared for western blot analysis of downstream molecules of AMPK signaling. Tubulin served as a loading control.

4.1.7. Human phospho-kinase assay after combinatorial treatment with METF and SAL

To get a broader view on signaling inhibition after combinatorial treatment of the HCC4006 and NCI-H1975 cells with METF and SAL, we utilized phospho-kinase array to investigate the phosphorylation of 43 kinases and 2 transcription factors (Figure 22A and B). As mentioned above, these two cell lines represent different EGFR mutation status related to Gefitinib sensitivity. In HCC4006 cells, phosphorylation of ten proteins (ERK1/2, AKT, CREB, β -catenin, Src, Lyn, Yes, Chk-2, FAK and P53) was downregulated following co-administration of 1 mM METF and 2.5 μ M SAL (Figure 22C). The phospho-status of these proteins became more notable when we applied both drugs to NCI-H1975 cells (Figure 22D); besides, ribosomal S6 kinase (rsk) family member phosphorylation also declined upon treatment in combination with 2.5 mM METF and 5 μ M SAL (Figure 22D). It is worth to note that in HCC4006 cells, activation of three Src family members did substantially respond to single agent, the same for SAL alone for treatment of NCI-H1975 cells. The finding that combined METF and SAL induced cell growth inhibition, suggests the multiple roles of this combination in reducing oncogenic effects of modules involved in EGFR, Wnt and AMPK signaling, cell adhesion and cell cycle regulation.

RESULTS

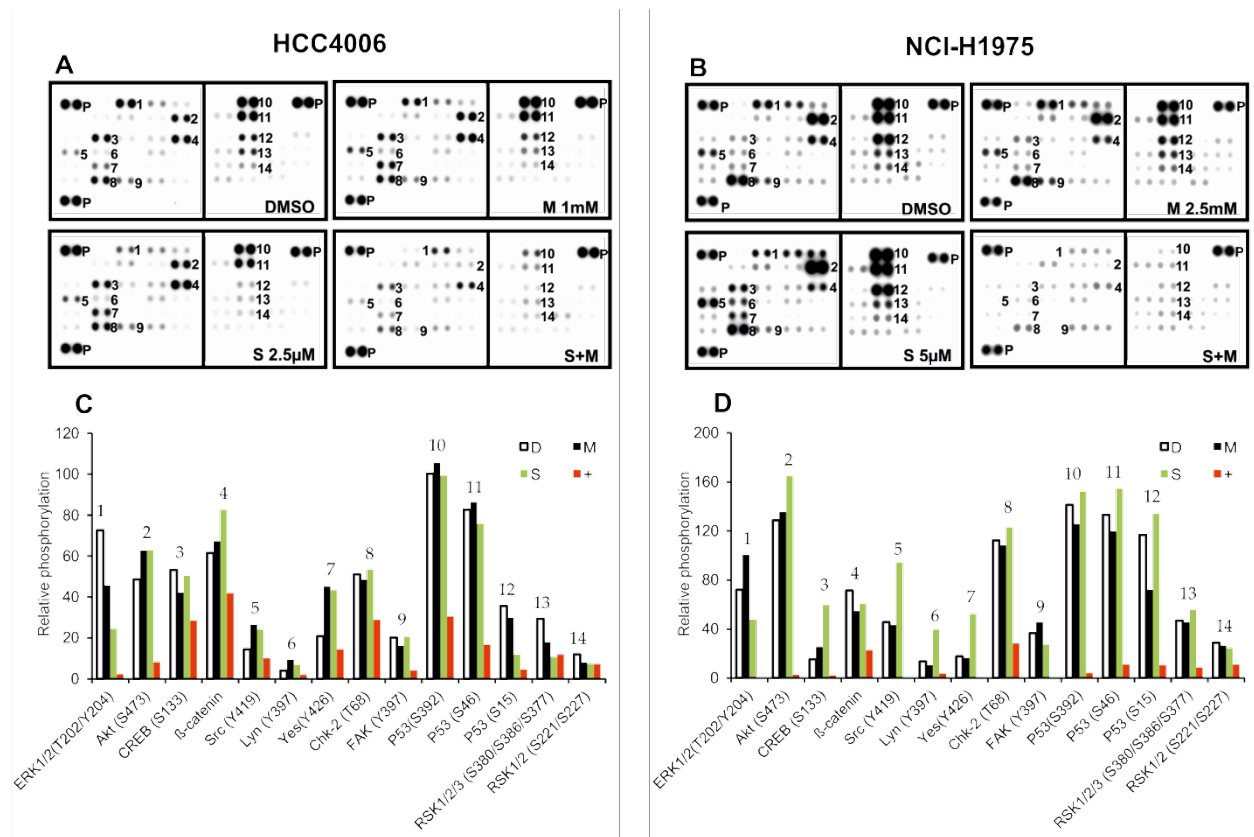


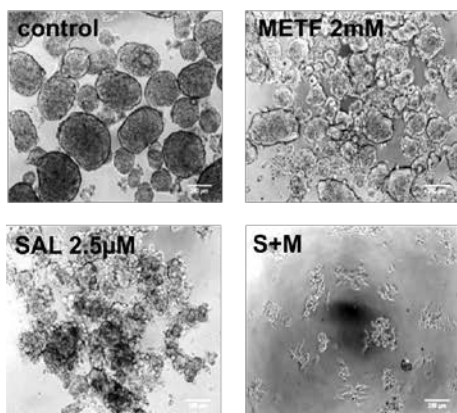
Figure 22. Phospho-kinase signaling after treatment of HCC4006 and NCI-H1975 with METF and SAL. (A and B) Whole-cell lysates from HCC4006 and NCI-H1975 after treatment with METF, SAL and combination were collected for human phospho-kinase array analysis. Each membrane contains kinase specific (number indicated) and positive control (P) antibodies spotted in duplicate. (C and D) Relative phosphorylation of spots was quantified by normalizing pixel density of the positive control to 100. Each bar is represented as mean of duplicate spots. D, DMSO; M, METF; S, SAL; +, combination of SAL and METF.

4.1.8. Combination of METF and SAL effectively inhibits sphere formation of NSCLC cell lines with different EGFR, KRAS, EML4/ALK and LKB1 status

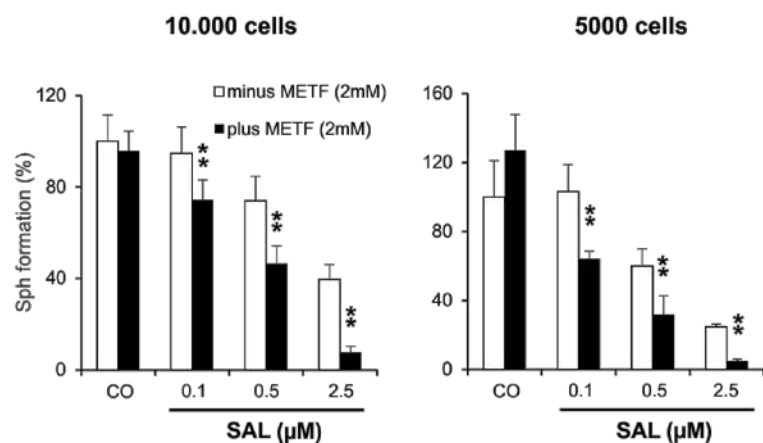
CSCs are characterized by their ability to form tumor spheres after seeding cells in serum-free media [141]. We therefore performed tumor-sphere assays with cells grown in the presence of METF, SAL, or both. Briefly, monolayer cells were treated with METF, SAL alone or in combination for 48 hours, then trypsinized and replated with 5,000 and 10,000 cells in ultra-low adherent 96-well plates for sphere generation with the continued presence of certain drugs. Representative images of spheroids indicated that in HCC4006 cells single agent SAL and, to a lesser extent, METF inhibited sphere formation (SF), whereas their combination prevented generation of spheroids most effectively (Figure 23A). At a density of 10,000 cells per well, all combinations especially with 2 mM METF and 2.5 μ M SAL showed statistically significant SF inhibition with ± 7 folds reduction compared to METF treatment (Figure 23B), and the effect of inhibition was more noticeable when 5,000 cells were seeded. Meanwhile, we noted that combinatorial treatment greatly reduced or abolished sphere generation under both amounts of seeded NCI-H1975 cells (Figure 23C and D). Similarly, co-administration of 50 nM SAL and 1 or 2.5 mM METF resulted in 2.5 and 3 folds decrease, respectively, in tumor SF in HCC95 cells (Figure 23E and F).

HCC4006

A

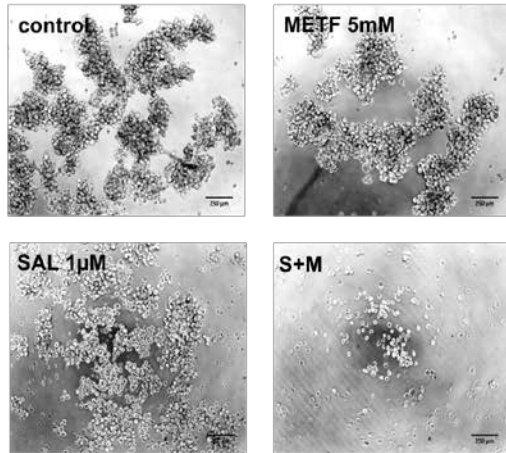


D

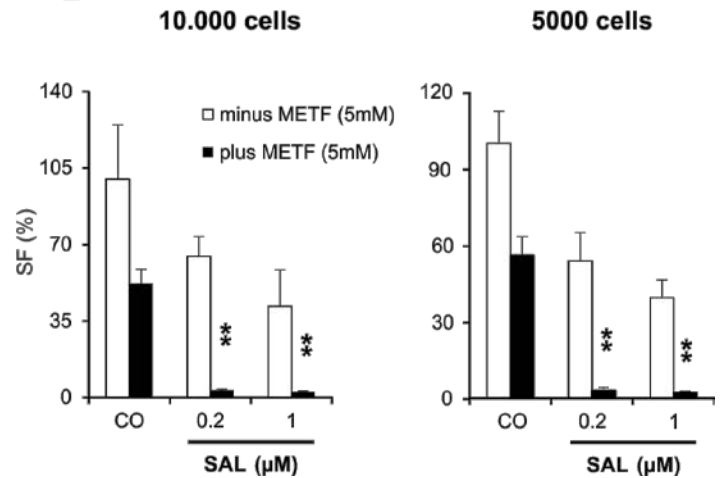


NCI-H1975

B

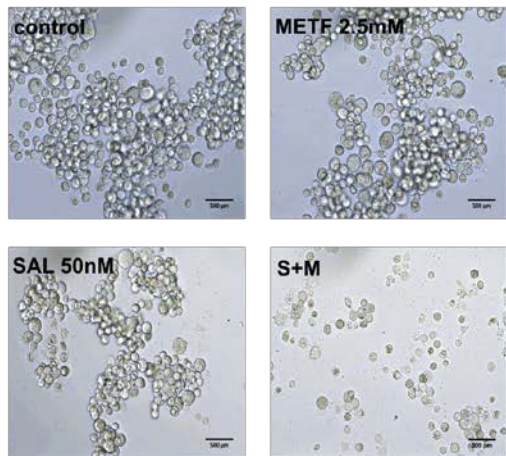


E



HCC95

C



F

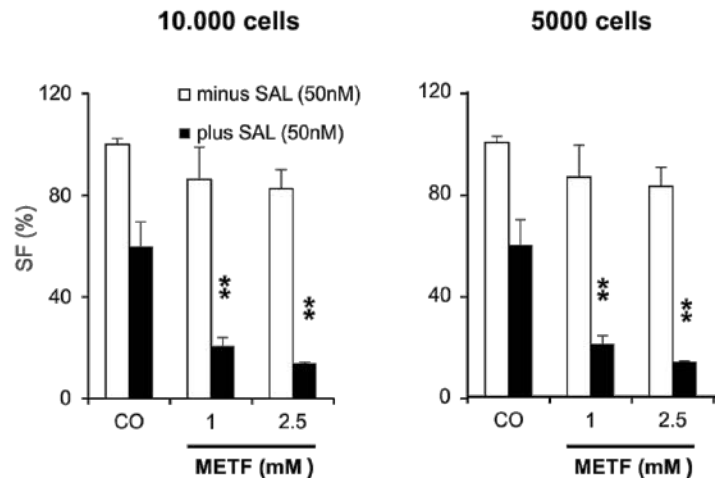


Figure 23. Combination of METF and SAL effectively targets CSCs. (A-C) Monolayer cells from HCC4006, NCI-H1975 and HCC95 after 48 hours treatment with indicated concentrations of METF and SAL were trypsinized and seeded with 10,000 cells into ultra-low adherent 96-well plate for three days of SF with further drug treatment. (D-H) After drug treatment of indicated cell lines, average cell numbers from formed spheroids were evaluated by CellTiter-Glo cell viability assay. CO, control; S+M, combination of SAL and METF.

To confirm these observations, we examined two other Gefitinib resistant NSCLC adenocarcinoma cell lines NCI-H3122 and NCI-H2122, with the same validation settings (Figure 24). SF analysis confirmed that combinatorial treatment caused a dramatic reduction in the number of spheroids derived from these two cell lines within 96 hours as a consequence of cell death. As an aside, NCI-H2122 spheres exhibited a large reduction of cell viability after SAL single agent treatment; however, co-exposure of METF still enhanced this effect. These data demonstrate the combination of METF and SAL could be a potent killer for lung cancer alveospheres/CSCs.

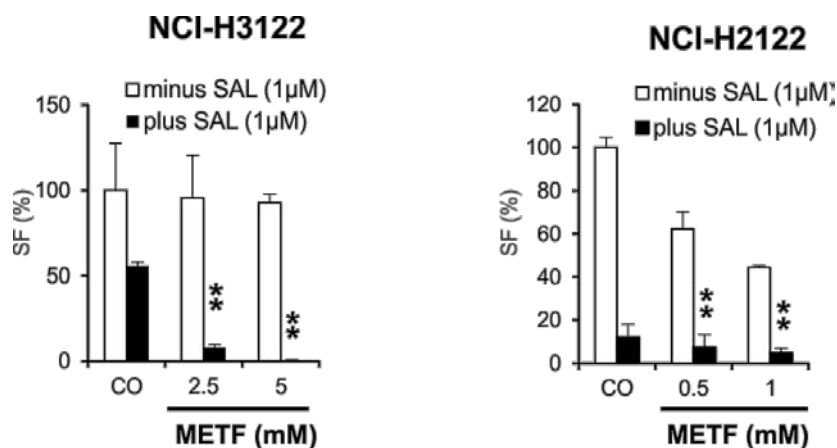


Figure 24. METF in combination with SAL markedly inhibits SF in NCI-H3122 and NCI-H2122 cells. Monolayer cells from NCI-H3122 and NCI-H2122 after 48 hours treatment with indicated concentrations of METF and SAL were trypsinized and seeded with 10,000 cells into ultra-low adherent 96-well plate for three days of SF with further drug treatment. After drug treatment of indicated cell lines, average cell numbers from formed spheroids were evaluated by CellTiter-Glo cell viability assay. CO, control.

4.1.9. Suboptimal Erlotinib stimulates SCM expression of EGFR wt NSCLC cell lines

Of note, in SF assays, exposure of HCC95 cells to 1 μ M Erlotinib increased the amount and size of spheroids (Figure 25A). To identify SCMs that are differentially regulated in generated compact spheres, we profiled gene expression relative to DMSO-treated control using real-time PCR. Obtained data indicated that the most widely used SCMs (Nanog, Sox2, CD44 and BMI1) were higher expressed after 1 μ M Erlotinib treatment of 3D cells, as anticipated (Figure 25B). Furthermore, the same strategy was applied to 6 other selected NSCLC cell lines, namely NCI-H2122, NCI-H1568, NCI-H3122, HCC4006, NCI-H1975 and NCI-H1650 (see cell line characteristic in Table 6). Here we noted the same tendency of SCM upregulation in the context of EGFR wt cells (Figure 25C-E).

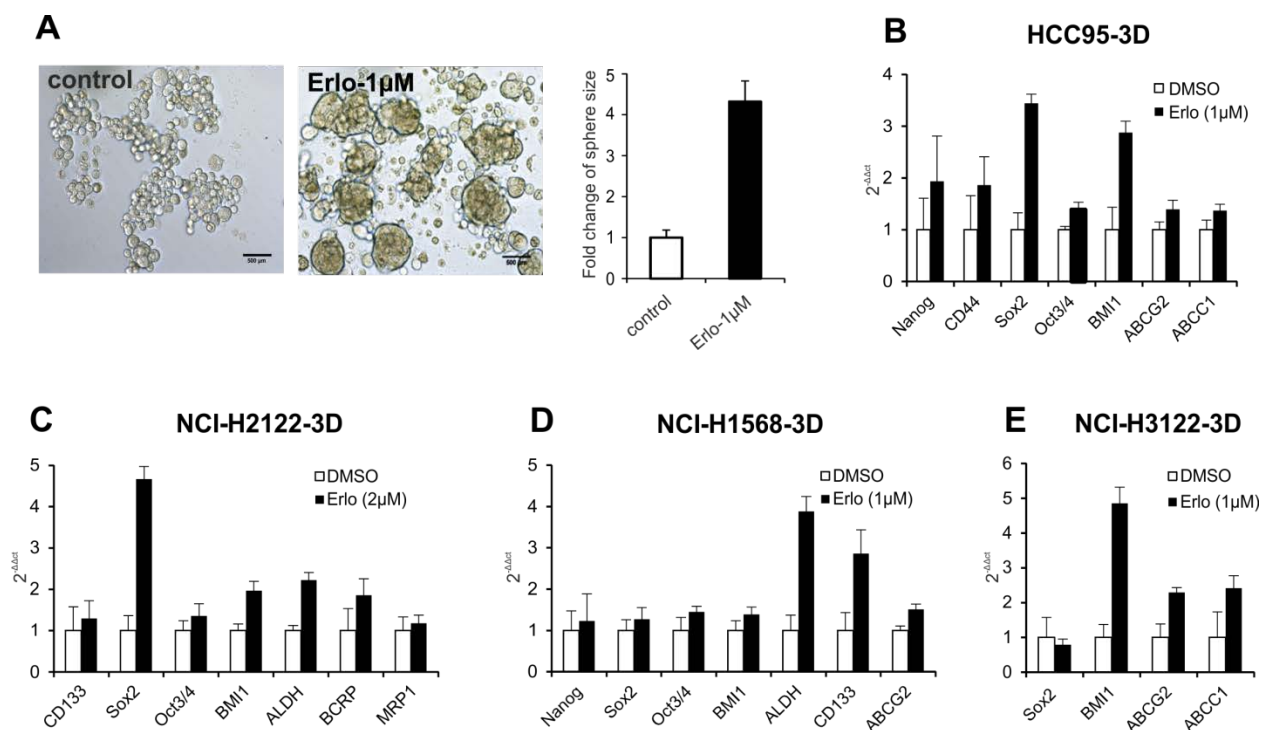


Figure 25. Elevated SCM expression upon insufficient Erlotinib treatment of EGFR wt NSCLC cell lines. (A) Phase-contrast micrographs of HCC95 spheroids. After 48 hours treatment with 1 μ M Erlotinib, 10,000 HCC95 monolayer cells were seeded into ultra-low adherent 96-well plate for three days of SF. (B-E) Real-time PCR analysis showed increased SCMs after low-dose Erlotinib treatment on formed spheres that were generated from indicated EGFR wt lung cancer cell lines. Erlo, Erlotinib.

However, there were no significant differences in gene expression levels (± 1.4 folds change) in EGFR mutated HCC4006 and NCI-H1975 cells upon 0.1 and 1 μ M Erlotinib treatment, respectively (Figure 26A and B). After exposing NCI-H1650 cells which harbor the inactivated tumor suppressor PTEN to 1 μ M Erlotinib, only CD133 and BMI1 showed less than 2 folds increase (Figure 26C).

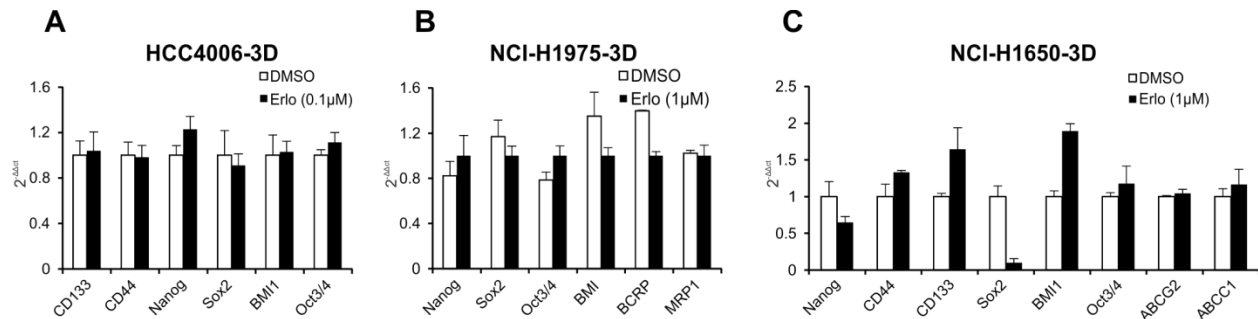


Figure 26. Stem cell marker expression under suboptimal doses of Erlotinib treated NSCLC cells with EGFR mutation. 2D cells from three EGFR mutated cell lines (HCC4006, NCI-H1975 and NCI-H1650) were exposed to 1/10 of IC₅₀ values of Erlotinib for 48 hours. Real-time PCR was applied to detect the difference of SCM expression of spheroids formed in non-adherent culture dishes compared with DMSO treatment. Erlo, Erlotinib.

Taken together, our results for the first time demonstrate that suboptimal doses of Erlotinib could stimulate stem cell associated gene expression profiles, suggesting a post-treatment transition towards properties of stem cells. We speculate an increased CSC population after insufficient-dose Erlotinib treatment of NSCLC cell lines with EGFR wt genotype could explain a possible association of 2D and 3D cells with acquired drug resistance.

4.1.10. METF abrogates Erlotinib induced apoptosis in NSCLC cell lines independent of the EGFR status

METF, as shown above, strongly exerted cell growth inhibition on all tested NSCLC cell lines (Figure 16 and 17). Next we would like to get more insight into the molecular mechanisms responsible for the cytotoxic effect of Erlotinib after co-administration of METF. Here we showed the data of cell lines with Erlotinib resistant (HCC95, NCI-H2122, NCI-H1650 and NCI-H1975) and sensitive genotype (HCC4006 and HCC827). EGFR downstream signaling evaluation indicated this combination, in comparison with single drug, strongly inhibited EGFR phosphorylation (Figure 27, upper part of each panel). Nevertheless, co-administration of METF reduced Erlotinib cytotoxicity via activation of AKT, a well-known anti-apoptotic signal regulator. Due to PTEN deletion in NCI-H1650 cells, AKT is continuously activated, however, we can still observe slight increase under 1 and 10 μ M Erlotinib alone treatment (Figure 27, middle part of each panel). As assessed by PARP cleavage, METF with IC₅₀ value, which didn't initiate significant apoptosis in comparison with control, reduced Erlotinib-induced PARP activation (Figure 27, bottom part of each panel). We further investigated whether the modulation of ERK1/2, involved in cell proliferation, responds to the cytotoxicity effect of METF. In two out of six cell lines (NCI-H2122 and NCI-H1650), METF stimulated the phosphorylation of ERK1/2 after co-administration of Erlotinib (Figure 27, lower part of each panel). Meanwhile, we also noticed this antagonistic effect in HCC95 cells treated with suboptimal doses of Erlotinib (0.1 and 1 μ M). Thus, our data argue against the involvement of ERK1/2 activity in METF-mediated cell inhibition, indicating METF abrogated Erlotinib cytotoxicity via activation of AKT, irrespective of the ERK1/2.

These data warrant caution when considering METF for type 2 diabetic lung cancer patients receiving Erlotinib or as adjuvant treatment in Erlotinib-based chemotherapeutic settings.

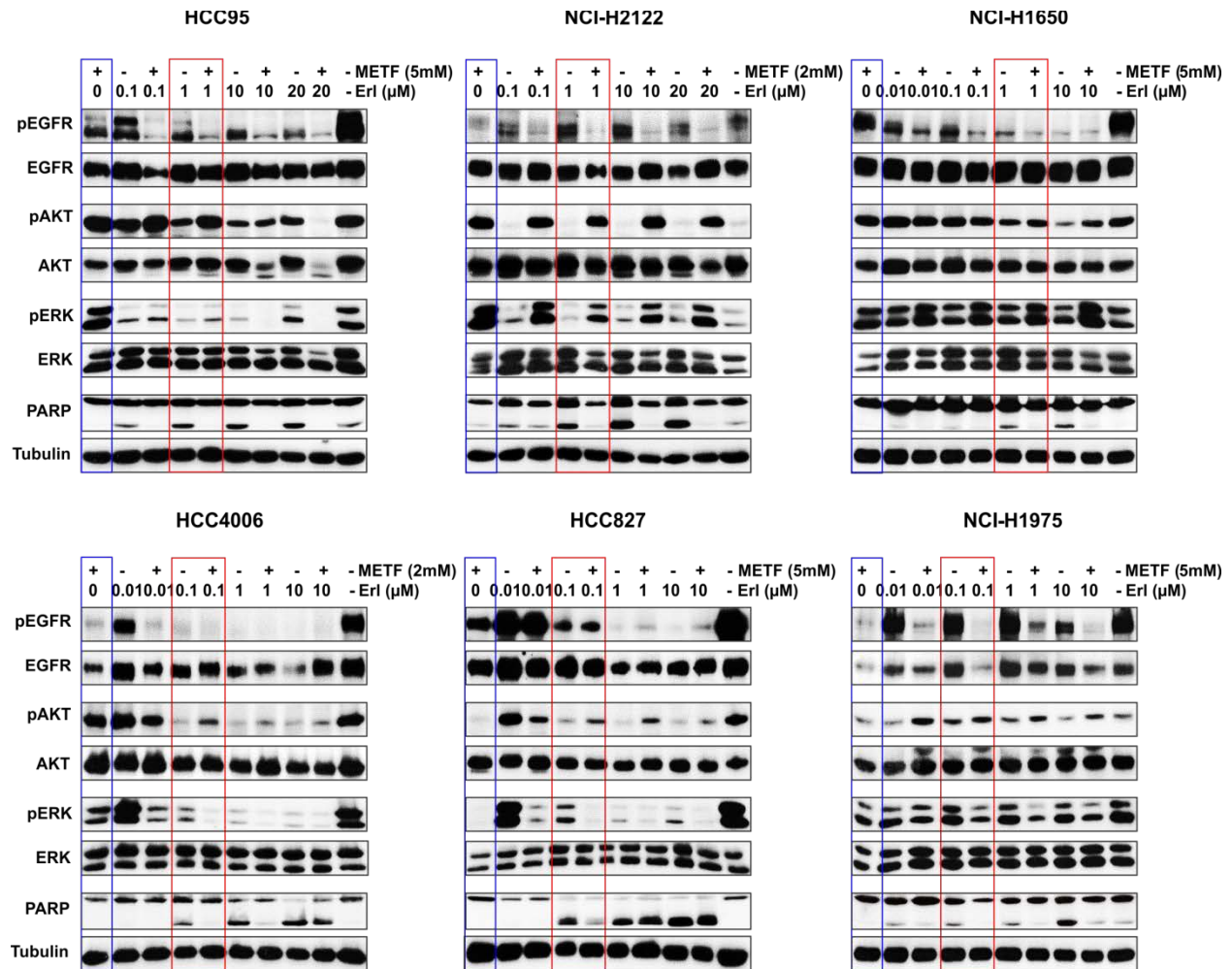


Figure 27. Effects of Erlotinib and METF on the EGFR signaling and downstream modules AKT, ERK1/2 and PARP. Four Erlotinib resistant (HCC95, NCI-H2122, NCI-H1975, NCI-H1650) and two sensitive (HCC4006, HCC827) NSCLC cell lines were exposed for 48 hours to the increasing amounts of Erlotinib with and without IC₅₀ value of METF. Western blots are shown for PARP, phospho- and total EGFR, AKT, ERK1/2. Tubulin served as a loading control. Erl, Erlotinib.

Chapter II

4.2. NSCLC cell line NCI-H1568 heterogeneity as a new approach to investigate chemoresistance

4.2.1. SAL interacts synergistically with Erlotinib on cell growth inhibition of NCI-H1568 wt/pool cells

Erlotinib which specifically targets mutated and overactive EGFR (see in introduction) is widely used for the treatment of NSCLC patients. In this study NCI-H1568 pool cells were investigated to determine how cells survive after treatment with different concentrations of Erlotinib (2.5, 5 and 10 μM). Real-time PCR demonstrated the elevated expression of stem cell markers at 24 and 48 checking points (Figure 28A and B). This could indicate that CSCs with an increased cell number survived Erlotinib application. We hypothesized that Erlotinib in NCI-H1568 wt cells targets rapidly proliferating cells, but spares slow-dividing cells representing chemoresistant phenotype. As published before, SAL is a promising killer of CSCs; we further investigated the growth inhibitory effect of combinatorial treatment with SAL and Erlotinib. First we treated NCI-H1568 wt cells with various concentrations of SAL and Erlotinib individually. Cell viability data indicated that NCI-H1568 wt cells were very resistant to Erlotinib with IC_{50} more than 20 μM , and resistant to SAL with IC_{50} around 2.5 μM (Figure 28C and D). In the further experiment, we combined three different concentrations of Erlotinib (0.2, 2 and 20 μM) with various concentrations of SAL, such as IC_{50} (2.5 μM), IC_{70} (0.5 μM) and IC_{90} (0.1 μM). Treatment of NCI-H1568 pool cells with combination of SAL and Erlotinib demonstrated enhanced growth inhibition over that observed with either agent exposure (Figure 28 E-G). The beneficial effect of combinatorial treatment is evident for all combinations with a more significant effect observed when a higher dose of SAL was used.

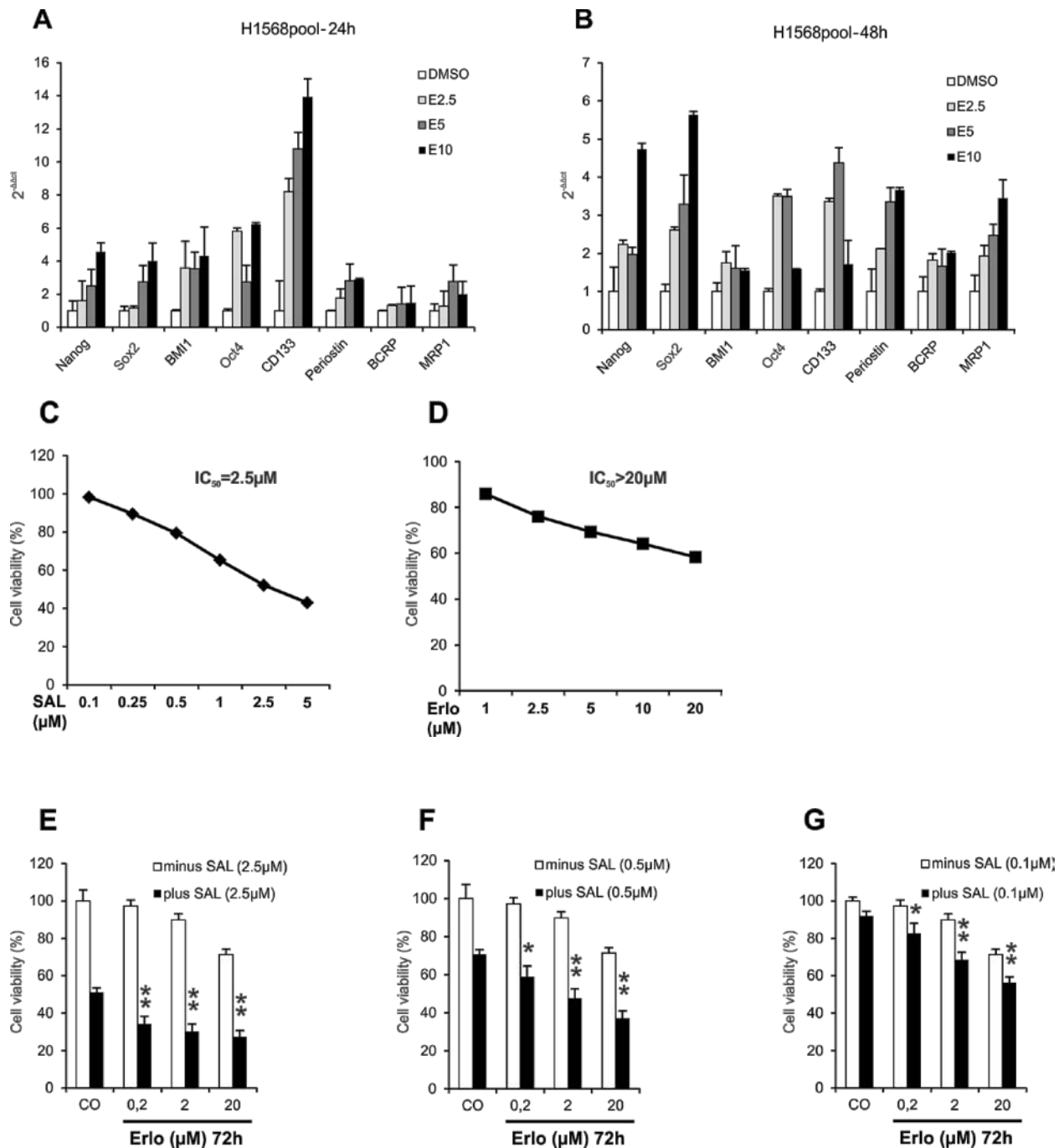


Figure 28. Effects of combinatorial treatment with Erlotinib and SAL on cell viability of NCI-H1568 cells. (A and B) Elevated SCM expression after 24 (A) and 48 hours (B) treatment upon various concentrations of Erlotinib of NCI-H1568 cells. (C and D) IC_{50} values of SAL (C) and Erlotinib (D) on NCI-H1568 cells. (E-G) SAL enhanced growth inhibition after co-administration of different concentrations of Erlotinib on NCI-H1568 cells. Culture NCI-H1568 pool cells for 72 hours in the

presence of increasing amounts of Erlotinib with and without SAL under concentrations of 2.5 (E), 0.5 (F) and 0.1 μM (G). Cell growth was assessed using CellTiter-Glo cell viability assay and plotted as a percentage of the viability of DMSO treated cells (control). The asterisks indicate significant differences versus SAL (** $P < 0.01$, * $P < 0.05$). CO, control; Erlo, Erlotinib.

4.2.2. Effect of SAL in combination with Erlotinib on EGFR signaling

To further estimate EGFR signaling that might correlate with the observed growth inhibition, we examined the effect of Erlotinib and SAL alone or in combination on the activation state of several key regulators involved in the EGFR signaling pathway. Western blot analysis identified that 48 hours treatment with the increasing concentrations of Erlotinib resulted in a gradual reduction in the activated forms of EGFR, HER2 and HER3, which were further reduced in the face of co-administration of SAL (Figure 29, upper panel). Suppression of phosphorylated ERK1/2, a downstream molecule of EGFR signaling, was observed with dual inhibition, but the extent of inhibition was much less than all the receptors above-mentioned (Figure 29, below panel). At this check points, AKT was strongly activated upon SAL monotherapy, whereas a remarkable upregulation was observed under higher dosage SAL (2.5 μM) application. Co-exposure to Erlotinib, which didn't induce AKT activation, suppressed the phosphorylation of anti-apoptotic protein AKT triggered by SAL (Figure 30, middle panel). Apoptotic response was further evaluated by examining the expression levels of PARP cleavage. Single-agent SAL or Erlotinib both elicited a dose-dependent activation of PARP, whereas a pronounced apoptosis activation was evident under combinatorial treatment (Figure 30, bottom panel). These results suggest that the inhibition of EGFR signaling achieved with the combination of SAL and Erlotinib can be augmented beyond that achieved using each agent individually, which is consistent with the speculation that the heterogeneity of cells is composed of SAL-targeted stem-like cells and Erlotinib-targeted differentiated cell population.

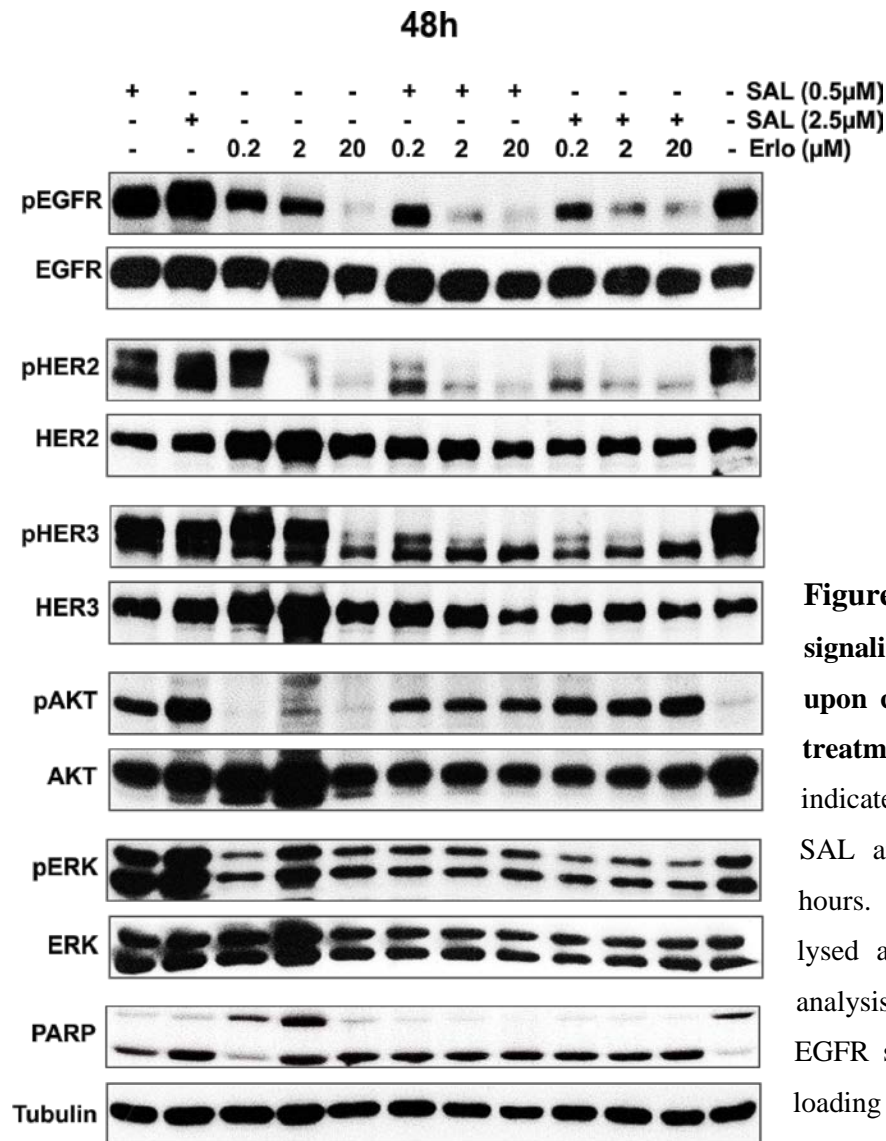


Figure 29. EGFR downstream signaling in NCI-H1568 cell lines upon combined Erlotinib and SAL treatment. Cells were exposed to the indicated concentrations of Erlotinib, SAL and their combinations for 48 hours. After harvesting, cells were lysed and prepared for western blot analysis of downstream molecules of EGFR signaling. Tubulin served as a loading control. Erlo, Erlotinib.

4.2.3. AKT activation by SAL treatment correlates with increased cellular apoptosis

To measure the relationship between the level of AKT activation and SAL toxicity, we analyzed the time- and dose-dependent effects of SAL on AKT phosphorylation. The pAKT positively correlated with SAL concentration, thereby suggesting that AKT activation by SAL correlates with increased cellular anti-apoptosis (Figure 30, upper panel). In parallel, we evaluated

RESULTS

apoptotic response by examining the PARP cleavage, and found similar activation patterns with dependence on dose of SAL treatment (Figure 30, middle panel).

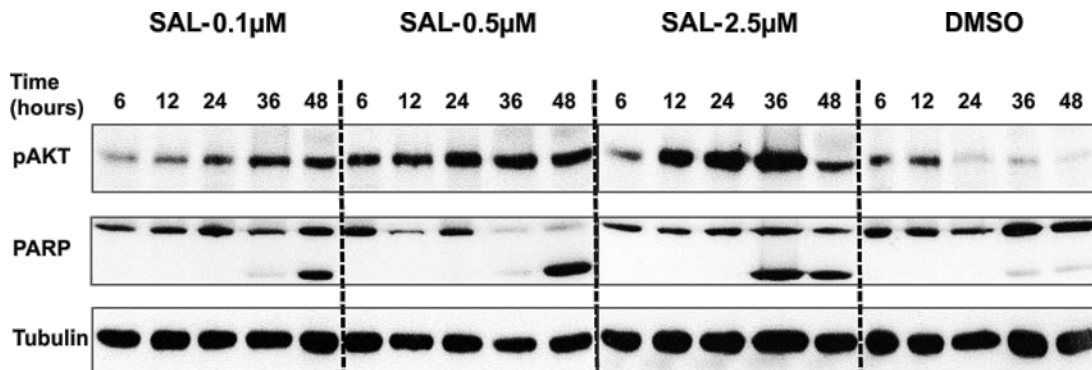
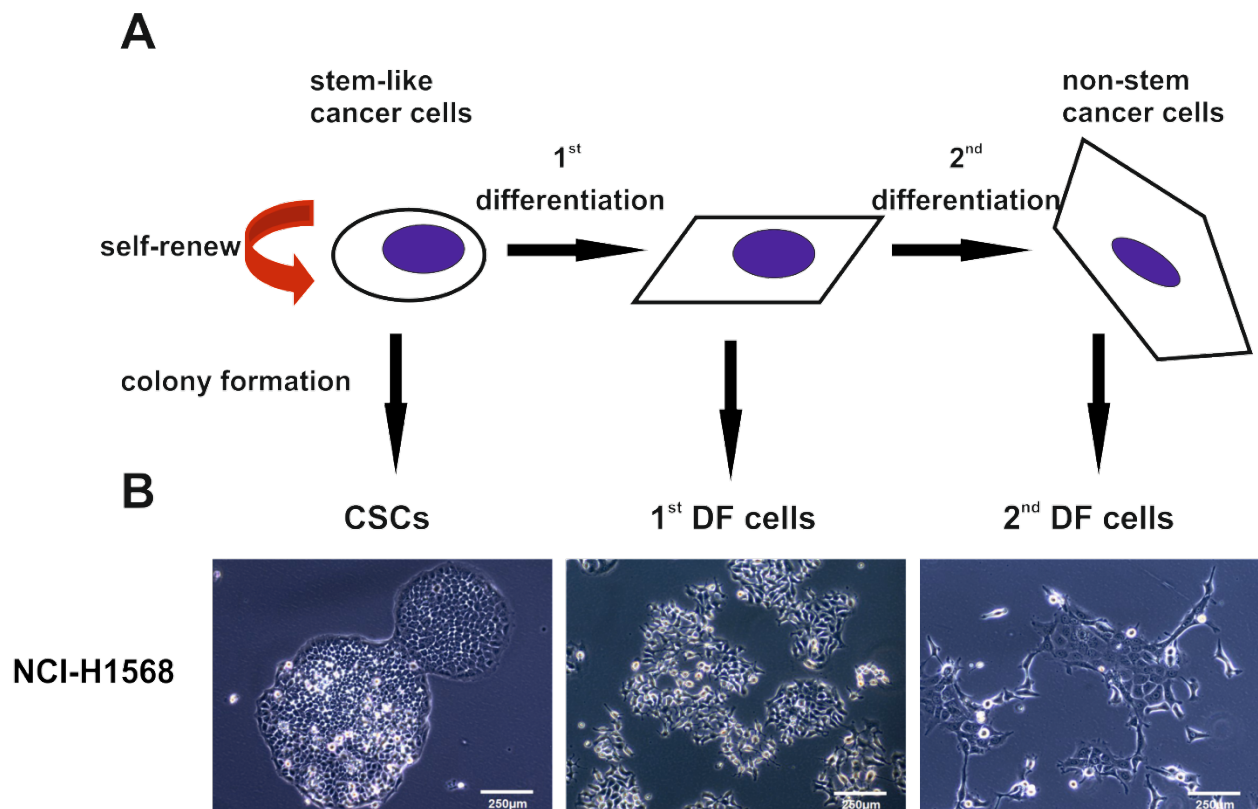


Figure 30. The time- and dose-dependent effect of SAL on apoptosis of NCI-H1568 cells. Western blot analyzed the expression levels of apoptosis related proteins pAKT and PARP of NCI-H1568 cells following incubation with SAL at the indicated concentrations (range 0.1 μ M to 2.5 μ M) and time courses (range 6 hours to 48 hours).

4.2.4. Lung cancer cell lines in clonal cultures exhibit distinct clonal morphologies

Since NCI-H1568 wt cells well responded to combinatorial treatment with Erlotinib and SAL, monoclonal cultivation and spheroid differentiation were carried out to determine the diversity of clonal morphologies. Based on differences in morphology, colonies were defined as CSCs, first line differentiation (1st DF) cells and second line differentiation (2nd DF) cells. Yann Barrandon and Howard Green for the first time classified the original clones of normal keratinocyte and described a method to analyze the potential of individual clones. Holoclones (holo = entire) form large rapidly growing colonies. Paraclones (para = beyond) are programmed for limited growth and consequently form uniformly small, terminal colonies. Meroclones (mero = partial) form two kinds of colonies – growing and terminal, which contain a proportion of cells that has degraded to paraclones [146] (Figure 31A). The distinction among clonal types in NCI-H1568 cell line indicated that CSCs were clusters of small, round and tightly packed cells with smooth colony

borderlines, and its perimeter is nearly circular, whereas 1st DF cells exhibited homogeneous cells with star shape (Figure 31B), and 2nd DF cells arranged fibroblast-like sharp, irregular and large cells. Similar experiments were carried out on cells derived from another five human NSCLC cell lines (NCI-H1975, NCI-H1650, NCI-H3122, HCC95 and HCC827), one immortalized human small airway epithelial cell line (SALE) and one SALER cell line (SALE transformed by KRAS G12V mutant form). All extended cell lines showed marked clonal heterogeneity and developed a range of colony morphologies paralleling the CSCs, 1st DF cells and 2nd DF cells, which are similar to NCI-H1568 cells. One exception is HCC827, in which 2nd DF cells are hard to discriminate (Figure 31C).



C

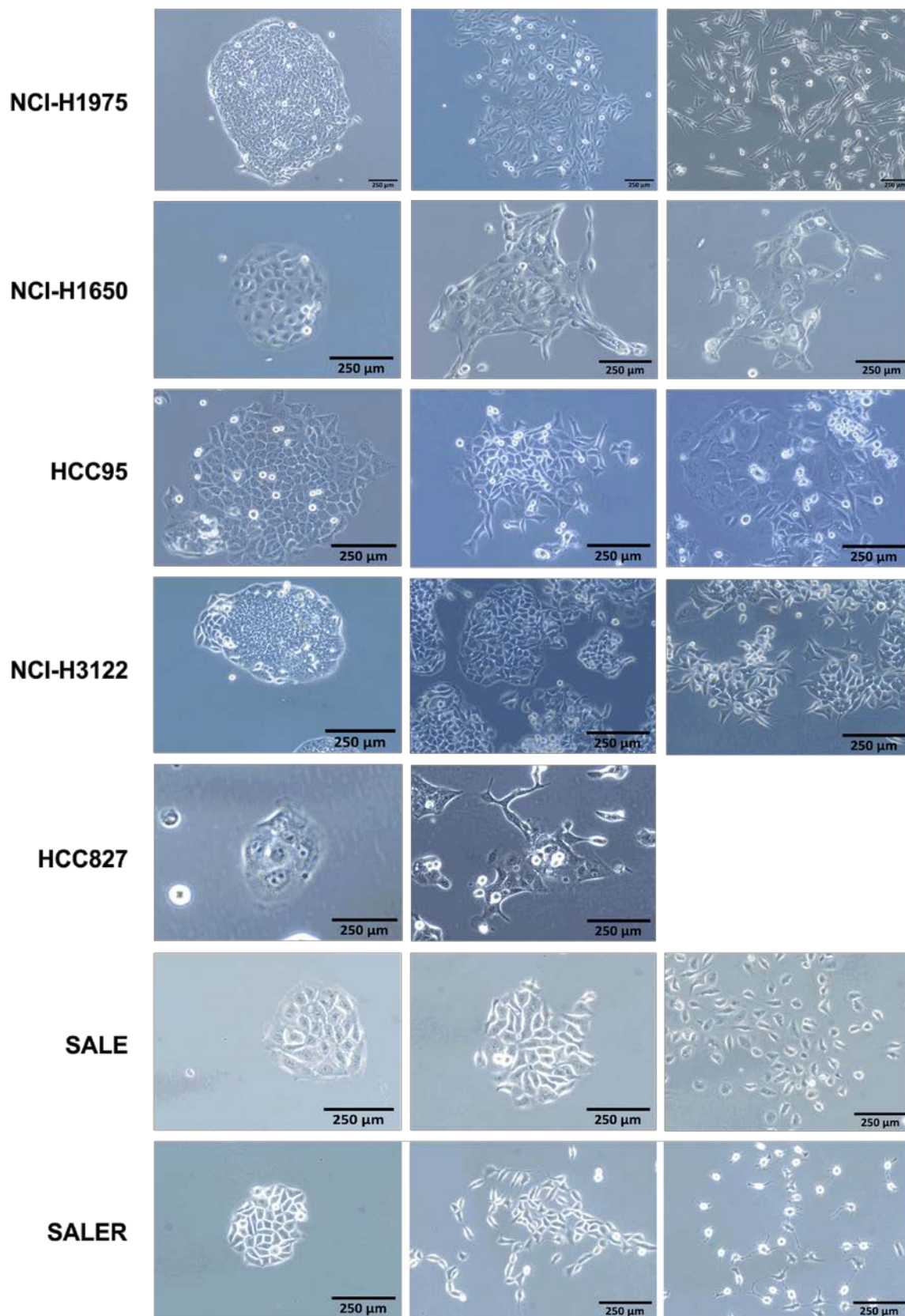


Figure 31. Phenotypic heterogeneity of NSCLC cell lines. (A) The model of hierarchical organization of lung cancer cell population. (B) Morphology of distinct colonies from cell lines NCI-H1568, NCI-H1975, NCI-H1650, NCI-H3122, HCC95, HCC827, SALE and SALER. The lung CSCs and their progenies in differentiation can develop to single colonies with different morphologies. Based on the in vitro characteristics, 1st DF cells correspond to the cells in the intermediate stage, while 2nd DF cells correspond to the fully differentiated cells.

4.2.5. Different NCI-H1568 cell clones possess distinct self-renewal

The ability of the CSCs to self-renew was assessed by a colony formation assay carried out with cell replated at low density. After two folds dilution, wells that contained only 1 viable cell have been marked and selected. At later times, intrinsic morphological differences in terms of the types of colonies produced by individual cells were apparent and persisted in the following 2 weeks. Among all 96-well plates studied, 200 wells satisfied our selection criteria and were followed up on the cell development at the clonal level (Figure 32A). Colonies were finally scored under the microscope, in which 36% clones developed into typical CSCs and 49% clones were 1st DF cells, whereas 15% formed 2nd DF cells (Figure 32B).

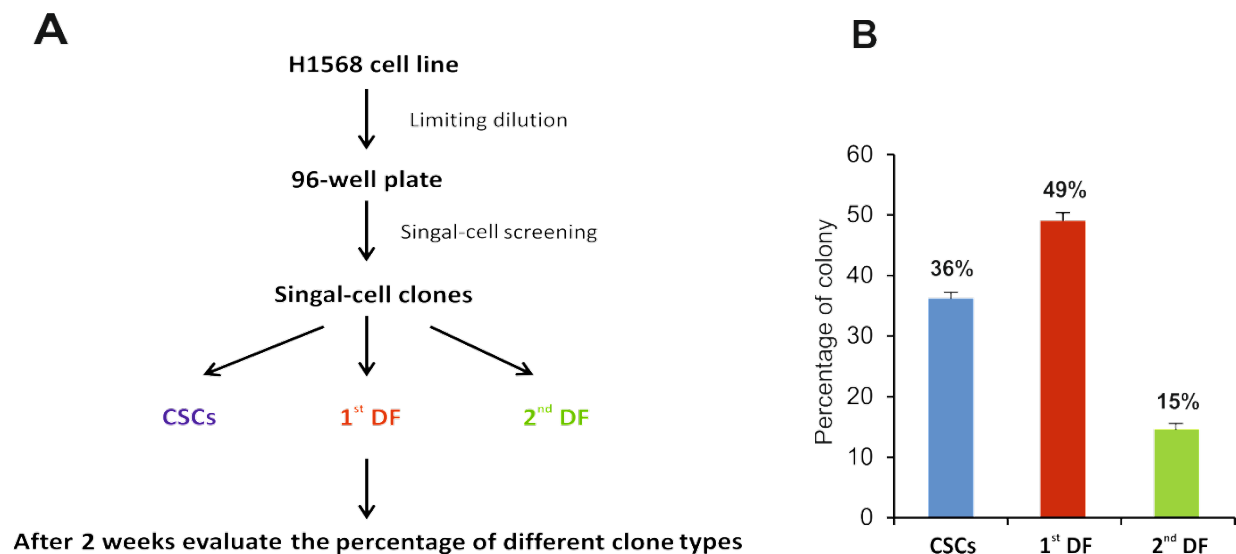
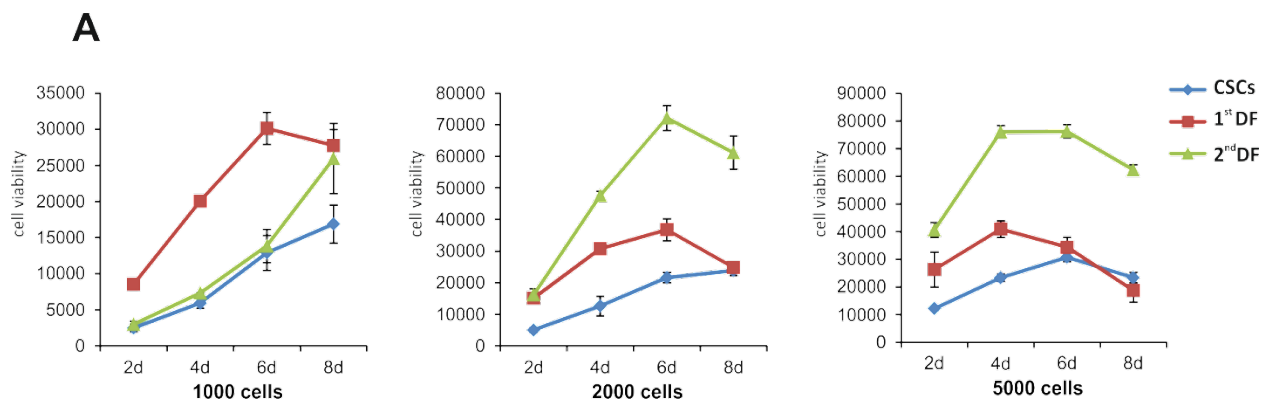


Figure 32. Clonal heterogeneity of NCI-H1568 cells. (A) Schematic depicting the procedure of deriving NCI-H1568 cell clonal cultures. (B) Quantification of each type of clones 2 weeks after plating.

4.2.6. Quiescence leads to low proliferative capacities of the CSCs

To evaluate long-term proliferation capacity, cells from all three types of colonies were isolated and seeded in 96-well plates at the density of 1000, 2000 and 5000 cells/well for proliferation capability. The stem-like cells are in a more quiescent state, which make them theoretically less sensitive to chemotherapeutics that target rapidly dividing cells (Figure 33). When the cells were seeded at low density (1000 cells/well), before 1st DF cells reaching the platform, the number of this type of cells was at least twice more than CSCs and 2nd DF cells at each check point (Figure 33A, left), while at higher cell density (2000 and 5000 cells/well), 2nd DF cells were extraordinary more proliferative than other two clones (Figure 33A, middle and right).

Proliferative activity of distinct subclones was further evaluated using the Ki-67 index. Colonies displayed strong cell nuclear staining of 2nd DF cells for Ki-67 antigen expression (Figure 33B, bottom) but with reduced reactivity of 1st DF cells (Figure 33B, middle). CSCs showed much lower proliferative capacity than 1st and 2nd DF cells, only a small population of large cells overlying the boundary of a cancer stem-like colony, possibly the 1st DF cells, showed staining for Ki-67 (Figure 33B, top).



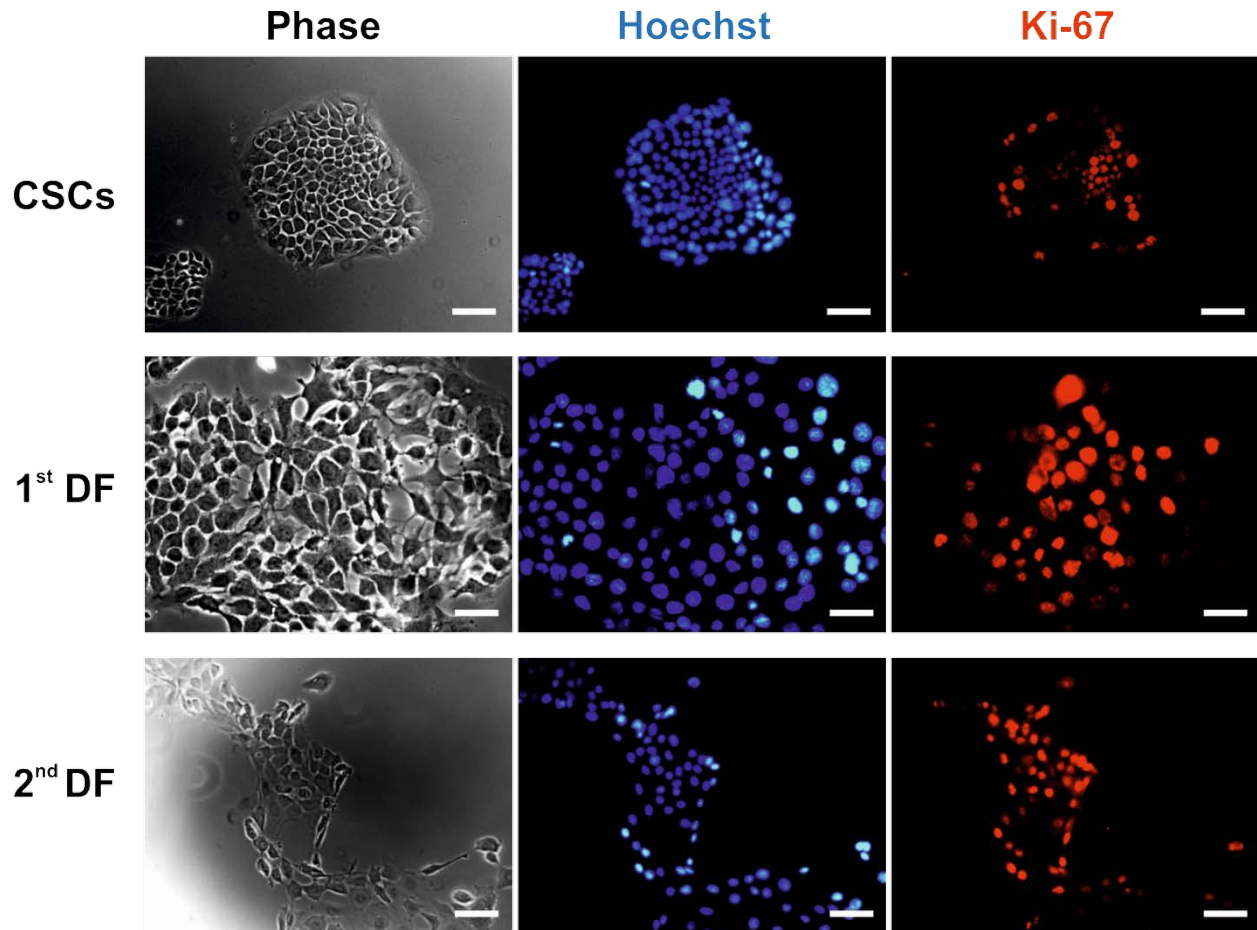


Figure 33. Evaluation of proliferative activity of distinct types of colonies. (A) Long-term propagation capacity of distinct types of colonies. Seeding 1000, 2000 and 5000 cells of each clones, CSCs (blue dolt), 1st DF (red square) and 2nd DF (green triangle), to 96-well plates, after each 2 days check the number of viable cells via CellTiter-Glo cell viability assay. Values represent the mean of three samples \pm SD. (B) Immunofluorescent staining of colonies. Sections of distinct clones were double-labeled with primary antibodies against the proliferation-associated nuclear antigen Ki-67 (red) and the nuclear stain, Hoechst 33342 (blue). Bar, 20 μ m.

4.2.7. CSCs isolated from NCI-H1568 cells spend longer in the G2 phase of the cell cycle

In conjunction with proliferation capability assay, FACS analysis indicated significant cell cycle differences between CSCs, 1st and 2nd DF cells by fluorescence labeling of DNA content to check cells' replication state. The proportion of cells in the G2-M phase of the cell cycle was

RESULTS

considerable higher in CSCs than in the 1st and 2nd DF cells, at the expense of G1 phase of the cell cycle (Figure 34A). CSCs in the G2-M phase were approximately 2 and 4 folds greater numbers than 1st and 2nd DF cells, respectively, with sequential percentages around 46, 21, and 14% (Figure 31B). Apoptotic cells were virtually undetectable in all cases. Stem-like cells were considered to have a resting or a slow mitotic index, while they continue to replicate through extending G2 phase and comprehensively repairing DNA damage to provide post-treatment recurrence.

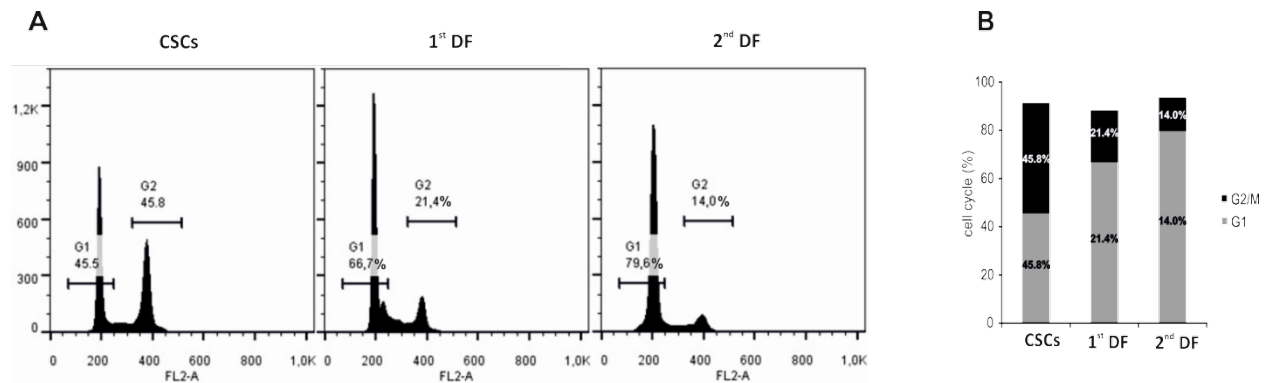


Figure 34. Cell cycle analysis on distinct types of clones. (A) Cell cycle analysis performed with propidium iodide staining and flow cytometry. (B) Percentage of G1 and G2-M phase on CSCs, 1st and 2nd DF cells of NCI-H1568 cell line.

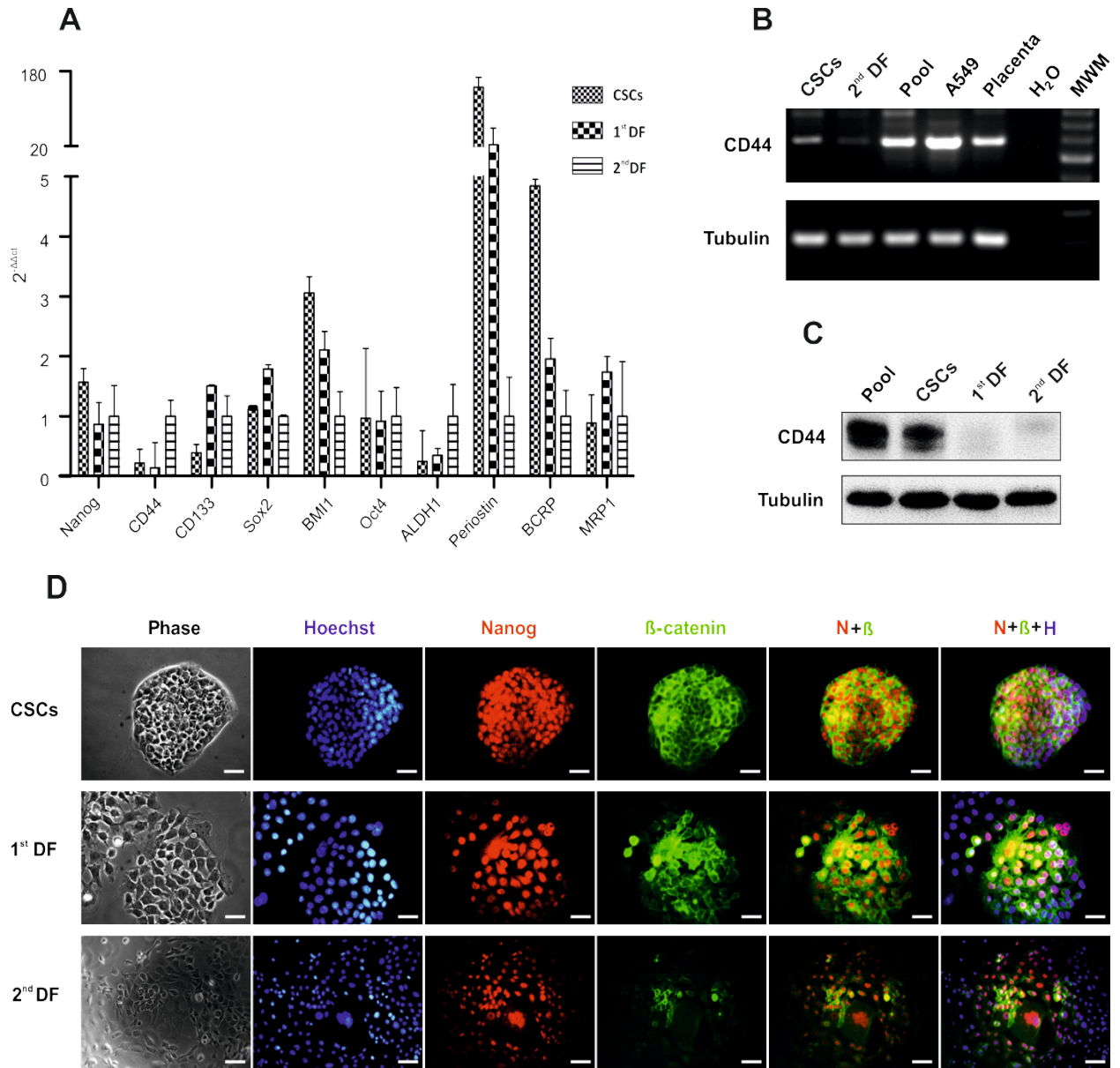
4.2.8. Evaluation of the expression of CSC related markers in distinct clones

Real-time PCR was employed simultaneously to examine the expression of a selection of genes with potential interest to CSCs, from which the expression of Nanog, BMI1 and BCRP was downregulated upon commitment to early and late differentiation, consistent with an intimate association with pluripotent stem cell identity (Figure 35A). However, increased expression of CD133 accelerated CSC differentiation. Similar expression patterns were observed for Sox2 and MRP1, the upregulation of which was less than 2 folds in 1st DF cells. Meanwhile, little differences between CSCs, 1st and 2nd DF cells were found for Oct4, a marker expressed at

higher levels on the stem cell fraction. Notably, very high levels of Periostin expression were measured in CSCs, and average expression levels were increased by 9 and 180 folds compared to 1st and 2nd DF cells, respectively. Surprisingly, CD44 expression levels were contrast with the previous observations, which reported CD44 can be used as the marker to detect and to sort CSCs. Additionally, conventional PCR and western blot assays were performed to detect CD44 levels and reversed real-time PCR data (Figure 35B and C).

RNA expression levels of Nanog and β -catenin were further analyzed by immunofluorescent staining (Figure 35D and E). Cells derived from distinct clones varied in their degree of staining with particular antibodies, but CSCs typically showed stronger staining than 1st and 2nd DF cells for molecules Nanog and β -catenin that are associated with stem-like cells. CSC colonies were near 100% positive for Nanog nuclear and β -catenin cell periphery staining. The majority of 2nd DF cells demonstrated low expression of β -catenin, and only a few distinct Nanog positive cells were detected in this population. Both antibodies were intermediate stained in 1st DF cells (Figure 35D). Figure 35E as a model demonstrated the initiation of differentiation of CSCs, from which we see the center of the colony is made up of tightly packed cobblestone shaped cells and slightly larger irregular cells at the edge. CSCs were considered as dormant less dividing cells and this concept was supported by the lesser DNA staining of center cells for Hoechst 33342. Although cells in the center of the colony showed strong staining for Nanog and β -catenin that are found at high levels on clonogenic cells, the staining was dramatically reduced, even vanished in peripheral cells.

RESULTS



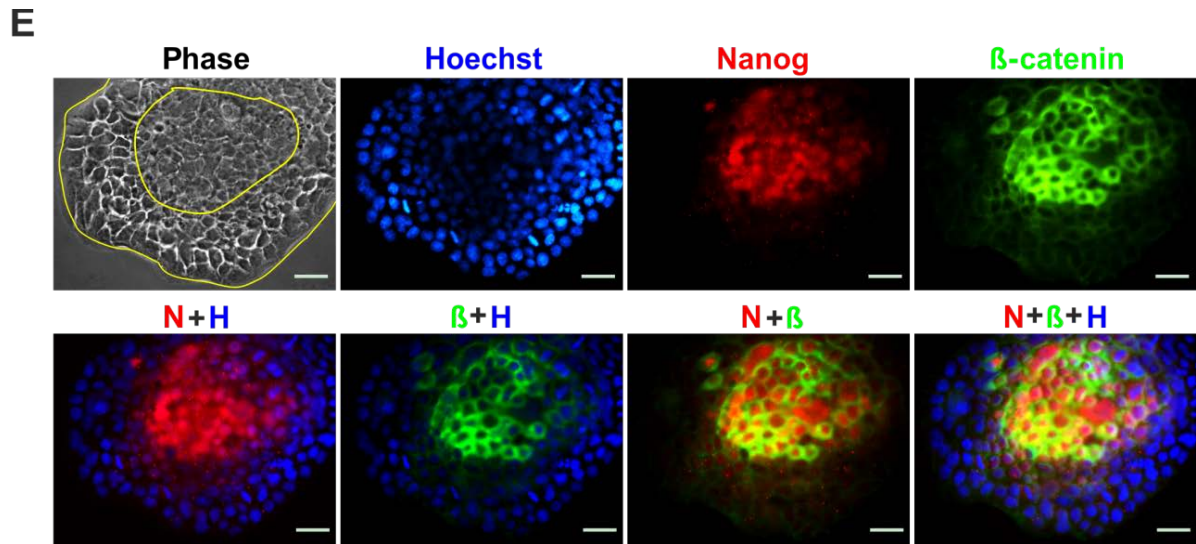


Figure 35. Different expressions of SCMs and multidrug resistant genes. (A) Stem cell related gene expression patterns assessed by quantitative PCR. mRNA levels of cancer stem cell markers and multidrug resistant genes in CSCs, 1st and 2nd DF cells were quantified with real-time PCR (hHPRT as the internal reference). CD44 expression level was further quantified by conventional PCR (B) and western blot (C). (D and E) Immunofluorescent staining patterns of distinct clones of NCI-H1568 cell line. Immunofluorescence was performed on paraformaldehyde fixed CSCs, 1st and 2nd DF cells with Nanog-specific (red) and β -catenin-specific (green) purified IgG, and counterstained with Hoechst 33342. Inner yellow line in E separated real CSCs from 1st DF cells in a colony. Bars, 20 μ m.

4.2.9. CSCs markedly enhanced the invasive potential of differentiated progeny

Invasion and metastasis are the most insidious and life-threatening aspects of cancer [147-149]. In vitro the invasive potential of the cells can be determined via migrating through the Matrigel. NCI-H1568 pool cells were initially checked to possess high capability of invasion (Figure 36A), after subcloning we would like to aware how invasion was distributed in various clones. Interestingly, we found that CSCs had obvious no invasion capacity based on Boyden chamber invasion assay (Figure 36B), whereas 2nd DF cells exhibited a greater than 2 and 4 folds increase in invasion compared to H1568 pool cells and 1st DF cells, respectively (Figure 36 A, C, D and G).

RESULTS

Cell-cell crosstalk is necessary for cells to carry out various functions. This raises the question of how cells communicate and influence one another to behave in irregular ways between different clones. To address the potential influence of CSCs on 1st and 2nd DF cell invasion, we co-cultured CSCs with 1st and 2nd DF cells at the same proportion for 48 hours through a direct contact. Surprisingly, the invasion was increased around 2 folds as a result of exposure of either 1st or 2nd DF cells to the co-culture condition (Figure 36 E, F, H and I). The observation can either indicated that direct contact or stimulatory factors secreted from 1st and 2nd DF cells drove CSCs to go for differentiation, or another way around that the addition of CSCs markedly enhanced the invasive potential of 1st and 2nd differentiated progeny of CSCs via expression of growth factors, like Periostin.

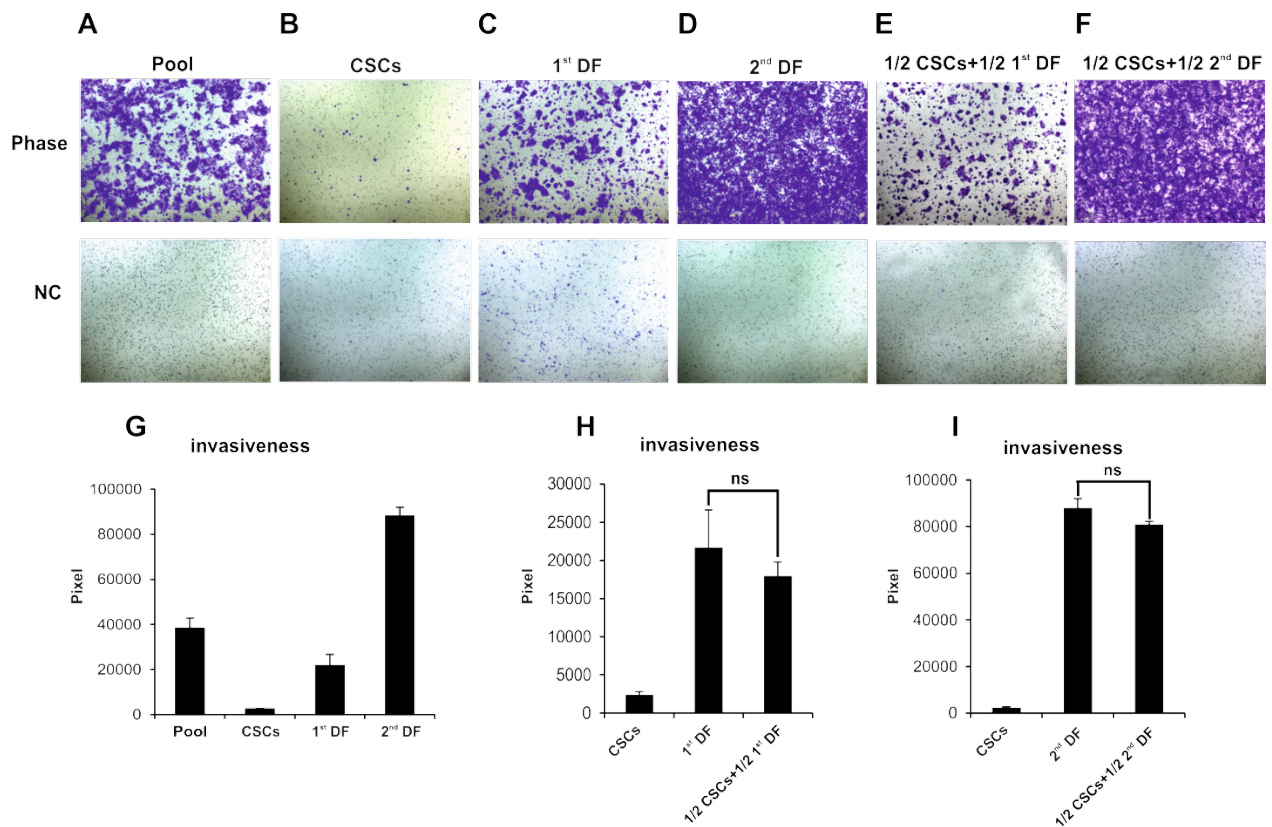
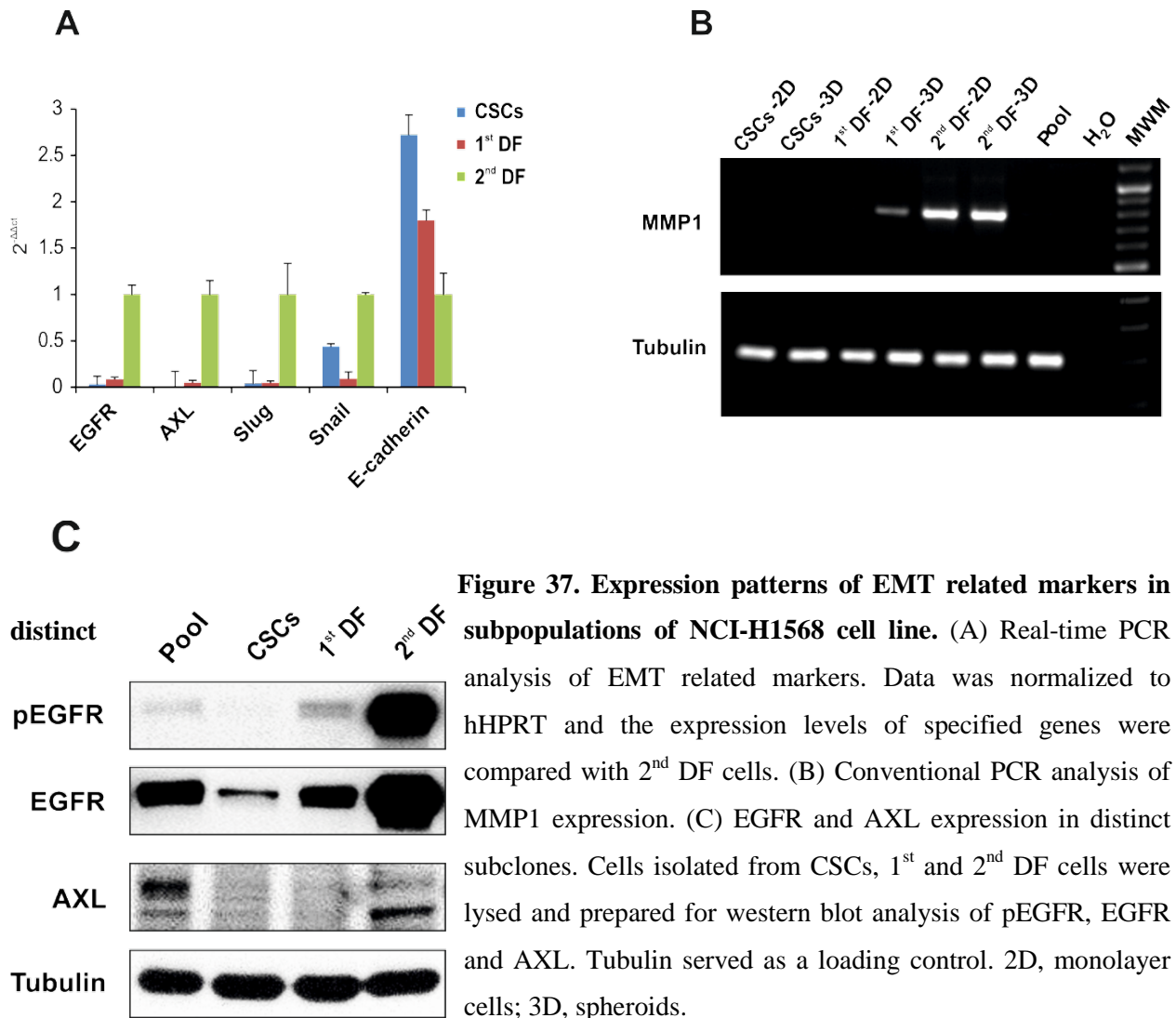


Figure 36. Invasivity of distinct clones by Boyden chamber invasion assay. (A-D) Representative images of NCI-H1568 pool cells and distinct clones. Phase, with chemoattractant; NC, negative control, and no chemoattractant were added. (E and F) Representative images of co-culture CSCs with 1st and 2nd DF cells at the same proportion. Cells were seeded into the Matrigel-coated inserts and permitted to migrate for 48 hours toward medium containing 10% FCS as a chemoattractant. Cells were visualized at 6

× magnification. (G) Quantification of invasive activity of distinct clones of NCI-H1568 cells. (H and I) Quantification of invasive activity of co-culture CSCs with 1st and 2nd DF cells at the same proportion. Cells were counted in triplicate wells and in three identical experiments. Values shown represent the mean ±SD of three independent experiments. ns, not significant.

4.2.10. EGFR plays a considerable role in mediating the invasive behavior

As indicated in Figure 31B, 2nd DF cells showed a scattered phenotype, losing their close cell-cell junctions and becoming spindle-shaped. These gradual morphological changes from CSCs to 1st DF, and then to 2nd DF cells are reminiscent of cells of the mesenchymal lineage. To evaluate the above observation, real-time PCR was undertaken to investigate the expression of epithelial-mesenchymal transition (EMT)-related genes. 2nd DF cells showed much higher expression of the mesenchymal markers Slug and Snail, and the concurrent attenuation of critical epithelial marker E-cadherin, differences in expression profile suggested the genotypic EMT (Figure 37A). It is well known that activity of MMP1, EGFR and AXL is positively correlated with an EMT-like morphological changes, tumor invasion and metastasis. Conventional and real-time PCR assays displayed gradual upregulation of all mentioned proteins in 1st DF cells compared to CSCs, and with a statistically significant increase in 2nd DF cells (Figure 37A and B). Western blot analysis was further performed to evaluate EGFR and AXL protein expression and EGFR phosphorylation of NCI-H1568 pool cells and the three subclones (Figure 37C). Expectedly, the data were corresponded to changes detected by real-time PCR. It should be noted that EGFR expression levels of NCI-H1568 pool cells and distinct clones are closely consistent with their respective invasion capacities.



According to the protein expression measured by western blot, we asked whether endogenous EGF receptor is playing a considerable role in mediating the invasive behavior. We performed a gene-silencing experiment utilizing double-stranded siRNA to silence the EGFR gene in the highly invasive 1st and 2nd DF cells. Western blot analysis revealed that EGF receptor was effectively knocked down by siRNA treatment compared to scramble treated cells, and same notable inhibition was seen of EGFR phosphorylation (Figure 38A). Moreover, as expected, the invasive activity in 2nd DF cells was almost abrogated by EGFR-specific inhibition (Figure 38D and E), but less so in 1st DF cells, with approximately 80% but sufficient inhibitory effect (Figure 38B and C). Taken together, these data demonstrate that EGFR expression is important for 1st and 2nd DF cells to drive their differentiated cancer cell invasion.

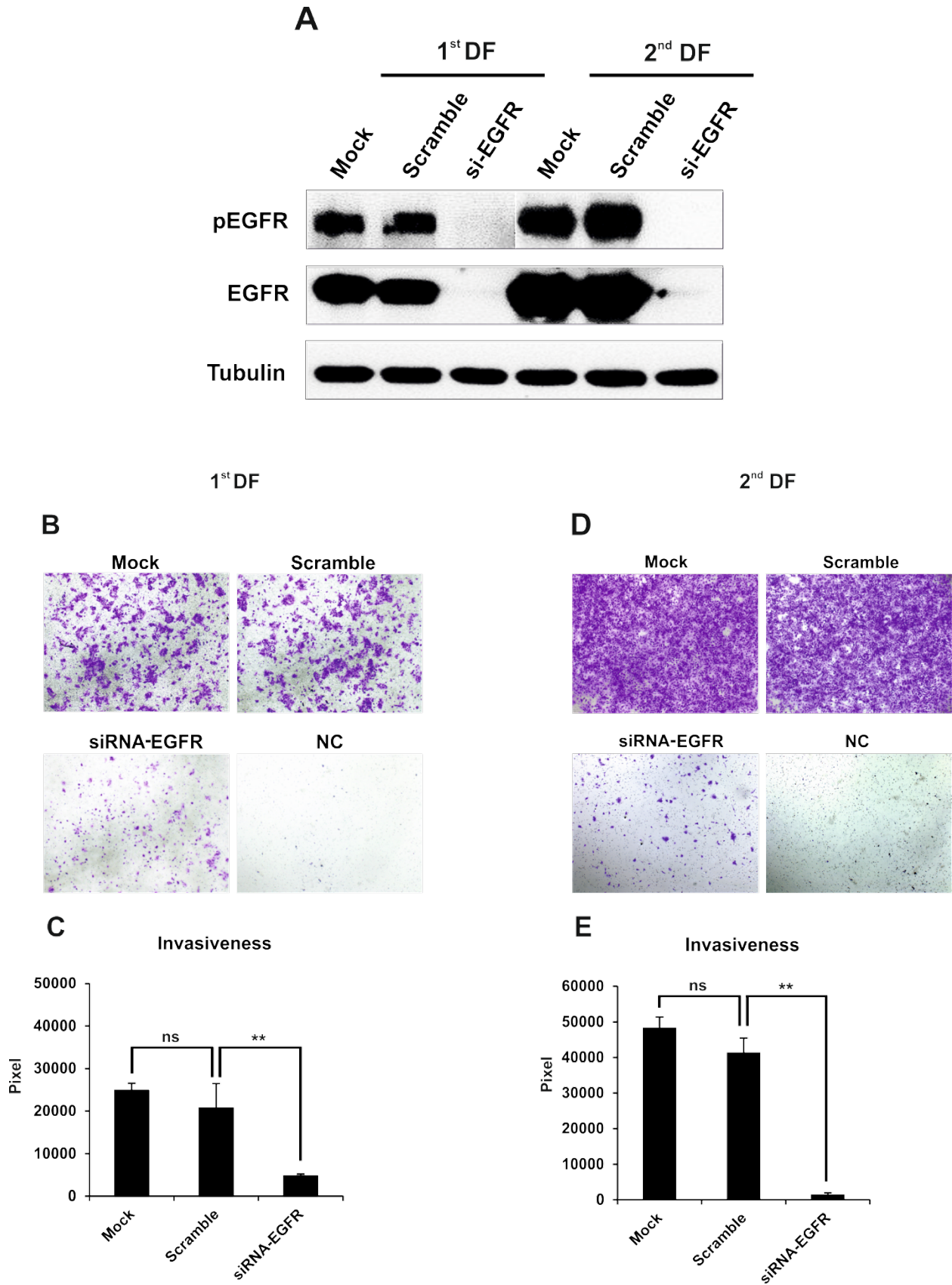
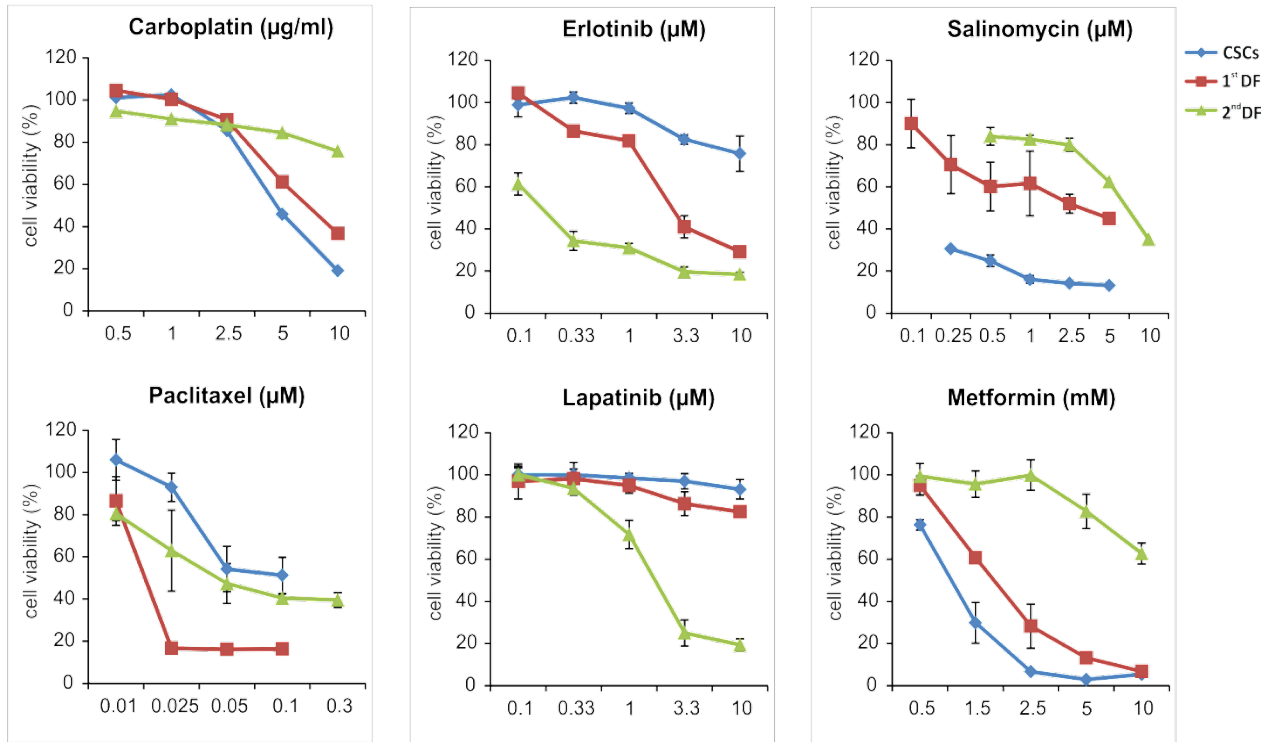


Figure 38. siRNA-EGFR downregulation of EGFR expression accompanied the reduction of cell invasion. (A) 1st and 2nd DF cells after transfection with siRNA-EGFR 72 hours were lysed and prepared for western blot analysis of pEGFR and EGFR. Tubulin served as a loading control. (B and D) Representative images showed reduced cell invasiveness due to EGFR knockdown compared to control cells. Invasion assays were performed using a Boyden chamber assay coated with Matrigel, which mimics the basement membrane composition. Cells were visualized at 6 × magnification. (C and E) Quantification of the invasion assays. Cells were counted in triplicate wells and in three identical experiments. Values shown represent the mean ±SD of three independent experiments. **P < 0.01; ns, not significant.

4.2.11. CSCs derived from NCI-H1568 cells survive chemotherapeutic agents and TKIs, but sensitive to the putative stem cell killers SAL and METF

CSCs have been shown to be associated with refractory to chemotherapy, to some extent explaining why tumors initially shrink after conventional treatment eventually recurrent. Hence, drug sensitivity of cells isolated from these three types of colonies was evaluated after applying the chemotherapeutic drugs (Carboplatin, Paclitaxel), TKIs (Erlotinib, Lapatinib) and the putative CSC killers (SAL, METF). Among the entire concentration range tested, the survival rates of CSCs were significantly higher than those from 1st and 2nd DF cells when treated with chemotherapeutic agent Paclitaxel and TKIs Erlotinib, Lapatinib. However, CSCs were highly sensitive to SAL, and sensitive to METF, as indicated low concentrations at 100 nM and 1 mM caused 50% cell growth inhibition, respectively (Figure 39A and B, right). Meanwhile, IC₅₀ of these two stem cell killers exhibited more than 2 and 7 folds increase in 1st and 2nd DF cells over CSCs (Figure 39B, right). Single agent treatment with Erlotinib or Lapatinib induced a substantial cell growth inhibition on 2nd DF cells, with IC₅₀ values of 0.2 and 2 μM, respectively (Figure 39A and B, middle). Among all the tested drugs, 1st DF cells showed highest sensitivity only to Paclitaxel, and the IC₅₀ value of which was reduced by 5 and 2.5 folds compared to CSCs and 2nd DF cells, respectively. Another chemotherapeutic drug Carboplatin at the entire tested concentrations caused a slight reduction of 2nd DF cells, but at a low dose 5 μg/ml led to growth inhibition at a large extent of CSCs and 1st DF cells (Figure 39A, upper left).

A



B

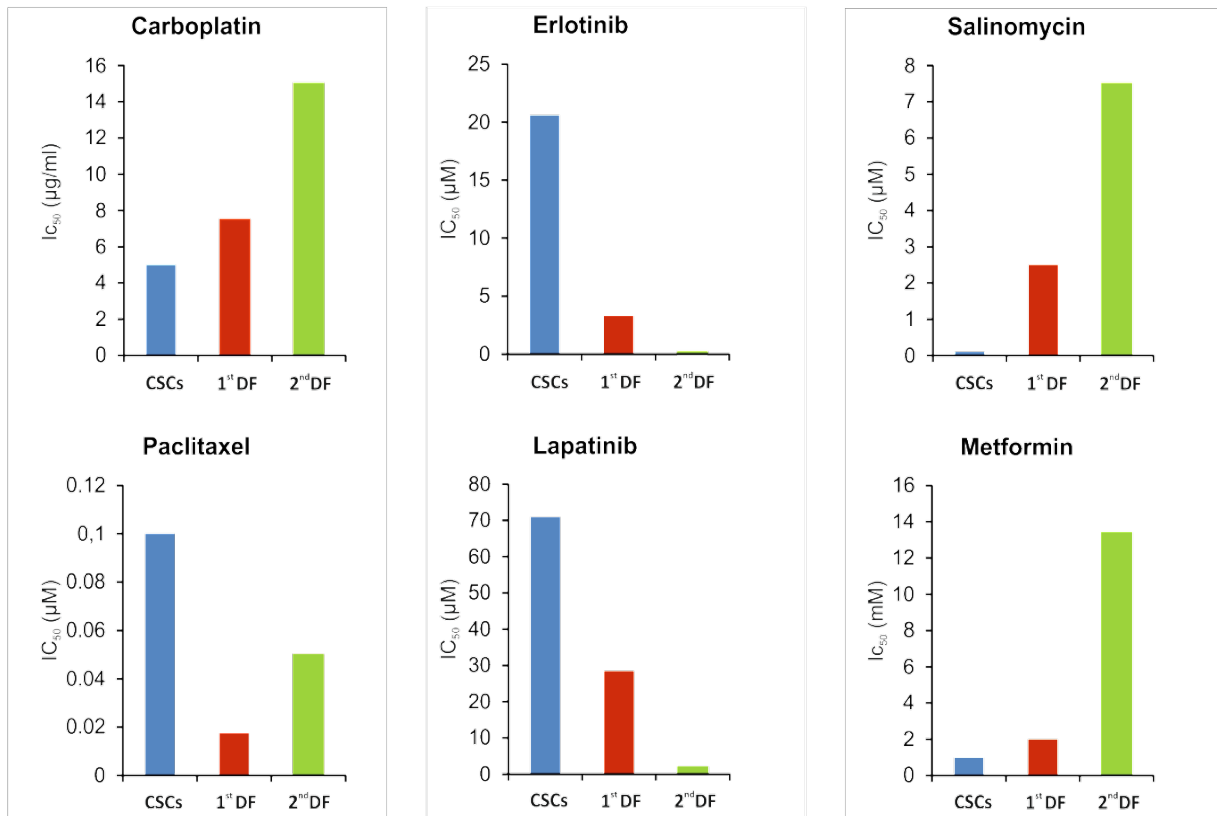


Figure 39. Drug sensitivity of NCI-H1568-derived unique clones. Response of CSCs (blue dolt), 1st DF cells (red square), and 2nd DF cells (green triangle) to treatment with Carboplatin, Paclitaxel, Erlotinib, Lapatinib, SAL and METF. (A) Cells were seeded in 96-well plates and grown one day in free drugs medium. Treatments were performed for 72 hours at the indicated drug concentrations. At the end of the treatment (96 hours after plating cells), the vitality of the cells was assessed by CellTiter-Glo cell viability assay. The data of the survival curves were plotted as percentages of DMSO controls. Each experiment consisted of at least four replicates for each point and the plotted data represent the average mean \pm SD of three independent experiments. (B) IC₅₀ values of indicated drugs on diverse subclones.

5. DISCUSSION

5.1. The addition of SAL doesn't commonly augment the antitumor activity over that achievable with 11 therapeutic drugs in tested NSCLC cell lines

NSCLC causes 1.4 million deaths worldwide every year [1]. Given a wide variety of therapies to which cancer cells are refractory, the CSC theory has brought awareness that eradicating CSCs may overturn the drug-resistance after chemoradiation or targeted therapy. In our study, we did multi-rounds drug treatment on the HCC4006, NCI-H1975 and HCC95 cell lines (with various EGFR status) under combination with the putative stem cell killer SAL and inhibitors for the non-CSC population, such as chemotherapeutic agents, EGFR humanized mAb Erbitux, and a panel of TKIs for EGFR, Src, PDGFR, KIT and VEGFR. The approach of combinatorial treatment with SAL and other inhibitors targeting both CSCs and transit-amplifying/differentiated cells has already been successfully applied to cancers as breast [150], pancreas [151] and sarcoma [152]. Unfortunately, as shown in Figure 15, SAL didn't enhance the effects of the tested drugs, suggesting ABC transporters that are associated with multidrug resistance may not be effectively targeted by SAL in these cell lines. These data are consistent with Larzabal's work [153], which showed differential effects of SAL and Paclitaxel targeting CSC and non-CSC populations, respectively, on lung primary tumors and metastases. However, a combination of both drugs did not improve the effect of single therapies. Collectively, of 12 therapeutic drugs available in the clinic, only METF elicits synergistic effects on the eradication of both differentiated cells and CSCs after co-administration of SAL, thus preventing cancer cell recovery in the tested NSCLC cell lines (Figure 15 and 16A).

5.2. METF modestly inhibits the growth of NSCLC monolayer cells and spheroids in a dose-dependent manner, interacting synergistically with SAL

METF is regarded as an anti-hyperglycaemic agent and developed for the treatment of type 2 diabetes. Besides its circulating insulin-lowering effects that reduce fasting blood glucose level, basic investigations demonstrated that METF also inhibited growth of various human cancer cell types, such as thyroid [110], prostate [111], gastric [112], breast [154] and glioblastoma [114]. In

line with these findings, we for the first time systematically showed that METF exerted a dose dependent growth-inhibitory effect on six NSCLC cell lines (HCC4006, NCI-H1975, HCC95, NCI-H1650, NCI-H2122, NCI-H3122) carrying various EGFR, KRAS, EML4/ALK and LKB1 genotypes irrespective of Gefitinib sensitivity. Furthermore, we found that SAL can sensitize cancer cells to the effects of METF treatment by enhancing inhibition of proliferation and cell death development, validated by CellTiter-Glo viability assay, cell and nuclear abnormalities, and PARP activation (PARP cleavage). Single treatment, such as METF, at the concentrations of 0.07, 0.15, 0.3 and 0.6 mM are without growth inhibition in HCC4006 cells, the same for 0.15 μ M SAL. However, in the presence of this combination, we observed a decreasing trend of cell viability that is consistent with METF doses. Here we speculated that, based on its small molecular property, METF, at a concentration less than 1 mM, could be hard to accumulate and can be quickly and effectively pumped out of the cells. Even though it has been approved to have anticancer effect on various cancer cell lines, the published data indicated that the minimum effective concentration of METF is 2 mM. In this case, SAL which acts as a possible inhibitor of P-glycoproteins to interfere with ABC transporters preserves the effect of METF even at low dose. Whether they are working synergistically as a complex or individually needs to be further dissected.

5.3. The inhibitory effect of METF/SAL is mediated by EGFR signaling

Understanding the molecular mechanism underlying the inhibitory activity of METF/SAL is pivotal to develop this combination as a novel therapy to reduce the risk of tumor relapse. EGFR is overexpressed in more than 60% of NSCLC cases and considered as a driving force in lung adenocarcinomas [40], so targeting EGF receptor to inhibit EGFR-mediated pro-survival and anti-apoptotic signals through the MAPK-ERK1/2 and PI3K-AKT pathways would be an effective lung cancer treatment. In HCC4006 cells, EGFR was continually activated in serum-starved conditions and completely abrogated upon EGFR specific TKI AG1478 treatment (Figure 13A). The question arose whether EGFR overexpression was necessary to activate AKT and drive cell survival? We found that knockdown of EGFR using siRNA markedly inhibited HER2 and HER3 phosphorylation, downregulated pAKT and pERK, and increased the levels of cleaved PARP (Figure 14). Jeffrey A. Engelman and colleagues [50] showed that MET

amplification or the EGFR T790M mutation is associated with Gefitinib resistance through HER3 dependent activation of PI3K/AKT in the presence of TKI. A novel finding of our work is that in NCI-H1975 cells, phosphorylation of AKT is driven by the maintenance of EGFR, as starving conditions sustained the absence of pHER3 (Figure 13B). Our data demonstrated that combinatorial treatment of the NSCLC cell lines with METF and SAL leads to a pronounced “unspecific” inhibition of EGFR, HER2, HER3 and the downstream regulators AKT and ERK1/2 expression and phosphorylation, via yet unknown mechanism, irrespective of the mutational status and protein expression. Phospho-kinase assay further indicated this combination worked more efficiently on cells harboring the gain-of-function mutant p53 than with wt P53, inducing an almost complete abolition of phospho-serine residues of P53 in Gefitinib resistant NCI-H1975 lung adenocarcinoma cell line. The significance of the P53 mutation for the resistance of this cell line has not been evaluated in our study; however, publicly available data indicated that P53-R273H could increase the resistance to chemotherapeutic drugs and TKIs [155]. Since FAK protein and Src family kinases are involved in cellular adhesion and spreading processes, combinatorial treatment induced the suppression of their activated forms could suggest that the cells are less aggressive after treatment.

There is increasing evidence that 3D spheroids more accurately reflect the in vivo microenvironment and are suitable as a platform in vitro for testing drug delivery, efficacy and CSC involvement. In our current study, cell viability and western blot assay both emphasized alveospheres are more resistant than monolayer cells upon METF alone treatment or co-administration of SAL. As shown in Figure 20A-C, higher doses of both drugs or more rounds of treatment are required to effectively inhibit alveosphere growth as compared to monolayer cells. In particular, an increased concentration of METF in combination with SAL better targeted spheres generated from squamous cell carcinoma HCC95 cells.

5.4. Combinatorial treatment with SAL and METF eradicates CSCs

Sphere formation assays have been widely used to identify stem cells based on their capacity of self-renewal and differentiation in vitro. Our present study demonstrated that single treatment with SAL and, to a less extent, with METF arrest spheroid generation, whereas their combination

significantly inhibited SF capability and substantially reduced their size in all tested 5 NSCLC cell lines, reflecting suppression of self-renewal of CSC (Figure 23). EGFR-targeting small-molecule inhibitors, such as Gefitinib and Erlotinib, were considered as the best front-line option for treating EGFR mutated NSCLC [156]. However, we observed that treatment of Erlotinib resistant NSCLC cell lines possessing EGFR wt genotype, with suboptimal dose inhibitor led to an increase in the “CSC population” evaluated by sphere formation assay (Figure 25A) and SCM profiling, which indicated an up to 5 folds difference between Erlotinib treated and DMSO control cells (Figure 25B-E). Although some reports demonstrated an enrichment of CSCs following therapy in breast, lung and ovarian cancers, it is still a relatively novel concept, as these identical results were obtained mainly after chemotherapeutic drug treatment, especially with Cisplatin [157-162]. Our data indicated that low or suboptimal doses of TKI Erlotinib, acting as a selective pressure on tumor cells, may spare the CSC and activate CSC renewal to substitute better targeted more differentiated and rapidly proliferating tumor cells. Of note, in our study, a manifestation of CSCs or transit-amplifying cells was observed in originally resistant NSCLC cell lines with EGFR wt.

5.5. Antagonistic effect of METF and Erlotinib is valuable for treatment on lung cancer patients with type 2 diabetes

Since METF significantly suppressed the growth of cancer cells, we conducted the experiment to investigate if co-administration of METF would increase the sensitivity of NSCLC to Erlotinib. Previous finding described by Morgillo et al. that METF and Gefitinib are synergistic in LKB1 wt NSCLC cells [163]. Data have been supported by Li et al., who showed METF might be used in combination with TKIs in patients with NSCLC harboring EGFR mutations [164]. In our study, assessed by PARP cleavage, apoptosis induction by METF treatment of indicated cell lines was very low, even lower than control group, suggesting an apoptosis-protective property of METF (Figure 27). Results obtained with the METF effect on cell cycle arrest and apoptosis are rather complicated [113, 165], which may reflected by the cell line context or tumor type specificity. Moreover, METF reduced PARP activation conducted by different concentrations of Erlotinib, and co-administration of METF declined Erlotinib cytotoxicity via activation of AKT, a well-known anti-apoptotic signal regulator. These results confirmed a recent study by

Janjetovic et al. who demonstrated the ability of METF to antagonize anticancer effect of Cisplatin in a variety of cancer cell lines, including glioma, neuroblastoma, fibrosarcoma and leukemia [166]. Antagonistic effect between METF and Erlotinib was not dependent on EGFR status, suggesting that AKT and ERK1/2, as downstream signaling of EGFR, can also be activated via other pathways, for instance, the complex pathways of insulin receptor, insulin-like growth factor receptor 1, AXL and MET. Future perspective studies are required to gain inside METF in combination with chemotherapeutic agents and other molecular targeted inhibitors to see if METF can synergistically act as a suitable candidate for co-administration to better treat lung cancer. METF antagonizes cytotoxic effect of Erlotinib in NSCLC cells, which warrant caution when considering METF for treatment of patients who simultaneously suffer from cancer and diabetes and already treated with Erlotinib, or as a potential adjuvant in Erlotinib-based chemotherapeutic regimens.

5.6. Quiescence emerges as a critical factor of CSC resistance to therapy

After monoclonal cultivation and spheroid differentiation, similar to the behavior of keratinocyte and some cancer cell lines [167-173], a serial colonies with diverse morphologies were developed in six human NSCLC cell lines, one immortalized human small airway epithelial cell line (SALE) and one SALER cell line (SALE transformed by KRAS G12V mutant form) (Figure 31). Based on the morphological diversity, distinct types of colonies named CSCs, 1st DF cells and 2nd DF cells were identified, which possessed differential capacity of self-renewal and proliferation rate. Harper et al states that normal and malignant epithelial cells with stem-like properties have an extended G2-cell cycle phase [174]. In consistent with their work, NCI-H1568 CSCs possessed the highest proportion of cells in the G2-phase, up to 4 folds greater number than 2nd DF cells (Figure 34). Proliferative quiescence was suggested to be related to therapeutic resistance. The greater proportion of CSCs observed to be present in G2 could result from a general increase in the time taken for CSCs to transit G2 or a more permanent block of a sub-fraction of the CSC population.

5.7. CSCs survive traditional chemotherapeutic agents and lead to cancer cell line recurrence

Chemotherapeutic agents and TKIs showed potency against differentiated progeny, but were less effective for quiescent primitive NCI-H1568 CSCs (Figure 32), which is consistent with the supportive role of CSCs in chemoresistance reported previously [170, 172]. In parallel, we for the first time claimed drug sensitivity of CSCs to SAL and METF, in addition to confirm the potential efficiency of these two drugs working as the putative stem cell killers, it also highlighted the possibility to specifically target the small subpopulation of CSCs. In response to drug treatments, the expression of ABC transporter gene ABCG2, of which the higher expression level was correlated with less efficiency of the drugs, was induced in CSCs preferentially (Figure 35A). This means the drug in-take will be increased more rapidly in 1st and 2nd DF cells than in CSCs, and to some extent explains why patients have a high response rate, but also frequent relapses, as established drugs can eradicate most of the tumor cells but spare the CSCs. This could be one of the potential origins of preferential survival of CSCs versus non-CSCs in chemotherapy.

5.8. EMT programs are regulated dynamically by contextual signals that carcinoma cells receive from the microenvironment

A fraction of CSCs seemed to be able to differentiate into progenitor cells, which might be responsible for higher metastatic potential of the cells after several passages. Interestingly, in our study molecules such as EGFR were gradually up-regulated in 1st and 2nd DF cells. By using siRNA against EGFR, we were able to inhibit invasion of 1st and 2nd DF cells, suggesting the functional role of EGFR in promoting metastasis. The epithelial-mesenchymal conversions are crucial for cell to migrate and invade into the surrounding stroma that take place during morphogenesis. Specifically, EMTs generate mesenchymal cell types from epithelial and endothelial precursors, in our case, at the early steps of metastasis, CSCs were converted into 1st and 2nd DF cells, but probably not completely, as indicated in Figure 36, cancer stem-like colony can serve as a good partner to stimulate 1st and 2nd DF cells for invasion, which can also protect 1st and 2nd DF cells from the effect of chemotherapeutic drugs. These alterations are essential to

completing the earlier steps of the metastatic cascade, i.e., local invasion, intravasation, survival while transiting through the circulation, and extravasation (Figure 7). Consequently, when these mesenchymal cells subsequently migrate and no longer experience these inciting contextual signals, they may revert via a MET to the epithelial state of their ancestors. Thus, EMT that are activated in the context of the primary tumor may empower carcinoma cells to translocate to anatomically distant sites, while the reverse process, termed MET may operate in these sites, enabling the disseminated cells to regain an epithelial phenotype (Figure 7). This reversion to an epithelial state may be critical to their successful colonization of distant organs.

5.9. Potential value of cancer stem-like clones in the study of CSCs

In present study, we demonstrated a series of stem cell properties of distinct subclones in NCI-H1568 cell line, which suggested the potential value of cancer stem-like clones in the study of CSCs. Taken together, the colonies with distinct morphologies and in different stages of differentiation can serve as a potential model for the analysis of CSCs. With this model, proteins and involved pathways potentially correlated with CSCs can be identified. More importantly, parallel evaluation of chemotherapeutic drugs can be carried out on CSCs and autologous non stem cancer cells. This means the clonal morphologies based CSC model will be useful to lead to the newer understanding of chemoresistance, which should be quite different from those obtained from heterogeneous cancer cell populations, and will be helpful to overcome the chemoresistance in cancer therapy.

6. SUMMARY

In the first part of this thesis, after screening of chemotherapeutic agents, TKIs or mAb in combination with the putative stem cell killer SAL, we found METF which modestly exerted a growth-inhibitory effect of monolayer cells and spheroids/CSCs on 6 NSCLC cell lines that possess different EGFR-TKI sensitivity, interacted synergistically with SAL. Inhibition of EGFR and mTOR signaling achieved with the combination of METF and SAL can be augmented beyond that achieved using each agent individually. Remarkably, significant reduction of tumor sphere formation was seen under combinatorial treatment in all treated NSCLC cell lines irrespective of their EGFR status. Furthermore, METF which didn't induce significant PARP activation, highly suppressed apoptosis caused in Erlotinib-treated cells via AKT activation and the inhibition of PARP cleavage. These data warrant caution when considering METF for type 2 diabetic lung cancer patients receiving Erlotinib or as adjuvant treatment in Erlotinib-based chemotherapeutic settings. Equally important, suboptimal Erlotinib induced enrichment of putative CSC markers in EGFR resistant NSCLC cells.

In the second part of this PhD study, according to the CSC model, cancer stem-like cells, 1st and 2nd DF cells were established through monoclonal cultivation and spheroid differentiation from several highly heterogeneous NSCLC cell lines, followed by assessment of self-renewal, proliferative capacities, cell cycle differences, stem cell related marker expression, invasivity and drug sensitivity. NCI-H1568 CSCs, expressing elevated SCMs and ABC transporters, were in a more quiescent state and showed a significantly higher proportion of cells in the G2-phase of the cell cycle. Boyden chamber invasion assay analysis revealed that the invasivity of CSCs, 1st and 2nd DF cells was arranged in ascending order, since the CSCs cannot drive cellular migration and invasion. Interestingly, invasivity of 1st and 2nd DF cells was 2 folds increased after co-cultivation with CSCs and can be abrogated by siRNA-mediated EGFR knock-down. Furthermore, CSCs surviving treatment with chemotherapeutic drugs (Carboplatin, Paclitaxel) and EGFR-TKIs (Erlotinib, Lapatinib) were highly sensitive to the potential CSC killers SAL and METF, while the progeny followed the opposite mode of action, suggesting the potential value of cancer stem-like clones in the study of CSCs and overcoming the chemoresistance in cancer therapy. It is worth to note that combinatorial treatment with Erlotinib and SAL

effectively inhibited NCI-H1568 cell growth, indicating drugs, such as SAL and METF, targeting lung CSCs have a promising therapeutic application.

7. ZUSAMMENFASSUNG

Im ersten Teil dieser Arbeit wurden Zelllinien, ein Screening chemotherapeutischer Agenzien, TKIs oder mAK in Kombination mit dem putativen Stammzellkiller SAL ergab, dass METF, welches einen moderat wachstumshemmenden Effekt auf Monolayerzellen und Sphäroide/CSCs in 6 NSCLC Zelllinien hat, die unterschiedliche EGFR-TKI-Sensitivität zeigen, synergistisch mit SAL interagiert. Die Hemmung von EGFR- und mTOR-Signalisierung durch METF oder SAL kann durch die Kombination von beiden verstärkt werden. Bemerkenswerterweise konnte in allen NSCLC Zelllinien unabhängig von ihrem EGFR-Status eine signifikante Reduktion der Tumorsphärenbildung beobachtet werden. METF, welches keine signifikante PARP-Aktivierung induziert, supprimierte zudem die Apoptose in Erlotinib-behandelten Zellen über AKT-Aktivierung und die Hemmung von PARP-Spaltung. Aufgrund dieser Daten sollte METF für Typ2-Diabetiker bei gleichzeitiger Erlotinib-Therapie mit Vorsicht eingesetzt werden. Gleiches gilt für eine adjuvante Behandlung bei erlotinib-basierter Chemotherapie. Bemerkenswerterweise induzierte eine suboptimale Erlotinib-Dosierung eine Anreicherung putativer CSC-Marker in EGFR-Wildtyp NSCLC-Zellen.

Im zweiten Teil dieser Arbeit wurden gemäß dem Krebsstammzell-Modell CSCs, 1st und 2nd DF Zellen aus mehreren stark heterogenen NSCLC Zelllinien durch monoklonale Kultivierung und Sphäroiddifferenzierung etabliert. Anschließend wurden deren Selbsterneuerungs- und Proliferationsfähigkeit, Zellzyklusunterschiede, Expression stammzellspezifischer Marker, Invasivität und Arzneimittelempfindlichkeit bewertet. NCI-H-1568 CSCs, die erhöhte Expression von Stammzellmarkern und ABC-Transportern zeigen, befanden sich im Ruhestadium mit signifikant erhöhtem Anteil an Zellen in der G2-Phase des Zellzyklus. Boyden Chamber-Invasionsassays ergaben, dass die Invasivität von CSCs über 1st zu 2nd DF Zellen ansteigt, da die CSCs nicht die Fähigkeit zu zellulärer Migration und Invasion besitzt. Interessanterweise war die Invasivität von 1st und 2nd DF Zellen nach Co-Kultivierung mit CSCs zweifach erhöht und konnte durch siRNA-vermittelten EGFR Knock-Down aufgehoben werden. Weiterhin waren CSCs, die die Behandlung mit First-Line-Medikamenten (Carboplatin, Paclitaxel) und EGFR-TKIs (Erlotinib, Lapatinib) überlebt hatten, gegenüber den potentiellen Stammzellkillern SAL und METF hochsensitiv während davon abstammende 1st und 2nd DF

Zellen dem umgekehrten Aktionsmodus folgen. Dies weist auf den potentiellen Wert von CSCs für die Untersuchung von Krebsstammzellen und die Überwindung von Chemoresistenzen in der Krebstherapie hin. Bemerkenswerterweise inhibierte die Behandlung mit Erlotinib und SAL das Wachstum von NCI-H-1568 Zellen effektiv, was darauf hindeutet, dass Medikamente, die auf Lungenkrebsstammzellen abzielen wie SAL und METF, eine vielversprechende therapeutische Anwendung darstellen.

8. REFERENCES

1. Siegel R, Ma J, Zou Z and Jemal A. Cancer statistics, 2014. *CA: a cancer journal for clinicians*. 2014; 64(1):9-29.
2. Cancer Facts & Figures 2011, Atlanta: American Cancer Society, 2011, copyright 2012 by American cancer society inc., surveillance research
3. Heighway J and Betticher DC. Solid Tumour Section. <http://AtlasGeneticsOncology.org>. 2004:139.
4. Bunn Jr PA, Franklin W and Doebele RC. The evolution of tumor classification: a role for genomics? *Cancer cell*. 2013; 24(6):693-694.
5. Collins LG, Haines C, Perkel R and Enck RE. Lung cancer: diagnosis and management. *American family physician*. 2007; 75(1):56-63.
6. Giangreco A, Groot KR and Janes SM. Lung cancer and lung stem cells: strange bedfellows? *American journal of respiratory and critical care medicine*. 2007; 175(6):547-553.
7. Rapp E, Pater JL, Willan A, Cormier Y, Murray N, Evans WK, Hodson D, Clark D, Feld R and Arnold A. Chemotherapy can prolong survival in patients with advanced non-small-cell lung cancer--report of a Canadian multicenter randomized trial. *Journal of Clinical Oncology*. 1988; 6(4):633-641.
8. Jackson EL, Willis N, Mercer K, Bronson RT, Crowley D, Montoya R, Jacks T and Tuveson DA. Analysis of lung tumor initiation and progression using conditional expression of oncogenic K-ras. *Genes & development*. 2001; 15(24):3243-3248.
9. Kim CFB, Jackson EL, Woolfenden AE, Lawrence S, Babar I, Vogel S, Crowley D, Bronson RT and Jacks T. Identification of bronchioalveolar stem cells in normal lung and lung cancer. *Cell*. 2005; 121(6):823-835.
10. Subramanian J and Govindan R. Lung cancer in never smokers: a review. *Journal of Clinical Oncology*. 2007; 25(5):561-570.
11. Crum CP and McKeon FD. p63 in epithelial survival, germ cell surveillance, and neoplasia. *Annual Review of Pathological Mechanical Disease*. 2010; 5:349-371.
12. Borthwick DW, Shahbazian M, Todd Krantz Q, Dorin JR and Randell SH. Evidence for stem-cell niches in the tracheal epithelium. *American journal of respiratory cell and molecular biology*. 2001; 24(6):662-670.

13. Hong KU, Reynolds SD, Watkins S, Fuchs E and Stripp BR. In vivo differentiation potential of tracheal basal cells: evidence for multipotent and unipotent subpopulations. *American Journal of Physiology-Lung Cellular and Molecular Physiology*. 2004; 286(4):L643-L649.
14. Kenfield SA, Wei EK, Stampfer MJ, Rosner BA and Colditz GA. Comparison of aspects of smoking among the four histological types of lung cancer. *Tobacco control*. 2008; 17(3):198-204.
15. Sutherland KD and Berns A. Cell of origin of lung cancer. *Molecular oncology*. 2010; 4(5):397-403.
16. Ullrich A, Coussens L, Hayflick J, Dull T, Gray A, Tam A, Lee J, Yarden Y, Libermann T and Schlessinger J. Human epidermal growth factor receptor cDNA sequence and aberrant expression of the amplified gene in A431 epidermoid carcinoma cells. 1984.
17. Coussens L, Yang-Feng TL, Liao Y-C, Chen E, Gray A, McGrath J, Seeburg PH, Libermann TA, Schlessinger J and Francke U. Tyrosine kinase receptor with extensive homology to EGF receptor shares chromosomal location with neu oncogene. *Science*. 1985; 230(4730):1132-1139.
18. Plowman GD, Whitney GS, Neubauer MG, Green JM, McDonald VL, Todaro GJ and Shoyab M. Molecular cloning and expression of an additional epidermal growth factor receptor-related gene. *Proceedings of the National Academy of Sciences*. 1990; 87(13):4905-4909.
19. Kraus MH, Issing W, Miki T, Popescu NC and Aaronson SA. Isolation and characterization of ERBB3, a third member of the ERBB/epidermal growth factor receptor family: evidence for overexpression in a subset of human mammary tumors. *Proceedings of the National Academy of Sciences*. 1989; 86(23):9193-9197.
20. Plowman GD, Culouscou J-M, Whitney GS, Green JM, Carlton GW, Foy L, Neubauer MG and Shoyab M. Ligand-specific activation of HER4/p180erbB4, a fourth member of the epidermal growth factor receptor family. *Proceedings of the National Academy of Sciences*. 1993; 90(5):1746-1750.
21. Roskoski Jr R. The ErbB/HER receptor protein-tyrosine kinases and cancer. *Biochemical and biophysical research communications*. 2004; 319(1):1-11.
22. Stein RA and Staros JV. Evolutionary analysis of the ErbB receptor and ligand families. *Journal of molecular evolution*. 2000; 50(5):397-412.

REFERENCES

23. Slamon DJ, Clark GM, Wong SG, Levin WJ, Ullrich A and McGuire WL. Human breast cancer: correlation of relapse and survival with amplification of the HER-2/neu oncogene. *Science*. 1987; 235(4785):177-182.
24. Graus-Porta D, Beerli RR, Daly JM and Hynes NE. ErbB-2, the preferred heterodimerization partner of all ErbB receptors, is a mediator of lateral signaling. *The EMBO journal*. 1997; 16(7):1647-1655.
25. Pinkas-Kramarski R, Soussan L, Waterman H, Levkowitz G, Alroy I, Klapper L, Lavi S, Seger R, Ratzkin BJ and Sela M. Diversification of Neu differentiation factor and epidermal growth factor signaling by combinatorial receptor interactions. *The EMBO journal*. 1996; 15(10):2452.
26. Brou C, Logeat F, Gupta N, Bessia C, LeBail O, Doedens JR, Cumano A, Roux P, Black RA and Israël A. A novel proteolytic cleavage involved in Notch signaling: the role of the disintegrin-metalloprotease TACE. *Molecular cell*. 2000; 5(2):207-216.
27. Linggi B and Carpenter G. ErbB receptors: new insights on mechanisms and biology. *Trends in cell biology*. 2006; 16(12):649-656.
28. Yarden Y and Pines G. The ERBB network: at last, cancer therapy meets systems biology. *Nature Reviews Cancer*. 2012; 12(8):553-563.
29. Seshacharyulu P, Ponnusamy MP, Haridas D, Jain M, Ganti AK and Batra SK. Targeting the EGFR signaling pathway in cancer therapy. *Expert opinion on therapeutic targets*. 2012; 16(1):15-31.
30. Chinchar E, Makey KL, Gibson J, Chen F, Cole SA, Megason GC, Vijayakumar S, Miele L and Gu J-W. Sunitinib significantly suppresses the proliferation, migration, apoptosis resistance, tumor angiogenesis and growth of triple-negative breast cancers but increases breast cancer stem cells. *Vascular Cell*. 2014; 6(1):12.
31. Engelman JA. Targeting PI3K signalling in cancer: opportunities, challenges and limitations. *Nature Reviews Cancer*. 2009; 9(8):550-562.
32. Arteaga CL and Engelman JA. ERBB Receptors: From Oncogene Discovery to Basic Science to Mechanism-Based Cancer Therapeutics. *Cancer cell*. 2014; 25(3):282-303.
33. Engelman JA, Janne PA, Mermel C, Pearlberg J, Mukohara T, Fleet C, Cichowski K, Johnson BE and Cantley LC. ErbB-3 mediates phosphoinositide 3-kinase activity in gefitinib-

- sensitive non-small cell lung cancer cell lines. *Proceedings of the National Academy of Sciences of the United States of America*. 2005; 102(10):3788-3793.
34. Pearson G, Robinson F, Beers Gibson T, Xu B-e, Karandikar M, Berman K and Cobb MH. Mitogen-activated protein (MAP) kinase pathways: regulation and physiological functions 1. *Endocrine reviews*. 2001; 22(2):153-183.
35. Roskoski Jr R. MEK1/2 dual-specificity protein kinases: structure and regulation. *Biochemical and biophysical research communications*. 2012; 417(1):5-10.
36. Lowenstein E, Daly R, Batzer A, Li W, Margolis B, Lammers R, Ullrich A, Skolnik E, Bar-Sagi D and Schlessinger J. The SH2 and SH3 domain-containing protein GRB2 links receptor tyrosine kinases to ras signaling. *Cell*. 1992; 70(3):431-442.
37. Hirsch FR, Varella-Garcia M, Bunn PA, Di Maria MV, Veve R, Bremnes RM, Barón AE, Zeng C and Franklin WA. Epidermal growth factor receptor in non-small-cell lung carcinomas: correlation between gene copy number and protein expression and impact on prognosis. *Journal of Clinical Oncology*. 2003; 21(20):3798-3807.
38. Kobayashi S, Boggon TJ, Dayaram T, Jänne PA, Kocher O, Meyerson M, Johnson BE, Eck MJ, Tenen DG and Halmos B. EGFR mutation and resistance of non-small-cell lung cancer to gefitinib. *New England Journal of Medicine*. 2005; 352(8):786-792.
39. Balak MN, Gong Y, Riely GJ, Somwar R, Li AR, Zakowski MF, Chiang A, Yang G, Ouerfelli O and Kris MG. Novel D761Y and common secondary T790M mutations in epidermal growth factor receptor-mutant lung adenocarcinomas with acquired resistance to kinase inhibitors. *Clinical cancer research*. 2006; 12(21):6494-6501.
40. Sharma SV, Bell DW, Settleman J and Haber DA. Epidermal growth factor receptor mutations in lung cancer. *Nature Reviews Cancer*. 2007; 7(3):169-181.
41. Choi YL, Soda M, Yamashita Y, Ueno T, Takashima J, Nakajima T, Yatabe Y, Takeuchi K, Hamada T and Haruta H. EML4-ALK mutations in lung cancer that confer resistance to ALK inhibitors. *New England Journal of Medicine*. 2010; 363(18):1734-1739.
42. Sasaki T, Koivunen J, Ogino A, Yanagita M, Nikiforow S, Zheng W, Lathan C, Marcoux JP, Du J and Okuda K. A novel ALK secondary mutation and EGFR signaling cause resistance to ALK kinase inhibitors. *Cancer research*. 2011; 71(18):6051-6060.
43. Pao W and Chmielecki J. Rational, biologically based treatment of EGFR-mutant non-small-cell lung cancer. *Nature Reviews Cancer*. 2010; 10(11):760-774.

REFERENCES

44. Katayama R, Shaw AT, Khan TM, Mino-Kenudson M, Solomon BJ, Halmos B, Jessop NA, Wain JC, Yeo AT and Benes C. Mechanisms of acquired crizotinib resistance in ALK-rearranged lung cancers. *Science translational medicine*. 2012; 4(120):120ra117-120ra117.
45. Turke AB, Zejnullahu K, Wu Y-L, Song Y, Dias-Santagata D, Lifshits E, Toschi L, Rogers A, Mok T and Sequist L. Preexistence and Clonal Selection of MET Amplification in EGFR Mutant NSCLC. *Cancer cell*. 2010; 17(1):77-88.
46. Ellis LM and Hicklin DJ. Resistance to targeted therapies: refining anticancer therapy in the era of molecular oncology. *Clinical cancer research*. 2009; 15(24):7471-7478.
47. Engelman JA and Settleman J. Acquired resistance to tyrosine kinase inhibitors during cancer therapy. *Current opinion in genetics & development*. 2008; 18(1):73-79.
48. Bean J, Riely GJ, Balak M, Marks JL, Ladanyi M, Miller VA and Pao W. Acquired resistance to epidermal growth factor receptor kinase inhibitors associated with a novel T854A mutation in a patient with EGFR-mutant lung adenocarcinoma. *Clinical cancer research*. 2008; 14(22):7519-7525.
49. Sequist LV, Waltman BA, Dias-Santagata D, Digumarthy S, Turke AB, Fidias P, Bergethon K, Shaw AT, Gettinger S and Cospers AK. Genotypic and histological evolution of lung cancers acquiring resistance to EGFR inhibitors. *Science translational medicine*. 2011; 3(75):75ra26-75ra26.
50. Engelman JA, Zejnullahu K, Mitsudomi T, Song Y, Hyland C, Park JO, Lindeman N, Gale C-M, Zhao X and Christensen J. MET amplification leads to gefitinib resistance in lung cancer by activating ERBB3 signaling. *Science*. 2007; 316(5827):1039-1043.
51. Postel-Vinay S and Ashworth A. AXL and acquired resistance to EGFR inhibitors. *Nature genetics*. 2012; 44(8):835-836.
52. Zhang Z, Lee JC, Lin L, Olivas V, Au V, LaFramboise T, Abdel-Rahman M, Wang X, Levine AD, Rho JK, Choi YJ, Choi CM, Kim SW, Jang SJ, Park YS, Kim WS, et al. Activation of the AXL kinase causes resistance to EGFR-targeted therapy in lung cancer. *Nature genetics*. 2012; 44(8):852-860.
53. Takezawa K, Pirazzoli V, Arcila ME, Nebhan CA, Song X, de Stanchina E, Ohashi K, Janjigian YY, Spitzler PJ and Melnick MA. HER2 amplification: a potential mechanism of acquired resistance to EGFR inhibition in EGFR-mutant lung cancers that lack the second-site EGFR T790M mutation. *Cancer discovery*. 2012; 2(10):922-933.

54. Sos ML, Koker M, Weir BA, Heynck S, Rabinovsky R, Zander T, Seeger JM, Weiss J, Fischer F and Frommolt P. PTEN loss contributes to erlotinib resistance in EGFR-mutant lung cancer by activation of Akt and EGFR. *Cancer research*. 2009; 69(8):3256-3261.
55. Roskoski Jr R. RAF protein-serine/threonine kinases: structure and regulation. *Biochemical and biophysical research communications*. 2010; 399(3):313-317.
56. Cheung HW, Du J, Boehm JS, He F, Weir BA, Wang X, Butaney M, Sequist LV, Luo B and Engelman JA. Amplification of CRKL induces transformation and epidermal growth factor receptor inhibitor resistance in human non-small cell lung cancers. *Cancer discovery*. 2011; 1(7):608-625.
57. Yano S, Wang W, Li Q, Matsumoto K, Sakurama H, Nakamura T, Ogino H, Kakiuchi S, Hanibuchi M and Nishioka Y. Hepatocyte growth factor induces gefitinib resistance of lung adenocarcinoma with epidermal growth factor receptor-activating mutations. *Cancer research*. 2008; 68(22):9479-9487.
58. Doebele RC, Pilling AB, Aisner DL, Kutateladze TG, Le AT, Weickhardt AJ, Kondo KL, Linderman DJ, Heasley LE and Franklin WA. Mechanisms of resistance to crizotinib in patients with ALK gene rearranged non-small cell lung cancer. *Clinical cancer research*. 2012; 18(5):1472-1482.
59. Gainor JF and Shaw AT. Emerging paradigms in the development of resistance to tyrosine kinase inhibitors in lung cancer. *Journal of Clinical Oncology*. 2013; 31(31):3987-3996.
60. Reya T, Morrison SJ, Clarke MF and Weissman IL. Stem cells, cancer, and cancer stem cells. *Nature*. 2001; 414(6859):105-111.
61. Sotiropoulou PA, Christodoulou MS, Silvani A, Herold-Mende C and Passarella D. Chemical approaches to targeting drug resistance in cancer stem cells. *Drug discovery today*. 2014.
62. Morshead CM, Reynolds BA, Craig CG, McBurney MW, Staines WA, Morassutti D, Weiss S and van der Kooy D. Neural stem cells in the adult mammalian forebrain: a relatively quiescent subpopulation of subependymal cells. *Neuron*. 1994; 13(5):1071-1082.
63. Dembinski JL and Krauss S. Characterization and functional analysis of a slow cycling stem cell-like subpopulation in pancreas adenocarcinoma. *Clinical & experimental metastasis*. 2009; 26(7):611-623.

REFERENCES

64. Chen J, Li Y, Yu T-S, McKay RM, Burns DK, Kernie SG and Parada LF. A restricted cell population propagates glioblastoma growth after chemotherapy. *Nature*. 2012; 488(7412):522-526.
65. di Fagagna FdA. Living on a break: cellular senescence as a DNA-damage response. *Nature Reviews Cancer*. 2008; 8(7):512-522.
66. Squatrito M, Brennan CW, Helmy K, Huse JT, Petrini JH and Holland EC. Loss of ATM/Chk2/p53 pathway components accelerates tumor development and contributes to radiation resistance in gliomas. *Cancer cell*. 2010; 18(6):619-629.
67. Bao S, Wu Q, McLendon RE, Hao Y, Shi Q, Hjelmeland AB, Dewhirst MW, Bigner DD and Rich JN. Glioma stem cells promote radioresistance by preferential activation of the DNA damage response. *Nature*. 2006; 444(7120):756-760.
68. Ropolo M, Daga A, Griffiero F, Foresta M, Casartelli G, Zunino A, Poggi A, Cappelli E, Zona G and Spaziante R. Comparative analysis of DNA repair in stem and nonstem glioma cell cultures. *Molecular Cancer Research*. 2009; 7(3):383-392.
69. Pajonk F, Vlashi E and McBride WH. Radiation resistance of cancer stem cells: the 4 R's of radiobiology revisited. *STEM CELLS*. 2010; 28(4):639-648.
70. Veis DJ, Sorenson CM, Shutter JR and Korsmeyer SJ. Bcl-2-deficient mice demonstrate fulminant lymphoid apoptosis, polycystic kidneys, and hypopigmented hair. *Cell*. 1993; 75(2):229-240.
71. Motoyama N, Wang F, Roth KA, Sawa H, Nakayama K-i, Negishi I, Senju S, Zhang Q and Fujii S. Massive cell death of immature hematopoietic cells and neurons in Bcl-x-deficient mice. *Science*. 1995; 267(5203):1506-1510.
72. Sanai N, Alvarez-Buylla A and Berger MS. Neural stem cells and the origin of gliomas. *New England Journal of Medicine*. 2005; 353(8):811-822.
73. Corbeil D, Röper K, Hellwig A, Tavian M, Miraglia S, Watt SM, Simmons PJ, Peault B, Buck DW and Huttner WB. The human AC133 hematopoietic stem cell antigen is also expressed in epithelial cells and targeted to plasma membrane protrusions. *Journal of biological chemistry*. 2000; 275(8):5512-5520.
74. Hilbe W, Dirnhofer S, Oberwasserlechner F, Schmid T, Gunsilius E, Hilbe G, Wöll E and Kähler C. CD133 positive endothelial progenitor cells contribute to the tumour vasculature in non-small cell lung cancer. *Journal of clinical pathology*. 2004; 57(9):965-969.

75. Liu G, Yuan X, Zeng Z, Tunici P, Ng H, Abdulkadir IR, Lu L, Irvin D, Black KL and John SY. Analysis of gene expression and chemoresistance of CD133+ cancer stem cells in glioblastoma. *Molecular cancer*. 2006; 5(1):67.
76. Todaro M, Alea MP, Di Stefano AB, Cammareri P, Vermeulen L, Iovino F, Tripodo C, Russo A, Gulotta G and Medema JP. Colon cancer stem cells dictate tumor growth and resist cell death by production of interleukin-4. *Cell stem cell*. 2007; 1(4):389-402.
77. Nanta R, Kumar D, Meeker D, Rodova M, Van Veldhuizen P, Shankar S and Srivastava R. NVP-LDE-225 (Erismodegib) inhibits epithelial–mesenchymal transition and human prostate cancer stem cell growth in NOD/SCID IL2R γ null mice by regulating Bmi-1 and microRNA-128. *Oncogenesis*. 2013; 2(4):e42.
78. Tang S-N, Singh C, Nall D, Meeker D, Shankar S and Srivastava RK. The dietary bioflavonoid quercetin synergizes with epigallocatechin gallate (EGCG) to inhibit prostate cancer stem cell characteristics, invasion, migration and epithelial-mesenchymal transition. *Journal of molecular signaling*. 2010; 5(1):14.
79. Dean M, Hamon Y and Chimini G. The human ATP-binding cassette (ABC) transporter superfamily. *Journal of lipid research*. 2001; 42(7):1007-1017.
80. Ashida H, Oonishi T and Uyesaka N. Kinetic analysis of the mechanism of action of the multidrug transporter. *Journal of theoretical biology*. 1998; 195(2):219-232.
81. Zhou S, Schuetz JD, Bunting KD, Colapietro A-M, Sampath J, Morris JJ, Lagutina I, Grosveld GC, Osawa M and Nakauchi H. The ABC transporter Bcrp1/ABCG2 is expressed in a wide variety of stem cells and is a molecular determinant of the side-population phenotype. *Nature medicine*. 2001; 7(9):1028-1034.
82. Haraguchi N, Utsunomiya T, Inoue H, Tanaka F, Mimori K, Barnard GF and Mori M. Characterization of a side population of cancer cells from human gastrointestinal system. *STEM CELLS*. 2006; 24(3):506-513.
83. Hu L, McArthur C and Jaffe R. Ovarian cancer stem-like side-population cells are tumourigenic and chemoresistant. *British journal of cancer*. 2010; 102(8):1276-1283.
84. Moserle L, Ghisi M, Amadori A and Indraccolo S. Side population and cancer stem cells: therapeutic implications. *Cancer letters*. 2010; 288(1):1-9.
85. Dean M, Fojo T and Bates S. Tumour stem cells and drug resistance. *Nature Reviews Cancer*. 2005; 5(4):275-284.

REFERENCES

86. Ginestier C, Hur MH, Charafe-Jauffret E, Monville F, Dutcher J, Brown M, Jacquemier J, Viens P, Kleer CG and Liu S. ALDH1 is a marker of normal and malignant human mammary stem cells and a predictor of poor clinical outcome. *Cell stem cell*. 2007; 1(5):555-567.
87. Pearce DJ, Taussig D, Simpson C, Allen K, Rohatiner AZ, Lister TA and Bonnet D. Characterization of cells with a high aldehyde dehydrogenase activity from cord blood and acute myeloid leukemia samples. *STEM CELLS*. 2005; 23(6):752-760.
88. Corti S, Locatelli F, Papadimitriou D, Donadoni C, Salani S, Del Bo R, Strazzer S, Bresolin N and Comi GP. Identification of a primitive brain-derived neural stem cell population based on aldehyde dehydrogenase activity. *STEM CELLS*. 2006; 24(4):975-985.
89. Li C, Heidt DG, Dalerba P, Burant CF, Zhang L, Adsay V, Wicha M, Clarke MF and Simeone DM. Identification of pancreatic cancer stem cells. *Cancer research*. 2007; 67(3):1030-1037.
90. Dylla SJ, Beviglia L, Park I-K, Chartier C, Raval J, Ngan L, Pickell K, Aguilar J, Lazetic S and Smith-Berdan S. Colorectal cancer stem cells are enriched in xenogeneic tumors following chemotherapy. *PloS one*. 2008; 3(6):e2428.
91. Fuchs E, Tumber T and Guasch G. Socializing with the neighbors: stem cells and their niche. *Cell*. 2004; 116(6):769-778.
92. Scadden DT. The stem-cell niche as an entity of action. *Nature*. 2006; 441(7097):1075-1079.
93. Watt FM and Hogan B. Out of Eden: stem cells and their niches. *Science*. 2000; 287(5457):1427-1430.
94. Li L and Neaves WB. Normal stem cells and cancer stem cells: the niche matters. *Cancer research*. 2006; 66(9):4553-4557.
95. Oskarsson T, Batlle E and Massagué J. Metastatic stem cells: sources, niches, and vital pathways. *Cell stem cell*. 2014; 14(3):306-321.
96. Reya T and Clevers H. Wnt signalling in stem cells and cancer. *Nature*. 2005; 434(7035):843-850.
97. Bar EE, Chaudhry A, Lin A, Fan X, Schreck K, Matsui W, Piccirillo S, Vescovi AL, DiMeco F and Olivi A. Cyclopamine-Mediated Hedgehog Pathway Inhibition Depletes Stem-Like Cancer Cells in Glioblastoma. *STEM CELLS*. 2007; 25(10):2524-2533.

98. Zhao C, Chen A, Jamieson CH, Fereshteh M, Abrahamsson A, Blum J, Kwon HY, Kim J, Chute JP and Rizzieri D. Hedgehog signalling is essential for maintenance of cancer stem cells in myeloid leukaemia. *Nature*. 2009; 458(7239):776-779.
99. Liu S, Dontu G, Mantle ID, Patel S, Ahn N-s, Jackson KW, Suri P and Wicha MS. Hedgehog signaling and Bmi-1 regulate self-renewal of normal and malignant human mammary stem cells. *Cancer research*. 2006; 66(12):6063-6071.
100. Merchant AA and Matsui W. Targeting Hedgehog—a cancer stem cell pathway. *Clinical cancer research*. 2010; 16(12):3130-3140.
101. Artavanis-Tsakonas S, Rand MD and Lake RJ. Notch signaling: cell fate control and signal integration in development. *Science*. 1999; 284(5415):770-776.
102. Farnie G and Clarke RB. Mammary stem cells and breast cancer—role of Notch signalling. *Stem cell reviews*. 2007; 3(2):169-175.
103. Fan X, Khaki L, Zhu TS, Soules ME, Talsma CE, Gul N, Koh C, Zhang J, Li YM and Maciaczyk J. NOTCH Pathway Blockade Depletes CD133-Positive Glioblastoma Cells and Inhibits Growth of Tumor Neurospheres and Xenografts. *STEM CELLS*. 2010; 28(1):5-16.
104. Fan X, Matsui W, Khaki L, Stearns D, Chun J, Li Y-M and Eberhart CG. Notch pathway inhibition depletes stem-like cells and blocks engraftment in embryonal brain tumors. *Cancer research*. 2006; 66(15):7445-7452.
105. Luqmani Y. Mechanisms of drug resistance in cancer chemotherapy. *Medical Principles and Practice*. 2008; 14(Suppl. 1):35-48.
106. Kourelis TV and Siegel RD. Metformin and cancer: new applications for an old drug. *Medical oncology*. 2012; 29(2):1314-1327.
107. Evans JM, Donnelly LA, Emslie-Smith AM, Alessi DR and Morris AD. Research Pointers: Metformin and reduced risk of cancer in diabetic patients. *BMJ: British Medical Journal*. 2005; 330(7503):1304.
108. Dowling RJ, Goodwin PJ and Stambolic V. Understanding the benefit of metformin use in cancer treatment. *BMC medicine*. 2011; 9(1):33.
109. Costa DB and Huberman MS. Improvement of type 2 diabetes in a lung cancer patient treated with Erlotinib. *Diabetes care*. 2006; 29(7):1711-1711.
110. Chen G, Xu S, Renko K and Derwahl M. Metformin inhibits growth of thyroid carcinoma cells, suppresses self-renewal of derived cancer stem cells, and potentiates the effect

REFERENCES

of chemotherapeutic agents. *Journal of Clinical Endocrinology & Metabolism*. 2012; 97(4):E510-E520.

111. Sahra IB, Laurent K, Loubat A, Giorgetti-Peraldi S, Colosetti P, Auberger P, Tanti J-F, Le Marchand-Brustel Y and Bost F. The antidiabetic drug metformin exerts an antitumoral effect in vitro and in vivo through a decrease of cyclin D1 level. *Oncogene*. 2008; 27(25):3576-3586.

112. Kato K, Gong J, Iwama H, Kitanaka A, Tani J, Miyoshi H, Nomura K, Mimura S, Kobayashi M and Aritomo Y. The antidiabetic drug metformin inhibits gastric cancer cell proliferation in vitro and in vivo. *Molecular cancer therapeutics*. 2012; 11(3):549-560.

113. Alimova IN, Liu B, Fan Z, Edgerton SM, Dillon T, Lind SE and Thor AD. Metformin inhibits breast cancer cell growth, colony formation and induces cell cycle arrest in vitro. *Cell cycle*. 2009; 8(6):909-915.

114. Isakovic A, Harhaji L, Stevanovic D, Markovic Z, Sumarac-Dumanovic M, Starcevic V, Micic D and Trajkovic V. Dual antiglioma action of metformin: cell cycle arrest and mitochondria-dependent apoptosis. *Cellular and molecular life sciences*. 2007; 64(10):1290-1302.

115. Anisimov VN, Berstein LM, Egormin PA, Piskunova TS, Popovich IG, Zabezhinski MA, Kovalenko IG, Poroshina TE, Semenchenko AV and Provinciali M. Effect of metformin on life span and on the development of spontaneous mammary tumors in HER-2/neu transgenic mice. *Experimental gerontology*. 2005; 40(8):685-693.

116. Hirsch HA, Iliopoulos D, Tsihchlis PN and Struhl K. Metformin selectively targets cancer stem cells, and acts together with chemotherapy to block tumor growth and prolong remission. *Cancer research*. 2009; 69(19):7507-7511.

117. Cufí S, Corominas-Faja B, Vazquez-Martin A, Oliveras-Ferraros C, Dorca J, Bosch-Barrera J, Martin-Castillo B and Menendez JA. Metformin-induced preferential killing of breast cancer initiating CD44⁺ CD24⁻/low cells is sufficient to overcome primary resistance to trastuzumab in HER2⁺ human breast cancer xenografts. *Oncotarget*. 2012; 3(4):395.

118. Rattan R, Ali Fehmi R and Munkarah A. Metformin: an emerging new therapeutic option for targeting cancer stem cells and metastasis. *Journal of oncology*. 2012; 2012.

119. Koo KH, Kim H, Bae YK, Kim K, Park BK, Lee CH and Kim YN. Salinomycin induces cell death via inactivation of Stat3 and downregulation of Skp2. *Cell death & disease*. 2013; 4:e693.

120. Gupta PB, Onder TT, Jiang G, Tao K, Kuperwasser C, Weinberg RA and Lander ES. Identification of selective inhibitors of cancer stem cells by high-throughput screening. *Cell*. 2009; 138(4):645-659.
121. Fuchs D, Daniel V, Sadeghi M, Opelz G and Naujokat C. Salinomycin overcomes ABC transporter-mediated multidrug and apoptosis resistance in human leukemia stem cell-like KG-1a cells. *Biochemical and biophysical research communications*. 2010; 394(4):1098-1104.
122. Kinashi H, Ōtake N, Yonehara H, Sato S and Saito Y. The structure of salinomycin, a new member of the polyether antibiotics. *Tetrahedron Letters*. 1973; 14(49):4955-4958.
123. Fuchs D, Heinold A, Opelz G, Daniel V and Naujokat C. Salinomycin induces apoptosis and overcomes apoptosis resistance in human cancer cells. *Biochemical and biophysical research communications*. 2009; 390(3):743-749.
124. Wang F, He L, Dai W-Q, Xu Y-P, Wu D, Lin C-L, Wu S-M, Cheng P, Zhang Y and Shen M. Salinomycin Inhibits Proliferation and Induces Apoptosis of Human Hepatocellular Carcinoma Cells In Vitro and In Vivo. *PloS one*. 2012; 7(12):e50638.
125. Al Dhaheri Y, Attoub S, Arafat K, AbuQamar S, Eid A, Al Faresi N and Iratni R. Salinomycin induces apoptosis and senescence in breast cancer: Upregulation of p21, downregulation of survivin and histone H3 and H4 hyperacetylation. *Biochimica et Biophysica Acta (BBA)-General Subjects*. 2013; 1830(4):3121-3135.
126. Kim K-Y, Yu S-N, Lee S-Y, Chun S-S, Choi Y-L, Park Y-M, Song CS, Chatterjee B and Ahn S-C. Salinomycin-induced apoptosis of human prostate cancer cells due to accumulated reactive oxygen species and mitochondrial membrane depolarization. *Biochemical and biophysical research communications*. 2011; 413(1):80-86.
127. Kim WK, Kim JH, Yoon K, Kim S, Ro J, Kang HS and Yoon S. Salinomycin, a p-glycoprotein inhibitor, sensitizes radiation-treated cancer cells by increasing DNA damage and inducing G2 arrest. *Investigational new drugs*. 2012; 30(4):1311-1318.
128. Riccioni R, Dupuis ML, Bernabei M, Petrucci E, Pasquini L, Mariani G, Cianfriglia M and Testa U. The cancer stem cell selective inhibitor salinomycin is a p-glycoprotein inhibitor. *Blood cells, molecules & diseases*. 2010; 45(1):86-92.
129. Li L and Neaves WB. Normal stem cells and cancer stem cells: the niche matters. *Cancer research*. 2006; 66(9):4553-4557.

REFERENCES

130. Takahashi-Yanaga F and Kahn M. Targeting Wnt signaling: can we safely eradicate cancer stem cells? *Clinical cancer research*. 2010; 16(12):3153-3162.
131. Lu D, Zhao Y, Tawatao R, Cottam HB, Sen M, Leoni LM, Kipps TJ, Corr M and Carson DA. Activation of the Wnt signaling pathway in chronic lymphocytic leukemia. *Proceedings of the National Academy of Sciences of the United States of America*. 2004; 101(9):3118-3123.
132. Funes JM, Quintero M, Henderson S, Martinez D, Qureshi U, Westwood C, Clements MO, Bourboulia D, Pedley RB and Moncada S. Transformation of human mesenchymal stem cells increases their dependency on oxidative phosphorylation for energy production. *Proceedings of the National Academy of Sciences*. 2007; 104(15):6223-6228.
133. Vander Heiden MG, Cantley LC and Thompson CB. Understanding the Warburg effect: the metabolic requirements of cell proliferation. *Science*. 2009; 324(5930):1029-1033.
134. Mitani M, Yamanishi T, Miyazaki Y and Ōtake N. Salinomycin effects on mitochondrial ion translocation and respiration. *Antimicrobial agents and chemotherapy*. 1976; 9(4):655-660.
135. Spitzner M, Ousingsawat J, Scheidt K, Kunzelmann K and Schreiber R. Voltage-gated K⁺ channels support proliferation of colonic carcinoma cells. *The FASEB Journal*. 2007; 21(1):35-44.
136. Agarwal JR, Griesinger F, Stühmer W and Pardo LA. The potassium channel Ether à go-go is a novel prognostic factor with functional relevance in acute myeloid leukemia. *Mol Cancer*. 2010; 9(18):2-16.
137. Pardo LA and Stühmer W. The roles of K⁺ channels in cancer. *Nature Reviews Cancer*. 2014; 14(1):39-48.
138. Chou T-C. Drug combination studies and their synergy quantification using the Chou-Talalay method. *Cancer research*. 2010; 70(2):440-446.
139. Kubo T, Yamamoto H, Lockwood WW, Valencia I, Soh J, Peyton M, Jida M, Otani H, Fujii T and Ouchida M. MET gene amplification or EGFR mutation activate MET in lung cancers untreated with EGFR tyrosine kinase inhibitors. *International Journal of Cancer*. 2009; 124(8):1778-1784.
140. Yamamoto H, Shigematsu H, Nomura M, Lockwood WW, Sato M, Okumura N, Soh J, Suzuki M, Wistuba II and Fong KM. PIK3CA mutations and copy number gains in human lung cancers. *Cancer research*. 2008; 68(17):6913-6921.

141. Pastrana E, Silva-Vargas V and Doetsch F. Eyes wide open: a critical review of sphere-formation as an assay for stem cells. *Cell stem cell*. 2011; 8(5):486-498.
142. Ho MM, Ng AV, Lam S and Hung JY. Side population in human lung cancer cell lines and tumors is enriched with stem-like cancer cells. *Cancer research*. 2007; 67(10):4827-4833.
143. Jiang F, Qiu Q, Khanna A, Todd NW, Deepak J, Xing L, Wang H, Liu Z, Su Y and Stass SA. Aldehyde dehydrogenase 1 is a tumor stem cell-associated marker in lung cancer. *Molecular Cancer Research*. 2009; 7(3):330-338.
144. Mano H. Non-solid oncogenes in solid tumors: EML4–ALK fusion genes in lung cancer. *Cancer science*. 2008; 99(12):2349-2355.
145. Tallarida RJ. Drug synergism: its detection and applications. *Journal of Pharmacology and Experimental Therapeutics*. 2001; 298(3):865-872.
146. Barrandon Y and Green H. Three clonal types of keratinocyte with different capacities for multiplication. *Proceedings of the National Academy of Sciences*. 1987; 84(8):2302-2306.
147. Duffy M. Inhibiting tissue invasion and metastasis as targets for cancer therapy. *Biotherapy*. 1992; 4(1):45-52.
148. Kohn EC and Liotta LA. Molecular insights into cancer invasion: strategies for prevention and intervention. *Cancer research*. 1995; 55(9):1856-1862.
149. Liotta LA and Stetler-Stevenson WG. Tumor invasion and metastasis: an imbalance of positive and negative regulation. *Cancer research*. 1991; 51(18 Supplement):5054s-5059s.
150. Oak PS, Kopp F, Thakur C, Ellwart JW, Rapp UR, Ullrich A, Wagner E, Knyazev P and Roidl A. Combinatorial treatment of mammospheres with trastuzumab and salinomycin efficiently targets HER2-positive cancer cells and cancer stem cells. *International Journal of Cancer*. 2012; 131(12):2808-2819.
151. Zhang G-N, Liang Y, Zhou L-J, Chen S-P, Chen G, Zhang T-P, Kang T and Zhao Y-P. Combination of salinomycin and gemcitabine eliminates pancreatic cancer cells. *Cancer letters*. 2011; 313(2):137-144.
152. Liffers S-T, Tilkorn DJ, Stricker I, Junge CG, Al-Benna S, Vogt M, Verdoodt B, Steinau H-U, Tannapfel A and Tischoff I. Salinomycin increases chemosensitivity to the effects of doxorubicin in soft tissue sarcomas. *BMC cancer*. 2013; 13(1):490.

153. Larzabal L, El-Nikhely N, Redrado M, Seeger W, Savai R and Calvo A. Differential Effects of Drugs Targeting Cancer Stem Cell (CSC) and Non-CSC Populations on Lung Primary Tumors and Metastasis. *PloS one*. 2013; 8(11):e79798.
154. Brown KA, Hunger NI, Docanto M and Simpson ER. Metformin inhibits aromatase expression in human breast adipose stromal cells via stimulation of AMP-activated protein kinase. *Breast cancer research and treatment*. 2010; 123(2):591-596.
155. Bamford S, Dawson E, Forbes S, Clements J, Pettett R, Dogan A, Flanagan A, Teague J, Futreal PA and Stratton M. The COSMIC (Catalogue of Somatic Mutations in Cancer) database and website. *British journal of cancer*. 2004; 91(2):355-358.
156. Köhler J and Schuler M. Afatinib, Erlotinib and Gefitinib in the First-Line Therapy of EGFR Mutation-Positive Lung Adenocarcinoma: A Review. *Onkologie*. 2013; 36(9):510-518.
157. Barr MP, Gray SG, Hoffmann AC, Hilger RA, Thomale J, O'Flaherty JD, Fennell DA, Richard D, O'Leary JJ and O'Byrne KJ. Generation and characterisation of Cisplatin-resistant non-small cell lung cancer cell lines displaying a stem-like signature. *PloS one*. 2013; 8(1):e54193.
158. Bertolini G, Roz L, Perego P, Tortoreto M, Fontanella E, Gatti L, Pratesi G, Fabbri A, Andriani F and Tinelli S. Highly tumorigenic lung cancer CD133+ cells display stem-like features and are spared by cisplatin treatment. *Proceedings of the National Academy of Sciences*. 2009; 106(38):16281-16286.
159. Hsieh J-L, Lu C-S, Huang C-L, Shieh G-S, Su B-H, Su Y-C, Lee C-H, Chang M-Y, Wu C-L and Shiau A-L. Acquisition of an enhanced aggressive phenotype in human lung cancer cells selected by suboptimal doses of cisplatin following cell deattachment and reattachment. *Cancer letters*. 2012; 321(1):36-44.
160. Levina V, Marrangoni AM, DeMarco R, Gorelik E and Lokshin AE. Drug-selected human lung cancer stem cells: cytokine network, tumorigenic and metastatic properties. *PloS one*. 2008; 3(8):e3077.
161. Liu Y-P, Yang C-J, Huang M-S, Yeh C-T, Wu AT, Lee Y-C, Lai T-C, Lee C-H, Hsiao Y-W and Lu J. Cisplatin selects for multidrug-resistant CD133+ cells in lung adenocarcinoma by activating Notch signaling. *Cancer research*. 2013; 73(1):406-416.

162. Xu Y, Hu Y-D, Zhou J, Zhang M-H, Yuan W-W and Luo Y. shRNA targeting Bmi1 impedes the self-renewal of cisplatin-enriched stem-like cells in human A549 cells. *Oncology reports*. 2012; 28(2):629-639.
163. Morgillo F, Sasso FC, Della Corte CM, Vitagliano D, D'aiuto E, Troiani T, Martinelli E, De Vita F, Orditura M and De Palma R. Synergistic effects of metformin treatment in combination with gefitinib, a selective EGFR tyrosine kinase inhibitor, in LKB1 wild-type NSCLC cell lines. *Clinical cancer research*. 2013; 19(13):3508-3519.
164. Li L, Han R, Xiao H, Lin C, Wang Y, Liu H, Li K, Chen H, Sun F and Yang Z. Metformin Sensitizes EGFR-TKI-Resistant Human Lung Cancer Cells In Vitro and In Vivo through Inhibition of IL-6 Signaling and EMT Reversal. *Clinical cancer research*. 2014.
165. Kitazono S, Takiguchi Y, Ashinuma H, Saito-Kitazono M, Kitamura A, Chiba T, Sakaida E, Sekine I, Tada Y and Kurosu K. Effect of metformin on residual cells after chemotherapy in a human lung adenocarcinoma cell line. *International journal of oncology*. 2013; 43(6):1846-1854.
166. Janjetovic K, Vucicevic L, Misirkic M, Vilimanovich U, Tovilovic G, Zogovic N, Nikolic Z, Jovanovic S, Bumbasirevic V and Trajkovic V. Metformin reduces cisplatin-mediated apoptotic death of cancer cells through AMPK-independent activation of Akt. *European journal of pharmacology*. 2011; 651(1):41-50.
167. Miloszevska J, Gos M, Przybyszewska M, Trembacz H, Koronkiewicz M and Janik P. Mouse sarcoma L1 cell line holoclones have a stemness signature. *Cell proliferation*. 2010; 43(3):229-234.
168. Locke M, Heywood M, Fawell S and Mackenzie IC. Retention of intrinsic stem cell hierarchies in carcinoma-derived cell lines. *Cancer research*. 2005; 65(19):8944-8950.
169. Harper LJ, Piper K, Common J, Fortune F and Mackenzie IC. Stem cell patterns in cell lines derived from head and neck squamous cell carcinoma. *Journal of Oral Pathology & Medicine*. 2007; 36(10):594-603.
170. Kalirai H, Damato BE and Coupland SE. Uveal melanoma cell lines contain stem-like cells that self-renew, produce differentiated progeny, and survive chemotherapy. *Investigative ophthalmology & visual science*. 2011; 52(11):8458-8466.
171. Manley Jr E and Waxman DJ. H460 non-small cell lung cancer stem-like holoclones yield tumors with increased vascularity. *Cancer letters*. 2013.

REFERENCES

172. Tan L, Sui X, Deng H and Ding M. Holoclone forming cells from pancreatic cancer cells enrich tumor initiating cells and represent a novel model for study of cancer stem cells. *PloS one*. 2011; 6(8):e23383.
173. Gammon L, Biddle A, Fazil B, Harper L and Mackenzie IC. Stem cell characteristics of cell sub-populations in cell lines derived from head and neck cancers of Fanconi anemia patients. *Journal of Oral Pathology & Medicine*. 2011; 40(2):143-152.
174. Harper LJ, Costea DE, Gammon L, Fazil B, Biddle A and Mackenzie IC. Normal and malignant epithelial cells with stem-like properties have an extended G2 cell cycle phase that is associated with apoptotic resistance. *BMC cancer*. 2010; 10(1):166.

9. APPENDIX

Abbreviations

ABC	ATP-binding cassette
AD	adenocarcinoma
ADAM	a disintegrin and metalloprotease
ALDH	aldehyde dehydrogenase
ALK	anaplastic lymphoma kinase
AMPK	AMP-activated protein kinase
APS	ammonium persulfate
ATCC	American type culture collection
ATM	ataxia telangiectasia mutated
ATP	adenosine triphosphate
ATR	ATM and Rad-3-related
AXL	tyrosine-protein kinase receptor UFO
BADJ	bronchioalveolar duct junction
BCRP	breast cancer resistance protein
BSA	bovine serum albumin
CBL	casitas b-lineage lymphoma
cDNA	complementary DNA
CO ₂	carbon dioxide
CSC	cancer stem cell
CHK1/2	checkpoint kinase 1/2
DF	differentiation
DNA	deoxyribonucleic acid
dNTP	deoxyribonucleoside triphosphate
DDR	DNA-damage-response
DMSO	dimethylsulfoxide
DTT	dithiothreitol
ECL	enhanced chemiluminescence
EGF	epidermal growth factor
EGFR	epidermal growth factor receptor
EML4	echinoderm microtubule-associated protein-like 4

APPENDIX

EMT	epithelial-mesenchymal transition
ErbB	Erythroblastosis B
ERK	extracellular signal-regulated kinase
FACS	fluorescence-activated cell sorting
FCS	fetal calf serum
FITC	fluorescein isothiocyanate
HER2, 3, 4	human EGF Receptor 2, 3, 4
Hh	Hedgehog
hHPRT	human hypoxanthine guanine phosphoribosyltransferase
HRP	horseradish peroxidase
IC ₅₀	half maximal inhibitory concentration
IL-4	interleukin-4
JM	juxtamembrane
JNK	c-Jun N-terminal kinases
LKB1	liver kinase B 1
MAPK	mitogen-activated protein kinase
MET	hepatocyte growth factor receptor
METF	Metformin
MMP	matrix metalloprotease
mTOR	mammalian target of rapamycin
NE	neuroendocrine
NEB	neuroendocrine bodies
NRG1/2/3/4	neuregulin1/2/3/4
NSCLC	non-small-cell lung cancer
PAGE	polyacrylamide gel electrophoresis
PARP	poly(ADP-ribose) polymerase cleavage
PBS	phosphate buffered saline
PCR	polymerase chain reaction
PIP2	phosphatidylinositol 4, 5-bisphosphate
PIP3	phosphatidylinositol 3, 4, 5-trisphosphate
PI3K	phosphatidylinositol 3-kinase
PKB/AKT	protein kinase B
PLC γ	phospholipase C
PMSF	phenylmethanesulfonyl fluoride
PNECs	pulmonary neuroendocrine cells

PTEN	phosphatase and tensin homologue deleted on chromosome 10
RNA	ribonucleic acid
rpm	rounds per minute
RPMI	roswell park memorial institute medium
RT	room temperature
RTK	receptor tyrosine kinases
SAL	Salinomycin
SCC	squamous cell carcinoma
SCLC	small cell lung cancer
SCM	stem cell marker
SD	standard deviation
SF	sphere formation
Shc	src homology 2 domain containing
siRNA	small interfering ribonucleic acid
SOS	son of sevenless
SP	side population
Src	homologue to v-src (sarcoma viral oncogene)
STAT	signal transducer and activator of transcription
S6K	ribosomal protein s6 kinase
TEMED	N, N, N', N'-tetramethylethylenediamine
TKI	tyrosine kinase inhibitor
TRAIL	TNF-related apoptosis-inducing ligand
vCE	variant Clara expressing cells
VEGF	vascular endothelial growth factor
wt	wild-type
2D	two-dimensional
3D	three-dimensional

Units

A	ampere
bp	base pairs
°C	degree Celsius
Da	dalton
g	gravitational force
kDa	kilodalton
m	milli
mA	milliampere
ml	milliliter
mM	millimolar
n	nano
ng	nanogram
nM	nanomolar
p	pico
μ	micro
μg	microgram
μl	microliter
μM	micromolar
V	volt

CURRICULUM VITAE

Personal Details

Name	Zhiguang Xiao
Date of Birth	11.01.1987
Place of Birth	Hunan, China
Nationality	Chinese

Education

June 2011-Feb 2015	PhD, Molecular Biology, Max Planck Institute of Biochemistry, Martinsried, Germany
Sep 2008-June 2011	Master, Preventive Veterinary Medicine, Chinese Academy of Agricultural Sciences, Beijing, China
Sep 2004-July 2008	Bachelor, Veterinary Medicine, Hebei University of Engineering, China

Awards and Fellowships

June 2011-Feb 2015	International Max Planck Research fellowship awarded by the Max Planck Society for PhD studies at the Max Planck Institute of Biochemistry
2008-2009	Advanced Individual of Cultural and Sports activities at Chinese Academy of Agricultural Sciences
2006-2007	Won the major award at Hebei University of Engineering
2004-2005	Merit Student, Model Student of Academic Records at Hebei University of Engineering

Publications

Zhiguang Xiao, Bianca Sperl, Axel Ullrich and Pjotr Knyazev. Metformin and salinomycin as the best combination for the eradication of NSCLC cell lines and their alveospheres (cancer stem cells) irrespective of EGFR, KRAS, EML4/ALK and LKB1 status. *Oncotarget*. 2014; 5(24):12877-12890.

Florian Kopp, Adam Hermawan, Prajakta Shirish Oak, Vijay Kumar Ulaganathan, Annika Herrmann, Nefertiti Elnikhely, Chitra Thakur, **Zhiguang Xiao**, Pjotr Knyazev, Beyhan Ataseven, Rajkumar Savai, Ernst Wagner and Andreas Roidl. Sequential salinomycin treatment results in resistance formation through clonal selection of epithelial-like tumor cells. *Translational Oncology*. 2014; 7(6):702-711.

XIAO Zhi-guang, LIU Xiao-min, WANG Li, LI Wei, WANG Wei, HU Wei-jie, WANG Jian-chao, MENG Qing-wen. Cloning and Tissue Expression of Mxl Gene in ICR Mouse. *Chinese Journal of Progress in Veterinary Medicine*. 2011,32(4):23-28

Talks (presenting author underlined)

Xiao Z., Knyazeva T., Oak P., Gautsch R., Sperl B., Wagner E., Roidl A., Ullrich A., Knyazev P. The role of HER2 in breast cancer stem cells and mammosphere formation. EMBL conference on ‘‘ Stem Cells in Cancer and Regenerative Medicine’’, Heidelberg, Germany, August 29-September 1, 2012

Xiao Z., Sperl B., Knyazev P., Ullrich A. Metformin and salinomycin as the best combination for the eradication of NSCLC cell lines and their alveospheres/cancer stem cells–irrespective of the EGFR status. <interact> Munich 2014, Munich, Germany, February 28, 2014

Poster presentation

Zhiguang Xiao, Bianca Sperl, Axel Ullrich, Peter G. Knyazev. Combinatorial treatment of lung cancer cell lines and their spheroids-cancer stem cells with standard therapeutic drug and salinomycin. 23rd EACR conference on ‘‘From Basic Research to Personalized Cancer Treatment’’, Munich, Germany, July 5-8, 2014

ATTEND:

Max-Planck-Gesellschaft Tagungsstätte Schloss Ringberg, Kreuth, Germany, June 10-13, 2014